Ph.D. THESIS

DYNAMIC MODELING OF THE HUMAN HEART

SÁNDOR MIKLÓS SZILÁGYI

Supervisor: Prof. Zoltán Benyó

Budapest University of Technology and Economics

Faculty of Electrical Engineering and Informatics

Department of Control Engineering and Information Technology

Budapest

2007

Table of Contents

1. Introduction

Sudden cardiac death, mostly caused by ventricular fibrillation, is responsible for at least five million deaths in the world each year. Despite several years of research, the responsible mechanisms for ventricular fibrillation are not yet well understood.

As most simulation studies are usually limited to planar simulations, the responsible mechanisms for the spatial phenomenon of ventricular fibrillation is not elucidated by far. It would be important to know how the most important heart parameters, such as heart's size, geometry, mechanical and electrical state, tissue homogeneity and fiber structure, affect the development of ventricular fibrillation.

The main difficulty in the development of a quantitatively accurate simulation of an entire three-dimensional human heart is the limited number of heart models and that the human heart muscle produces rapidly varying, highly localized fronts.

Moreover, in pathological cases, the most relevant parameters of the conduction properties are highly changed that can produce spiral, self-inducing depolarization waves, which often transforms into ventricular fibrillation. These regional alterations of conduction properties are highly patient specific. To approach toward the solution of these problems, a complex modeling of the heart is necessary.

This thesis focuses on the adaptive ECG analysis and heart modeling. In the second chapter a detailed ECG processing method is presented that uses an iterative filtering and parameter estimation technique to obtain the aimed results. This algorithm is capable to properly adapt itself to patient specific demands. Instead of the direct or transformation-based processing methods that cannot cover the uncommon waveforms even if using large sample databases, this feature-specific ECG estimation method can handle almost all perturbed waveform. The signal estimation and efficient compression processes are highly correlated by the a priori determined medical parameters. The advanced distortion analysis allows to adaptively modify the compression rate assuring a pre-defined quality of the biological parameters.

In the third chapter a dynamic heart model is presented. The model is capable to simulate almost all important pathological cases. The depolarization waveform is simulated at a dynamically, locally and temporally variable resolution that yields a fast simulation keeping estimation error at a reasonable level. The adaptive mesh refinement method uses the first derivative of the intracellular potential to determine the proper local resolution. The whole method is highly parallelized, so video cards can efficiently perform the bulk of the calculation.

In the fourth chapter, the simultaneous processing of the ECG signal and echocardiographic image sequence determines the latent connection between the heart's electric and mechanic properties. This connection can be used to realize the electric-mechanic model of the heart.

The massive amount of a priori medical information can be used to determine the spatial coordinates of the heart's walls. Using a time dependent surface, we could determine the 4D model of the heart. This spatio-temporal model was determined for normal and ectopic beats.

In the fifth chapter, an advanced accessory pathway localization method is presented using the standard 12-lead ECG record. Although the published localization methods (Arruda, Fitzpatrick) yields an almost 90% recognition rate, the weak points of the Arruda localization method can be exploited partially by the replacement of a weak point using a heart model simulation. The obtained clinical data evaluation supported our heart model based considerations.

2. ECG Signal Processing

2.1. General Presentation

The electrical surface electrocardiograph (ECG) signal is generated by the heart's muscle and measured on the skin surface of the body. It has a great importance in diagnosis and monitoring of the heart's condition. The ECG can be measured as a multi- or single- channel signal, depending on the application. During regular measurement of standard clinical ECG, 12 different leads (channels) are recorded from the body surface (skin) of a resting patient. In arrhythmia analysis only one or two ECG leads are recorded or monitored to investigate life-threatening disturbances in the rhythm of the heartbeat.

Nowadays the most important health problem affecting large groups of people is related to the malfunctions of the heart, usually caused by heart attack, rhythm disturbances and pathological degenerations. One of the main goals of health study is to predict these kind of tragic events, and by identifying the mostly exposed patients, it becomes possible to apply a preventing therapy.

The computerized ECG signal processing, after several years of significant progress, can be considered a well-developed application. An efficient real-time analyzer and encoder system, based on filtering, beat detection (recognition and clustering), classification, storage and diagnosis, must be able to evaluate the signal with maximum few seconds delay to recognize in time the potentially dangerous and life threatening arrhythmia. Despite the presence of serious noise, a reliable analysis must involve at least the detection of QRS complex, T and P waves, automatic rhythm analysis, classification and diagnosis, allowing physicians to derive more information for cardiac disease diagnosis. It is important to determine the correct position and amplitude of every characteristic event.

As in paper (Provazník, 2001) is epitomized, in cardiology research the computerized ECG analysis is exploited in numerous areas such as:

- cardiac pattern characterization (Senhadji *et al.*, 1995)
- QRS and T wave morphology analysis (Lemire *et al.*, 2000), (Couderc *et al.*, 1998), (García *et al.*, 2000)
- Bayesian ECG signal modeling (Prado *et al.*, 2001)
- electrocardiographic signal compression (Ahmed *et al.*, 2000), (Istepanian *et al.*, 2000), (Provazník *et al.*, 1997)
- high resolution ECG analysis (Colella *et al.*, 1994), (Gomis *et al.*, 1997)
- body surface potential mapping (BSPM) (Mirvis, 1998), (Lux *et al.*, 1978)
- heart rate variability analysis (HRV) (Joho *et al.*, 1999), (Struzik, 2000), (Tkacz *et al.*, 2000)
- heart rate turbulence analysis (HRT) (Schmidt *et al.*, 1999), (Watanabe, 2003), (Ghuran *et al.*, 2002)
- detection of conduction block (Evans *et al.*, 1999)
- ventricular arrhythmia analysis (Afonso *et al.*, 1995), (Evans *et al.*, 1999)
- late potentials analysis and localization (Meste *et al.*, 1994), (Rix *et al.*, 1997)
- WPW syndrome analysis (Wellens *et al.*, 1987), (Wellens *et al.*, 1990), (Fitzpatrick *et al* 1994), (Reddy *et al.*, 1987), (Arruda *et al.*, 1998)
- ventricular pressure variability analysis (Joho *et al.*, 1999)
- heart sound processing (Wood *et al.*, 1995)
- fetal ECG extraction (Khamene *et al.*, 2000)

- spatial heart reconstruction by inverse electrocardiography (Huiskamp *et al.*, 1997), (Guanglin *et al.*, 2001), (Shahidi *et al.*, 1994).

Starting from the list of enrolled cardiologic research areas we could realize that the correct ECG analysis is a crucial point of heart study. Many attempts were made until now to correctly identify the characteristic points of the ECG. The most relevant ECG analyzing methods can be divided into three functional groups:

1) Direct methods: where the samples of the signal are used to perform the detection. The morphological-operator- based algorithm in presence of high level noise can produce only mediocre results (Trahanias, 1993)

2) Transformation methods: where the original samples are subjected to a transformation and the detection is performed in the new domain. One of the most promising methods belonging to this group is the Wavelet transform (Li *et al.*, 1995)

3) Parameter estimation methods: where a preprocessing is employed to "learn" some features that are used during the detection. Some methods belonging to this group are: linear and nonlinear prediction methods, syntactic methods and neural nets methods (Xue *et al.*, 1992).

The performance of an optimally functioning computerized ECG filtering algorithm is limited by the ability to separate the signal from artifacts, and by the amount and nature of distortion introduced by the filter. As a filter can perform much better using some predefined patient specific information, it is desired to use a post-filtering step to reduce the signal distortion. The speed and accuracy requirements during ECG processing represent a hard task, the varying shape of the ECG and the subjectivity of the diagnosis make it even harder.

The most important task in the ECG signal processing is the accurate localization of QRS complexes. The established QRS places constitute the basic a-priori information for all further processing steps. Many times the recorded ECG is disturbed by different kind of noises that can imply a pre-filtering or discarding of the studied segment. To assure the good quality of the ECG, and to prevent the loss of clinically significant information, the usage of human and artificial noise detection schemes is required. As the perturbing noise can only be diminished, but not eliminated from the measured signal, it is important to use processing methods with good noise susceptibility. The non-linear behavior of the human body requires adaptive processing that follows the patient's state.

The design of an optimal matched filter can increase the signal-to-noise ratio, but the non stationary nature of the signal and noise in an ECG represents an obstacle in the application of these filters for QRS detection. A linear filter cannot properly whiten the non-linear ECG signal. Artificial neural networks (ANN) (Xue *et. al*, 1992) are inherently non-linear models, so an ANN based filtering is potentially useful. In practical use, the ANN model can adapt far better than linear models. The number of input units corresponds to the filter order that should not be increased too much, in order to assure constantly good transient properties. The selection of the right number of hidden layers is important to provide good learning speed and adaptation at the same time. After pre-processing, filtering, evaluation and model's parameter estimation, the signal reconstruction is needed. In this step, the post-filtering method knows the main ECG specific information, and can better separate all artificial noises. An efficient filter has to use all ECG and patient dependent information. This problem can be handled only if the computer knows the formation of the ECG signal.

The collected noise during ECG signal acquisition makes almost meaningless the usage of loss-free compression (Nave *et al.*, 1993). In this paper we focused on lossy methods as a compromise between bandwidth and final reconstruction possibility, using sophisticated medical knowledge-based reconstruction algorithms (Szilágyi *et al.*, 2003c). The signal's main characteristics are represented by exponential parameterization that is delivered by a processing system that uses support vector machine (SVM) (Osowski *et al.*, 2004). This robust model involves the filtering, analysis and compression step of an automatic ECG evaluation method.

2.2. The Problem of Noise Filtering

Owing to the intensive recent progress of personal computers (PC) the automated ECG analysis is prospering in the last decade. Unfortunately despite all computational efforts of the researcher community, they could not develop a totally credible QRS detection method. The main reason of this fiasco is caused by a high variability of the measured signal and noise characteristic.

The measured ECG data apart the useful signal often contain high amplitude noise. These perturbations may counteract to succeed with a proper detection of QRS beats. Despite adaptation of most evaluated filtering techniques the insurance of the clinically useful data could not be guaranteed in all circumstances. The most important aspect of a performing QRS detection method is a low sensitivity to various noises that allows the development of a clinically robust solution. Electrocardiographic records may be altered by various kinds of noise. Most common cases are (Friesen *et al.*, 1990):

1. power line interference
2. electrode contact noise
3. motion caused artifacts
4. muscle contraction (electromyographic, EMG)
5. baseline drift and ECG amplitude modulation with respiration
6. instrumentation noise generated by electronic devices used in signal processing
7. electrosurgical noise
8. other, less significant noise sources presented in paper (Webster, 1978)

In the followings a brief presentation of each described noise type, and methods that can handle these perturbations will be discussed. The pertinent characteristics of each noise type will be given.

2.2.1. Power line interference

Inward of all electric current consumer apparatus an electromagnetic field is generated that assist to the outward situated electric network generated base-harmonic and their harmonics caused perturbations. Unfortunately these disturbances exists inward all electric appliances, and with proper screening their effect can be decreased but not abolished. The base frequency of this noise is place dependent, for example 50Hz in Europe and 60Hz in US.

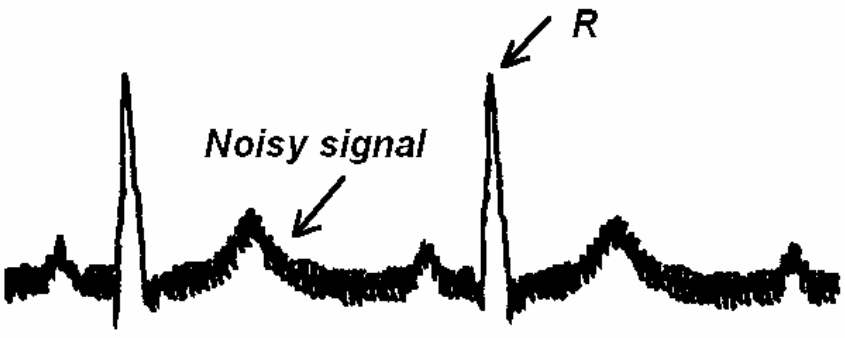

Fig. 2.1. An ECG sequence altered by the electric network caused perturbation

This jamming is composed by a set of sinusoid signals. Allowing stationary measuring conditions, the characteristics of these sinusoidal terms are fairly estimable. Notwithstanding the main properties of the noise are constant with time its behaviors may alter slightly. Equation (2.1) describes the time variant form of this perturbation:

$$N_{PLI}(t) = \sum_{i=1}^{n} A_i \cdot \sin\left(PLF \cdot i \cdot t + \varphi_i\right), \tag{2.1}$$

where *PLI* represent the generated disturbance in the electric network, *PLF* is the base frequency, A_i personates the amplitude of various harmonics, φ_i pictures the phase of harmonics and n symbolize the number of regarded components. Usually the highest frequency of a QRS complex situates below 1000Hz, so parameter n is considered less than 20. Empirical data reflects that the maximal amplitude of harmonics can reach half size of R wave in lead D2 (considering a normal ECG waveform) (see Fig. 2.1).

2.2.2. Electrode contact noise

The improper contact of the electrodes interrupts for a short period the connection between patient and measuring system, creating the electrode contact noise. The loss of contact can be permanent or intermittent, as in case when a loose electrode is brought in and out of connection with the patient's skin as a result of vibration or movement. This switching action at the input of measuring apparatus generates an abrupt, high amplitude artifact that decays to isoelectric line exponentially, since the ECG signal is usually capacitively coupled to the system. Shortly after the pretermitter event the amplitude of power line interference may be significant. In the followings when the connection is regained the level of the power line interference drops in approximately one second to the average amplitude prior disconnection.

Fig. 2.2. Loose contact effect on an ECG sequence

As Fig. 2.2 presents, the amplitude of the artifact can reach the maximal recorder output with duration of few seconds. The random property counteracts us to describe by practically useful mathematical equations, so an adequate estimation can be realized only from model-based processing of the circumambient signal.

2.2.3. Motion caused artifacts

The measured ECG signal is inseparable from alteration caused by the specific movements of the studied patient. Motion artifacts are transient but not step-like baseline changes caused by modification in the electrode-skin impedance due electrode motion, as presented in Fig. 2.3.

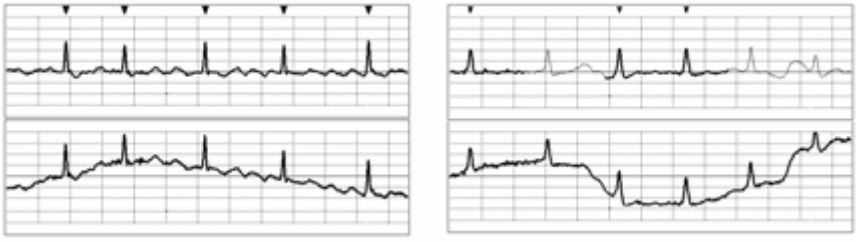

Fig. 2.3. Various motion-caused perturbed ECG signals, after and before filtering. The small black triangles indicate the recognized QRS complexes

A typical cause of motion artifacts is assumed to be vibrations or movements of the subject. The shape of the iso-electric line perturbation can be considered to be a biphasic signal resembling one cycle of a sine wave with duration of 100-500ms and maximal amplitude that can reach 500% of the height of a normal QRS beat. The filtering of such a signal is considered to be hard, especially when the measured value reaches one of the limiting degrees. In this case the disturbed interval cannot be processed, so the highly altered QRS beats become unrecognizable.

2.2.4. Muscle contractions (electromyographic, EMG)

Muscle contraction generates millivolt-level artifactual potentials. Usually these currents extinct each other so the recognition of QRS beats is not hardened, but they can decrease the detection rate of other waves, like P, S, T, U. The average value of the artifact is close to baseline with amplitude 10% of normal QRS and a duration of 50ms. Its frequency may vary from low components until 10kHz.

2.2.5. Breath caused baseline movement

The drift of the iso-electric line with respiration can be approximated with a simusoidal component at the frequency of respiration added to the ECG signal. The amplitude of the drift may be at least five times smaller than the size of a normal QRS beat. As the respiration frequency of a normal patient is about 0.15-0.30Hz this artifact changes slowly and may alter in 2-5 period of ECG. Such a noise type sparely aggreges the recognition of QRS beats.

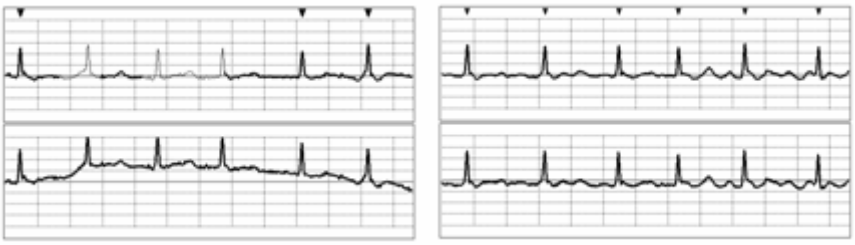

Fig. 2.4. The effect of respiration on the measured ECG. QRS complexes cannot be determined from the filtered signal if the measured signal reached the upper limit of measuring domain (left side)

2.2.6. Instrumentation noise generated by electronic devices used in signal processing

Artifacts generated by electronic devices in the instrumentation system did not acquit the white noise condition, namely their average value differs from zero. Therefore the measuring amplifier whose filtering allows an integrative property will saturate the signal direct proportionally with the amplitude of averaged noise. This phenomena can inchoate the decadence or losing of the useful signals dynamic (see Fig. 2.5). To assure a zero compensation of the input amplifier allowing its functioning in the proper measuring interval it is necessary to build a feed-back connection.

Fig. 2.5. The saturation of the ECG signal

It is not possible to correct the measured signal with conventional algorithms because a proper rectification supposes the complete understood of the ECG evolvement. Practically the correct detection of the QRS beats may allow the evaluation of the disturbed intervals, but because a high error probability the deteriorated section is often discarded.

The saturation of the input amplifier causes a total loss of the signal dynamic, so we have no information about the measured signal. In such cases an alarm must sound to alert the ECG technician to take a corrective action.

2.2.7. Electrosurgical noise

The electrosurgical noise completly destroys the ECG and can be represented as a large amplitude sinusoid with high frequencies (approximately 100kHz and 1MHz). Its duration vary from few tenth second to seconds. Since the sampling rate of the ECG is much lower (about 200Hz to 2000Hz) an aliased version of this signal would be added to the ECG. This perturbation manifest as a high amplitude white noise on the ECG. If low-pass filtering cannot solve the problem the studied segment must be rejected. With an aggresive increment of the sampling rate (a high order oversampling) the amplitude of the noise is reducible but not eliminatible.

2.3. Motivation of Filtering

An optimal computerized ECG filtering algorithm's performance mainly depends on the ability to separate the signal from artifacts, and on the amount and nature of distortion introduced by the filter. A post-filtering step is essential to reduce the signal distortion. Both guidelines are quite hard to evaluate, because the diagnosis is subjective and depends on the shape of the ECG signal.

The most important task in the ECG signal processing is the accurate detection of the QRS complexes. All further processing steps are based on the position of the QRS waves as basic information. Unfortunately the recorded ECG is often disturbed from different kinds of noises. Data corrupted with noise must be pre-filtered or discarded.

The ECG quality assurance requires human and artificial noise detection schemes in order not to lose clinically significant information. During ECG recording the noise can only be diminished but not eliminated, so it is important to use a method with good noise susceptibility.

ECG filtering algorithms generally contain a band-pass filter with a centre frequency in the range of 11-16 Hz. After passing through the filter, the signal may be squared or averaged over a number of samples to obtain the place of QRS waves. Unfortunately these static techniques suffer from two major problems:

- QRS waveform varies from patient to patient, and depends on the state of the patient;
- Noise and QRS complex pass bands overlap.

The non-linear behavior of the human body implies that all processing methods must be capable during measurement to change their state otherwise they introduce a huge amount of artificial noise. The design of an optimal matched filter can increase the signal-to-noise ratio (SNR), but the non-stationary nature of the signal and noise involved in the measured ECG obstruct to put into practice these filters for QRS detection. A linear filter cannot whiten the noise of a non-linear ECG signal effectively.

Artificial neural networks (ANN) have several interesting biomedical applications in the area of data processing (Minami *et al.*, 1999). The best known neural solutions involve multilayer perceptrons, Kohonen self-organizing networks, fuzzy or neuro-fuzzy systems, genetic algorithms and the

combination of various solutions within a hybrid system (Lagerholm *et al.*, 2000). A complex ECG analyzer system applies many neural networks and chooses the best one, while discarding the rest. Most efficient approaches usually are based on the combination of many classifiers utilizing either different classifier network structures or different data preprocessing methods (Osowski *et al.*, 2001) (Osowski *et al.*, 2004).

The support vector machine (SVM), pioneered by (Vapnik, 1998), had to solve the main drawbacks of conventional artificial neural networks such as:

- Modern biological problems are high-dimensional, and if the underlying mapping is not very smooth, the linear paradigm needs an exponentially increasing number of terms with an increasing dimensionality of the input space, that means an increase in the number of independent variables. This is known as 'the curse of dimensionality';
- The real-life data generation laws may typically be far from the normal distribution and a model-builder must handle this difference in order to construct an effective learning algorithm;
- The maximum likelihood estimator (and consequently the sum-of-error-squares cost function) should be replaced by a new induction paradigm that is uniformly better, in order to model properly non-Gaussian distributions.

SVM classifiers became quite popular due to their robustness and stability (Vapnik, 1998). A SVM used in a ECG processing and parameter extraction system is rigorously based on statistical learning theory and simultaneously minimizes the training and test errors. Apart from that, they produce a unique globally optimal solution and hence are extensively used in diverse applications including medical diagnosis (Smola *et al.*, 1998).

Artificial neural networks are inherently non-linear models, so an ANN-based filtering is potentially useful (Xue *et al.*, 1992). In case of a complex, heavily non-linear behavior signal, like almost all biological ones, we should use two hidden layers that generally provide good approximation results and allow good learning speed and adaptation at the same time. In practical use, the ANN model can adapt far better than linear ones. The number of input units corresponds to the filter order that should not be increased too much, in order to allow constantly good transient properties.

After pre-processing, filtering, evaluation and model parameter estimation, a signal reconstruction is needed. In this stage, the post-filtering algorithm 'knows' the main ECG specific information, so it can better separate all artificial noises from the signal. In order to develop a high performing filter, the application of ECG and patient depending information is necessary. This problem can be handled only if the computer knows the formation of the ECG signal.

In most cases, due to the collected noise during measurement, there is almost no reason to use loss-free compression (Nave *et al.*, 1993). In this paper we focused on loosely methods as a compromise between bandwidth and final reconstruction possibility, using sophisticated medical knowledge-based reconstruction algorithms (Szilágyi *et al.*, 2003c). The signal's main characteristics are represented by exponential parameterization that is delivered by a processing system that uses an SVM-based UNN (Vapnik, 1998). This robust model involves the filtering, analysis and compression step of an automatic ECG evaluation method.

2.4. Processing Methods

2.4.1. Wavelet transform

Let $\Psi(t)$ be a complex valued function in $L^2(R)$, whose Fourier transform $\hat{\Psi}(\omega)$ satisfies:

$$\int_{-\infty}^{+\infty} \frac{|\hat{\Psi}(\omega)|^2}{|\omega|} d\omega = C_\Psi < +\infty \,. \tag{2.2}$$

Let $\Psi_s(t) = \frac{1}{s} \cdot \Psi(\frac{t}{s})$ be the dilation of $\Psi(t)$ by a scale factor of s>0 (Eq. (2.2)). The WT of a function $f(t) \in L^2(R)$ at scale s and position τ is defined by:

$$Wf(s,\tau) = \frac{1}{s} \cdot \int_{-\infty}^{+\infty} f(t) \cdot \Psi^*(\frac{t-\tau}{s}) dt \,, \tag{2.3}$$

where * denotes the complex conjugation. In case of the WT (Eq. (2.3)) is invertible (Mallat *et al.*, 1992), the $f(t)$ can be obtained by:

$$f(t) = \frac{1}{C_\Psi} \cdot \int_{-\infty}^{+\infty} \int_{-\infty}^{+\infty} Wf(s,\tau) \cdot \Psi^*(\frac{\tau-t}{s}) d\tau \frac{ds}{s^2} \,. \tag{2.4}$$

The selected wavelet is:

$$\Psi(t) = \frac{1}{\sqrt{2 \cdot \pi} \cdot \sigma} \cdot e^{-\frac{t^2}{2 \cdot \sigma}} \cdot \sin(\alpha \cdot t \cdot e^{\beta \cdot t}) \,, \tag{2.5}$$

where α and β is selected according to the highest frequency in ideal (noise free) ECG signal and σ is the dispersion, used to modify the wavelets shape. In our experiment we used $\alpha = 200 \cdot \pi$, $\beta = -1/3$. The WT depends upon two parameters, scale s and position τ. The dyadic wavelet is determined using a scale $s = 2^j$, where $j \in Z$ and Z is the integral set. The WT (Eqs. (2.4), (2.5) at scale $s = 2^j$ is obtained by:

$$Wf(2^j,\tau) = \frac{1}{2^j} \cdot \int_{-\infty}^{\infty} f(t) \cdot \Psi^*(\frac{t-\tau}{2^j}) dt \,. \tag{2.6}$$

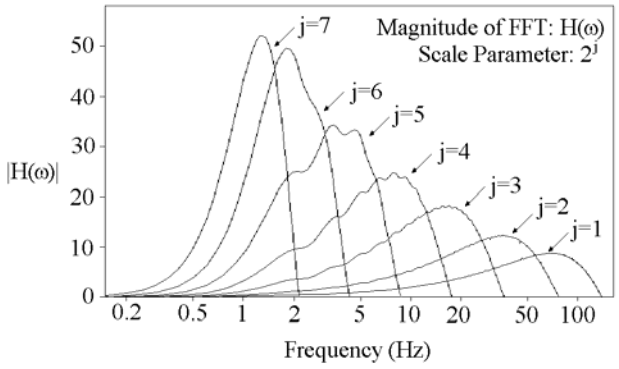

Fig. 2.6. Fourier transform of wavelets at different scales.

Table II.1. The wavelets frequency response at various scales *s*.

Scale *s*	Lower 3dB Frequency [Hz]	Higher 3dB Frequency [Hz]
2^1	35.8	99.1
2^2	17.8	54.4
2^3	8.0	23.8
2^4	4.2	12.3
2^5	1.86	6.09
2^6	1.25	2.92
2^7	0.89	1.67

Fig. 2.6. illustrates the Fourier transform of the wavelets at different scales $s = 2^j$ (Eq. (2.6)), and their 3-dB band-widths are listed in Table II.1.

2.4.2. Support vector machine learning

The problem of learning SVM (Vapnik, 1998) is formulated as a task of separating learning vectors X_i into two classes of destination values $d = +1$ or $d = -1$, using maximal possible separation margin, that allows a high robustness to the obtained solution. The maximization task of function $Q(\alpha)$ is defined in (Smola *et al.*, 1998) and (Burges, 2000) as follows:

$$Q(\alpha) = \sum_{i=-p}^{p} \alpha_i - \tfrac{1}{2} \cdot \sum_{i=-p}^{p} \sum_{j=-p}^{p} \alpha_i \cdot \alpha_j \cdot d_i \cdot d_j \cdot K(x_i \cdot x_j), \tag{2.7}$$

with linear constraints $\sum_{i=-p}^{p} \alpha_i \cdot d_i = 0$, where $0 \le \alpha_i \le C$. The α values are Lagrange multipliers, and function *K* represents the kernel, *p* is the number of learning pairs and *C* is a user defined constant (in our study *C* was selected between 0.1 and 0.5). In this case we applied radial Gaussian kernel function. The output signal $y(x)$ of the SVM network in retrieval mode (after learning) is determined as the combination of kernels

$$y(x) = \sum_{i=1}^{N_{SV}} \alpha_{SVi} \cdot d_i \cdot K(x_{SVi} \cdot x) + w_{opt}, \tag{2.8}$$

where N_{SV} is the number of support vectors and w_{opt} is the optimal weight vector. Although SVM separates the data into two classes, the recognition of more ones is straightforward by applying either 'one against one' or 'one against all' methods (Crammer *et al.*, 2000).

2.4.3. Unified neural networks

If we focus on the two-class classification case and consider linear discriminant functions, the respective decision hypersurface in the *n*-dimensional feature space is a hyperplane, that can be described as:

$$g(x) = w^T \cdot x + w_0 = 0, \tag{2.9}$$

where $w = [w_1, ..., w_n]^T$ is known as the weight vector and w_0 as the threshold value. For a given vector x_d, if the function $g(x_d) = 0$ then is x_d situated on the decision hyperplane. The distance z of a vector x from the decision hyperplane can be computed as: $z = |g(x)| / \|w\|$, where $\|w\| = \left(\sum_{i=1}^{n} w_i^2 \right)^{1/2}$. In a classification problem, our purpose is the optimization of vector w in such a way, that the criteria function $J(w)$ is minimized. Let ω_1 and ω_2 be the two classes that we need to separate. We assume this task can be performed using a linear relation. This means that there exists at least one such w_{sol} hyperplane that fulfils the following relations:

$$\begin{aligned} {w_{sol}}^T \cdot x > 0 \ \text{ for } \ \forall x \in \omega_1 \\ {w_{sol}}^T \cdot x < 0 \ \text{ for } \ \forall x \in \omega_2 . \end{aligned} \tag{2.10}$$

If we design a classifier, where the desired output is $y_{des} = +1$ for $\forall x \in \omega_1$ and $y_{des} = -1$ for $\forall x \in \omega_2$, and try to modify weights in vector w in such a way that the criteria function

$$J(w) = \sum_{i=1}^{N} (y_{des,i} - f_s(w^T \cdot x_i))^2 \tag{2.11}$$

is minimized, then we have constructed a root mean square (RMS) error based separator method. In the previous formula, f_s denotes a sigmoid function.

The SVM-s based classifier algorithms are very popular due their robustness. The main concept incorporates the search for the 'most robust solution' vector w_{sol} that gives the maximum possible margin. The margin is represented by the minimal distance $z = |g(x)|/\|w\|$. This means the minimization of $\|w\|$.

Although both these methods, the traditional RMSE approximation and SVM-based classification, deliver good results in a certain noise-free environment, in biomedical simulation such sterile conditions never occur, mainly because of measurement errors and the improper estimation of unmeasurable biological parameters.

The root mean square classifiers have the following drawbacks:

- Improper solution in case of asymmetric transfer functions;
- Large estimation error of the criteria function in case of border-close high dispersion (uncertain) inputs;
- In a noisy environment, the criteria function may possess multiple local minimal solutions that may cause low quality results;
- The white noise is 'un-learnable' so the function $J(w)$ will saturate at an uncontrollable error level.

The SVM produces a considerably superior result in hostile environment, and can avoid the above mentioned problems, but fails to take into consideration the topology of the input vectors, as presented in Fig. 2.7.(a). This topology becomes more important is case of multi-dimensional spaces and non-linear separation borders, than in case of linear separation in a two dimensional space.

To overcome the above mentioned problems for both presented classification metods, we propose for classification a UNN. The main difference between UNN and the described classifiers consists in the equation of its criteria function:

$$J(w) = \lambda_d \cdot \sum_{i=1}^{N} (y_{des,i} - f_s(w^T \cdot x_i))^2 + \lambda_m f_m(z) + \lambda_u \cdot \sum_{i=1}^{N} f_u(w^T \cdot x_i), \tag{2.12}$$

that is composed by three additive terms responsible for the difference error, margin and smoothness, respectively. The function $f_u(\alpha) = \alpha^{-2}$ represents a repelling force that doesn't let the boundary be close to any of the vectors x_i. Coefficients λ_d, λ_m, λ_u adjust the tradeoff among these three terms. The margin value is represented by *z*.

The presented UNN can work in non-linear environment, too. In this case the distance of a point from the separation hyperstructure is considered the closest distance from any point of it. The SVM formulation can work in the same manner, the structure tries to have a shape that keeps maximal distance from the clusters elements. The third term forces the separation structure to places that suffer from minimal repelling force.

The non-linear form of the criteria function takes into consideration the topology of the separation hyperstructure as presented in Figure 2.7.(b). For example, the two closest × and • have the same distance from the non-linear separation barrier, but the × has better topology (the adjacent calculated distances are shorter for × than for the • point) so is considered closer than the • point.

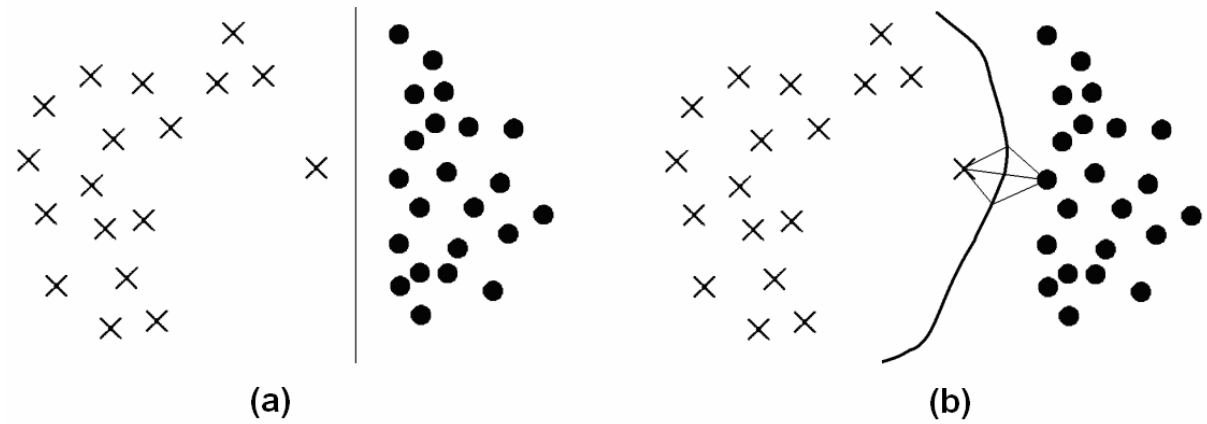

Fig. 2.7. A two-class separation problem: (a) linear separation performed by SVM-based classifier cannot yield optimal solution in all cases; (b) distance of an object from the non-linear separation barrier should depend on the topology of the classes

2.5. General presentation of processing

2.5.1. The processed ECG records

In our investigation we have focused on the evaluation of own measurements (sampled at 200-500Hz with 12-bit resolution), but to allow a good comparability of the algorithm with other works we applied our processing on the well-known MIT-BIH arrhythmia database too (sampled at 360Hz with 11-bit resolution). Most of these files contain one or two channels, but numerous registrations have 12 leads. The performance of the processing method is complex and was determined by the number of estimation parameters, estimation error, robustness of the solution, stability criteria, diagnostic performance, smoothing strength, applied resolution and sampling rate.

As initial information the processing algorithm had only a basic (short) template bank and in time of usage, a patient-specific classifier was created without human supervision. At the learning phase, to allow significant performance improvement, we applied a maximum 1-3 minute manually processed ECG record.

2.5.2. The structure of the processing algorithm

In a conventional physiologist-based ECG signal evaluation a pre-filtered signal is directly used to perform diagnosis. As not every physiologist is an ECG expert they may need to perform a computer aided diagnosis. The short presentation of this methodology is presented in Fig. 2.8.

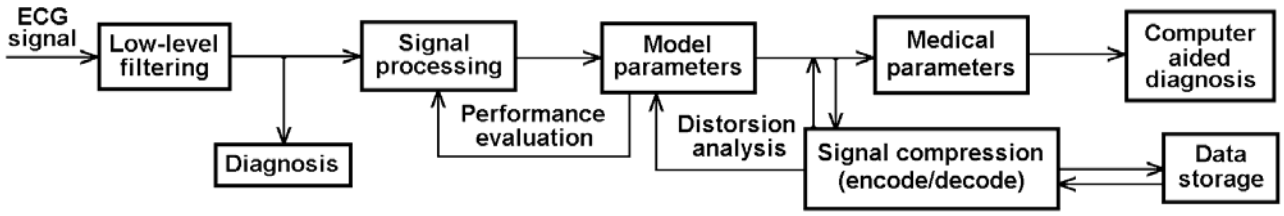

Fig. 2.8. A brief scheme of the conventional and computer aided diagnosis

As Fig. 2.8. presents, the measured ECG signal is pre-filtered using simple band-pass schemes or analogue solutions. These filtered signals are the input parameters of a conventional diagnosis.

However these samples may contain several artifacts that can alter the reliability of such a process. The computer-aided diagnosis can help a non ECG expert physician to take more reliable diagnosis.

To perform a computer-aided diagnosis the pre-filtered signal is processed in order to determine the model parameters. The iterative evaluation of the model may force to effectuate the processing step more times. After the model parameters are determined the computer can calculate medical parameters. These results are well-known for physicians and all conventional diagnostic method is created as a decision-tree using the obtained medical parameters. In case of signal compression a distortion analysis is performed to verify the diagnostic usefulness of the encoded-decoded signal. A complex ECG signal filtering method must take into consideration to biological formulation of the studied signal. This means the usage of some a priori information about various waveforms, the adaptive behavior to handle patient-dependent data and a capability to efficiently separate the measured artifact from the useful signal. This style of planning demands a three-layer filtering, as presented in Figure 2.9.

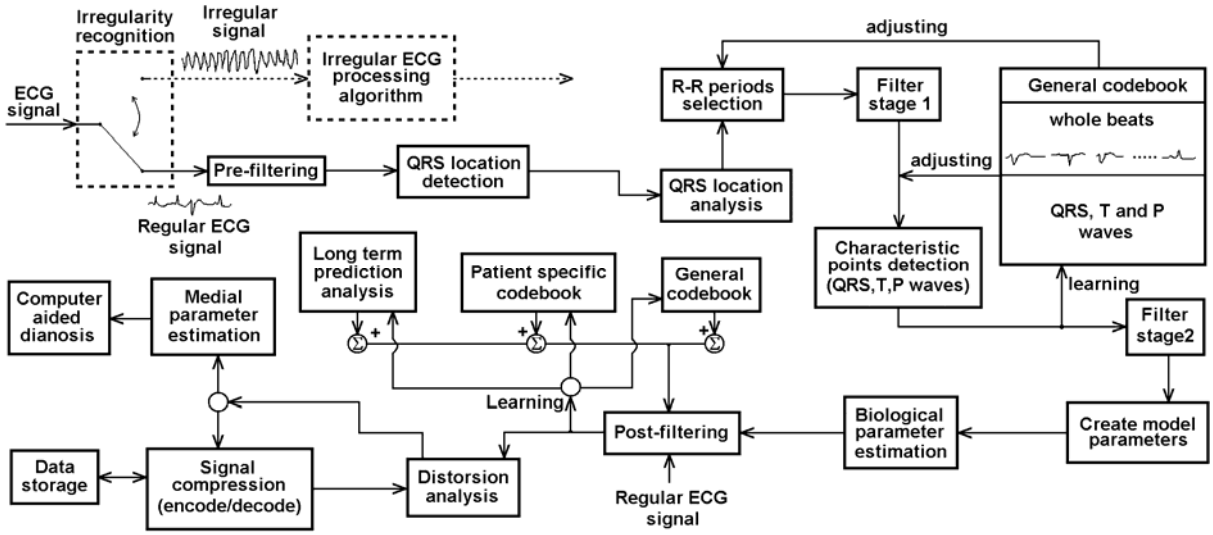

Fig. 2.9. A detailed scheme of computer aided ECG processing, diagnosis, and efficient data storage

The two major tasks in ECG signal processing is parameter extraction to perform automated diagnosis and efficient data storage (Zigel *et al.*, 2000b). As both tasks are based on proper parameter estimation and efficient signal reconstruction their main steps are common (see Figure 2.9.). As Figure 2.9. shows, the first step of ECG signal processing is related to a coarse classification of the recorded data as regular or irregular. If a segment of signal is considered too noisy or manifest uncommon shape it is considered irregular. Such an irregular data did not contain any estimable biological information, so medical parameters cannot achieve any advantage. This property of the data inhibits the usage of model based processing and encoding. Conventional voice processing methods may be used to encode-store-decode the recorded data.

A regular ECG signal contains the main characteristics such as QRS beats, base-line and other waves. The semi-periodic behavior of the ECG implies for every few second long data sequence to contain at least one R-R period that may be most easily recognize by looking for QRS beats. A pre-filtering step has the task to enlighten the selection of the QRS beats.

After a pre-filtering step the recognition of each QRS beat can be done easily. However the exact place of such beats is quite important during further analysis. It may appear one-two second long perturbations that can pass the first irregularity test but can hide few valid QRS beats. If sophisticated shape analysis methods cannot determine the place of these disturbed waves we can get erroneous results. In such cases a logical selection of valid R-R segment separator QRS beats is essential. To perform this step we must apply some biological parameter analysis, such as R-R distance.

Once correct R-R distances are determined and the perturbed data segments are marked, the recorded signal is ready to perform a completely new filtering based on QRS periods. The main idea lays in a logical consideration that supposes a much higher noise tolerance of the QRS beats than other waveforms due to its higher amplitude.

In Fig. 2.9., the filter stage 1 step is totally based on R-R segmented ECG signal. The resulting signal may be included in the general codebook during a learning step. This codebook contains whole beats, QRS, T and P beats. The existence of a huge amount of a-priori waveform family in the general codebook is essential, otherwise the waveform recognition step cannot be performed with acceptable accuracy. In case of beat shape miss (the studied beat cannot be found in the codebook) the R-R periods selection may be revised.

The output of the first filtering step may be adjusted using whole beats information from the general codebook. This could be important in case of abrupt baseline movement. After the adjusting step from general codebook the recognition of various characteristic waveforms, such as QRS beats, T, P waves is effectuated.

As all important waves are recognized the recorded ECG may be filtered using all known medical information. This kind of filtering is performed in filter stage 2. The output of this filtering step may be used to create the model parameters. These parameters can be used to obtain some biological parameters that are well-known by physiologists.

Using the obtained biological parameters and the original ECG signal a post-filtering step is performed. This step uses the general codebook, the patient specific codebook and a long term prediction analysis. This long term prediction supposes that the consecutive QRS beats are much similar than any average beats. Logically this consideration is only true if the prediction is applied for the same type of beat. For example a normal, followed by a ventricular beat may differ completely.

During a learning process the output of the post-filtered signal may be used to adjust the patient specific codebook and the long term prediction. Another important task is the distortion analysis of the filtered signal. In case of uncompressed signal this kind of analysis is obsolete, but the usage of a relatively high compression rate signal compacter method implies advanced distortion analysis. A high distortional coefficient may cause wrong medical parameter estimation that may cause erroneous computerized diagnosis. This consideration is also true if the signal is compressed but the diagnosis is performed by physicians. A relatively low alteration of the S-T segment may cause false S-T elevation or depression which is a typical characteristic of the heart infarct.

The proposed complex ECG signal compression algorithm can be divided into the following steps:

- Irregular signal recognition and processing;
- Pre-filtering;
- Segmentation into R-R intervals;
- R-R period based filtering;
- Create/update a temporal template bank for whole beats;
- Determine all recognizable characteristic points (for R, T and P waves);
- R, T and P wave location based filtering;
- Extract the waveform estimation model's parameters;
- Biological parameter estimation;
- Perform a post-filtering using pattern database and the model-based estimation;
- Complete the general and patient specific template bank for all recognized waves;
- Adjust long term prediction;

- Adaptive smoothing and advanced distortion analysis;
- Residual signal estimation, entropy coding, data storage and back-estimation;
- Medical parameter estimation and computer aided diagnosis.

2.5.3. Irregular signal recognition and processing

A regular ECG signal possesses a quasi-periodical behavior. The main redundancies in the signal exist in the form of correlation among consecutive beats (inter-beat correlation) and correlation between adjacent samples (intra-beat correlation) (Nave *et al.*, 1993). The high inter-beat correlation suggests the usefulness of the long term prediction (LTP). The frequent appearance of abnormal beats implies the usage of a wave codebook, containing the most typical forms.

The intra-beat correlation is parlayed by a short term prediction (STP). Such estimation may not use any biologic-related information, only general signal estimation models (for example a short term prediction works in the same manner in case of ECG, EEG or recorded sound).

An ECG sequence is considered regular if it contains the PQRST characteristic points. The most important task is to identify due to its high amplitude the QRS wave. If a signal sequence did not contain the QRS, the LTP cannot be applied. These signals are classified irregular which may be measured in case of ventricular fibrillation (VF), ventricular tachycardia (VT) or heavily noise polluted signal. The algorithm of irregular signal detection and compression is described in paper (Zigel, 1998).

2.5.4. Elimination of the electric noise

If a signal sequence contains regularly occurring QRS beats that have similar shape, the LTP is usable, and the studied data is considered regular. However a regular signal by far not means a directly processed one. Before recognizing the characteristic waveforms (R, T and P waves) of the ECG and performing an accurate segmentation, we need to pre-filter the signal in order to eliminate all perturbing phenomena, like noise caused by the electrical network, the perturbing artifacts caused by bad contacts, motion or breathing.

The elimination of the noise caused by the electrical network is recommended by windowed FFT and IFFT combined with a parameter estimator and filter, which contains the following steps:

- Perform a windowed FFT for an interval of length between five and twenty seconds. All intervals are overlapped by at least fifty percent of their length;
- Estimate the amplitude and phase of the 50 (60) Hz component and its higher harmonics from the amplitudes and phases of the adjacent frequencies;
- Modify the signal spectra;
- Process the IFFT algorithm;
- The final step of pre-filter module is performed by a regressive method to eliminate the artificial noise caused by modifications in the signal's spectra.

In our approach, because the studied signal has a non-linear behaviour, we define a non-linear adaptive estimation algorithm. The main drawback of this method is the cumbersomeness to determine the optimal phase of the 50 (60) Hz component of the measured ECG signal. Details on how to handle this problem are presented in (Szilágyi *et al.*, 2003b).

A similar solution considers that although the phase appraisement is hard and much more sensitive to perturbations than amplitude estimation, the presented phase assessment method solves this task. The basic idea starts from the considerations that the electrical noise frequency overlaps with the ECG,

and the amplitude and phase of the real biological signal cannot vary too fast with a slight modification of the frequency (all biological signals have relatively smooth modification of the amplitude and phase along the signal's spectra). The amplitude and phase of the measured signal determined at 50 (60) Hz frequency involves the electric noise and the real ECG components.

Let A_{EN}^{1} be the amplitude of the first harmonic of the electrical noise, along a window of $N = 2\delta + 1$ sample width, situated symmetrically around the sample at position ξ. Such a chosen window implies that the sum of the sine components is zero. Applied the same conditions the sum of the cosine components will be a nonzero value. To allow a zero sum for both components, we must shift the window with one position to left and right, respectively. Theoretically, from two vectors we could be able to determine the cosine component, but to reach higher precision, we should use both shifted windows. The amplitude for *i*-th harmonic is given by:

$$A_{EN}^{i} = \frac{1}{N} \cdot \sum_{k=-\delta}^{\delta} X(\xi + k) \cdot \sin\left(2\pi \cdot \frac{f_{EN,i}}{f_s} \cdot k \right), \tag{2.13}$$

where $f_{EN,i}$ represents the frequency of the i-th harmonic of the electrical noise and f_s is the sampling rate. To determine the estimated amplitude and phase for *i*-th harmonic, we must choose two from the three vectors. The selection highly depends on the angles between these vectors (the angle between the projection of the selected two vectors must be maximal for the most robust estimation). Fig. 2.10. visualizes the determination process of the amplitude and phase for a higher harmonic. After obtaining the amplitude and phase of electric noise we made an averaging process that minimizes the abrupt leap of the phase by the following relation:

$$J(A_{EN}^{i}) = \sum_{i=1}^{k} c_i \cdot \varphi(A_{EN}^{i}), \tag{2.14}$$

where *J* is the criteria function, *i* represents the harmonic, c_i is a harmonic dependent coefficient, and φ represents the phase of a given harmonic.

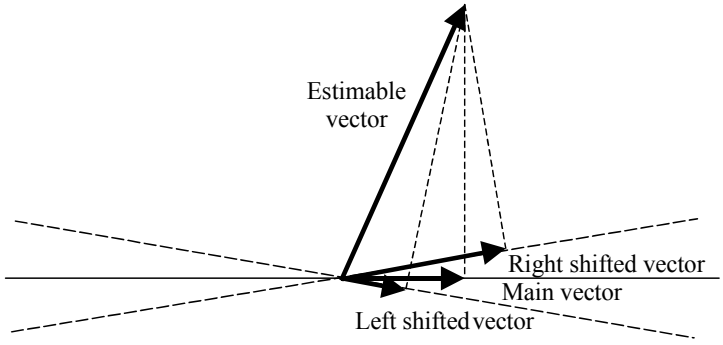

Fig. 2.10. The estimable vector can be determined more exact if the angle between orthogonal projections of the selected vectors is higher (always less than π).

2.5.5. Oversampling as a low-pass filter

Let be $F_{sampl.}$ the applied sampling rate, and $F_{max.}$ the maximal achievable rate. In this case exists a number $q \le F_{max.} / F_{sampl.}$ that can be applied as an oversampling value. Let be $X(n)$ the *n*-th measured value. If an oversampling is applied, the measured value $X(n)$ can be determined by the relation: $X(n) = q^{-1} \sum_{i=1}^{q} X_{meas.}(n,i)$. A big deficiency of this approximation consists in the immission of the wrong measured values in the final calculation. Such an equipartition weighting may cause altered estimated values. An important issue is the usage of the most probable values in

measured level estimation. This means a non-linear weighting of the measured samples. Let be $X_{meas.}(n) = \{X_{meas.}(n,1),..,X_{meas.}(n,q)\}$ a set of measured values. The oversampling number q limit the size of set $X_{meas.}(n)$. Each element of this set possesses a probability value that can be determined by the mean value and dispersion. In our consideration these samples obey a Gauss distribution. The relatively low level of q (much lower than 100) inhibits the calculation of the real distribution of the measured samples. Using a dispersion

$$\sigma(n) = \sqrt{\frac{1}{X(n)^2}\sum_{i=1}^{q}\left(X_{meas.}(n,i) - X(n)\right)^2}\,, \tag{2.15}$$

and a mean value $X(n) = q^{-1}\sum_{i=1}^{q} X_{measured}(n,i)$, the probabilities of each measured value $p(X_{meas.}(n,i))$ is calculated. Starting from these probability levels, the estimated value $\widetilde{X}(n)$ can be determined using the relation

$$\widetilde{X}(n) = \frac{\sum_{i=1}^{q} p(X_{meas.}(n,i)) \cdot X_{meas.}(n,i)}{\sum_{i=1}^{q} p(X_{meas.}(n,i))}. \tag{2.16}$$

The so obtained value is considered the measured value. In this case this process behaves as a low-pass filter with $F_{upper}(n) = F_{sampl.}/2$.

2.5.6. IIR filters to eliminate wrong values

In numerous situations it is not possible to use a high oversampling value. In this case in the measured signal may appear acicular shapes, caused by wrongly recorded values. An IIR filter allows the correction of altered values if most samples have reliable level. This kind of signal correction method uses samples recorded with a few ms delay.

Let be $X(n)$ the *n*-th measured ECG value and $Y(n)$ the output of the IIR filter. The time moment will be $t = \Delta \cdot n$, where Δ represents the sampling period. The $Y(n)$ output of the applied IIR filter will be: $Y(n) = \sum_{i=1}^{p} a(i) \cdot Y(n-i) + \sum_{i=1}^{p} b(j) \cdot X(n-j)$, where the **a** and **b** vectors determine the filter characteristics and values *p* and *q* regulates the power. With a proper adjustment of the *p*, *q*, **a**, **b** values the aimed filtering can be performed.

Usually the ECG signal contains much low level noise that perturbs the adjacent beats. This event limits the useful power of the IIR filter. Using a regular ECG recording the optimal value of *p* and *q* is under 10. The **a** and **b** vector elements are considered in the interval (-2, 2).

2.5.7. The description of pre-filtering

2.5.7.1. The importance of pre-filtering

The most important task of pre-filtering is the transformation of the measured signal in an easily processable format. Its importance consists in making able the computer to correctly determine various events that appear in the recorded signal. This task can be accomplished by using a pre-filter process that can recognize and eliminate various artifacts, otherwise the processed signals characteristic may be altered that can degenerate to wrong diagnosis.

2.5.7.2. The structure of pre-filtering process

The principal role of the pre-filtering is to enlighten the precise localization of the QRS beats. In most standard leads the detection of the QRS beat can be realized by the localization of the R peak (positive or negative). The proposed pre-filtering algorithm contains the following procedures:

- Spectral band filtering (to separate the non-ECG related low and high frequency components);
- The elimination of the wrongly measured samples (see oversampling and IIR-based filtering);
- The elimination of artifacts caused by electric network;
- Separation of other kind of artifacts from useful signal;
- Elimination of internal noises by a whitening filter.

Due to the various disturbing phenomena, the ECG measuring procedure must obey some rules that allow the possibility to separate most artifacts from the signal. The most important parameters that influence the measured ECG signal are:

- The level and nature of the recorded artifacts during measurement;
- The accuracy and sampling frequency.

The proper sampling accuracy is important, otherwise the fine characteristics of the signal remains hidden. A relatively high sampling rate is necessary to visualize the dynamics of the signal. If the measuring circumstances allows it is important to use an oversampling that can help to eliminate acicular artifacts. A band-pass filter allows the separation of high frequency peaks from the useful signal. Unfortunately the low frequency artifact components partially overlap with the useful signal. The separation of these data cannot be realized with low-pass filtering.

An opportunity to eliminate the artifacts from the recorded signal is by using whitening filters (Xue *et al.*, 1992). These filters estimates the colored noise but not biological waves, such as QRS beat. As the filter names suggest, the whitening filter transforms all recognized colored noise to white noise. Due to the low amplitude of T and P waves, these waves are considered colored noise, so the filter eliminates them. After the whitening process is performed the output signal contains white noise and regular QRS beats. The obtained data can be processed with transform-based methods, like Wavelets, regression (non-linear methods) and stochastic algorithms (unified neural networks, hidden Markov models). A proper recognition of the QRS waves enlightens the segmentation of the ECG signal.

2.5.8. Approximation function set

After the electric noise and acicular values are eliminated, it is possible to estimate the signal's value at a certain time. The separation of high frequency noise using non-linear parameter estimation methods generally provides higher performance than applying transformation methods. In our approach, due to the non-linear behaviour of the studied signal, we applied a non-linear adaptive estimation algorithm. This approximation is based on a set S of basic estimation functions that usually are non-linear and can be parameterized by some certain values. In the under-mentioned and incomplete set S, we describe some basic approximation functions, where q^{-1} represents one sample period long dead time, α , a and b are internal parameters such that $a^2 + b^2 = 1$ (see Eq. (2.17)).

$$S(X) = \left\{ \begin{array}{c} f_1(X) = X; f_2(X) = \frac{1}{N_2} \cdot X^2; f_3(X) = \frac{1}{N_3} \cdot X \cdot \left(X \cdot q^{-1}\right), \\ f_4(X) = \frac{1}{N_4} \cdot \sqrt{X}; f_5(X) = \frac{1}{N_5} \cdot e^{\alpha \cdot X}; f_6(X) = \frac{1}{N_6} \cdot e^{\alpha \cdot \left(a \cdot X - b \cdot \left(X \cdot q^{-1}\right)\right)}; \ldots \end{array} \right\}. \qquad (2.17)$$

2.5.9. Estimation of the ECG signal

In high frequency noise elimination, the non-linear parameter estimation methods could reach better performance than transformation methods.

Let $\hat{X}_L(n)$ and $\hat{X}_R(n)$ the *n*-th left and right aimed estimation, defined as:

$$\hat{X}_L(n) = p_L \cdot \widetilde{X}_L(n) = p_L \sum_{i=-q}^{q} a_{L,i} X(n-i) + (1-p_L) \sum_{i=1}^{q} b_{L,i} \hat{X}_L(n-i), \tag{2.18}$$

$$\hat{X}_R(n) = p_R \cdot \widetilde{X}_R(n) = p_R \sum_{i=-q}^{q} a_{R,i} X(n-i) + (1-p_R) \sum_{i=1}^{q} b_{R,i} \hat{X}_R(n+i), \tag{2.19}$$

where $a_{L,i}$, $a_{R,i}$, $b_{L,i}$ and $b_{R,i}$ are prediction coefficients, p_L and p_R are balance probabilities determined by the dispersions $\sigma_{\hat{X}_L - X}(n,l)$, $\sigma_{\hat{X}_R - X}(n,l)$, $\sigma_{\widetilde{X}_L - X}(n,l)$ and $\sigma_{\widetilde{X}_R - X}(n,l)$. For better separation of the signal from the noise, the length *l* should select more than one R-R period. During on-line processing, the estimation is delayed with at least $3 \cdot q$ samples, but preferably with more than one R-R interval, in order to minimize the differences of the efficiency between $\hat{X}_L(n)$ and $\hat{X}_R(n)$; $(p_L + p_R = 1)$. The resulting sample $\hat{X}(n)$ is obtained by the following formula:

$$\hat{X}(n) = p \sum_{i=-q}^{q} a_i \hat{X}_L(n-i) + (1-p) \sum_{i=-q}^{q} b_i \hat{X}_R(n-i). \tag{2.20}$$

2.5.10. Segmentation into R-R intervals

A segmentation process of the recorded ECG into R-R intervals has three important parts:

- Locate the possible QRS beats using direct, transformation or regression method (in this study a Wavelet-based transformation method is used)
- Analyze the location of the recognized beats
- Selection of the R-R periods

2.5.10.1. Recognition of QRS beats using Wavelet-transform

In a heavily noise tainted environment, a parameter extraction model could be less robust, than a good transformation algorithm. One of the best transformation methods for R wave detection uses wavelets. The selected mother wavelet is:

$$\Psi(t) = \frac{1}{\sqrt{2\pi}\sigma} \cdot \exp\left(-\frac{t^2}{2\sigma}\right) \cdot \sin(\alpha \cdot t \cdot \exp(-\beta|t|)). \tag{2.21}$$

The parameters α and β are selected according to the highest frequency in ideal (noise free) ECG signal, and σ is the dispersion, used to modify the wavelet's shape.

After the analysis of more than 100 recordings, we obtained as a good robust result $\alpha = 200 \cdot \pi$ and $\beta = 1/3$. The robustness in this step is far more important, than a local performing index. The WT depends upon two parameters, scale *s* and position τ.

The dyadic wavelet is determined by a scale $s = 2^j$ with integer *j*. The wavelet transform at scale $s = 2^j$ is obtained by:

$$Wf(2^j,\tau) = \frac{1}{2^j} \cdot \int_{-\infty}^{\infty} f(t) \cdot \Psi^*(\frac{t-\tau}{2^j}) dt \,. \tag{2.22}$$

Experiments show that this kind of wavelet allows the creation of more robust algorithms than using conventional ones. This property is due to the sinusoidal term, which can realize a correlation not only with the adjacent beats (the ECG signal is more or less semi-periodical).

2.5.10.2. Validation of the obtained QRS positions

After the location of the QRS beats is obtained a biologic-parameter-based analysis is performed. There are numerous biological aspects, such as possible R-R distance, frequency and rhythm analysis.

In some circumstances the measured T wave may be as high as the R beat. In this case the unique separation possibility is the morphological analysis of the wave. Each wave at each standard measuring lead has a well-known generic form. Using this aspect of waves we can eliminate the T wave caused false positives even if it contains almost the same frequency components.
The main biological aspects that are studied during the beat location validation process are:

- Distance from adjacent beats
- Shape of beat
- Rhythm analysis aspects (this information is well-presented in any cardiology handbook)
- R-R period variance in function of beats shape (the possible variance margins are QRS beat shape dependent)

2.5.11. Build up or update the temporal template bank

2.5.11.1. QRS location specific filtering

The template banks build or update, and even a comparison is preceded by the filter stage one (see Fig. 2.9.). The principal role of this procedure is to exploit the information obtained from the preliminary localized beats. Previous filters, such as the pre-filtering step has no information about the quasi-periodicity of the ECG. Using the shape, size and location of each QRS beat it become possible to handle much easier the recoded artifact and noise. A noise perturbed ECG segment may cause the pollution of the template bank with un-proper results that cause slower speed and limited performance.

2.5.11.2. ECG segment clustering

Largely the signal's power is included in the QRS beats, so a template collection is essential. During signal processing, the pre-constructed wave database should be alterable. Although automated waveform classification based on a decision-tree algorithm could produce remarkable results, the new self-organizing (SO) adaptive clustering (Smola *et al.*, 1998) based method has several advantages:

- It is not susceptible to variations of beat morphology and temporal characteristics;
- It can perform a real-time unsupervised learning;
- It needs much less amount of knowledge for the same performance.

The clusters (see Fig. 2.11.) are built up according to the following rules:

- $\sigma_i \leq \sigma_{Max}$; σ_{Max} is predetermined; i=0..n;

- The mean value of a cluster is M_i and is determined in such a way, that σ_i to be minimal;
- For every R (T and P) wave, which belongs to a cluster, $\|X\| = \sum_{i=0}^{N} \left((X_i - M_i)/\sigma_i\right)^2 \le R_{MAX}$ where R_{MAX} is predetermined; X is a vector, representing a wave in the space;
- X may belong to more cluster;
- The total number of the clusters for a predetermined R_{MAX} is minimized.

Each waveform in the template bank is represented by 8 characteristic points that were selected using a shape estimation error minimization process. The indicator vector of each waveform is represented as $\overline{X}^t = (p_0(X),..., p_{n-1}(X))$ where n is the number of clusters and $p_I(X)$ is the probability that X belongs to the cluster C_I, having the value:

$$p_I(X) = \prod_{k=0}^{7} \frac{1}{\sigma_{I,k}} \exp\left(-\frac{(X_k - M_{I,k})^2}{2\sigma_{I,k}} \right). \tag{2.23}$$

The clustering process must work properly even if the studied patient manifests abnormal QRS wave patterns. To assure this, the main database must contain the most specific abnormal waveforms that are patient-free. It case of heavily patient dependent waveforms, such as ectopic beats, the studied waveforms are collected and included in a new, patient dependent cluster. These clusters are representative only for a patient but not for a larger group.

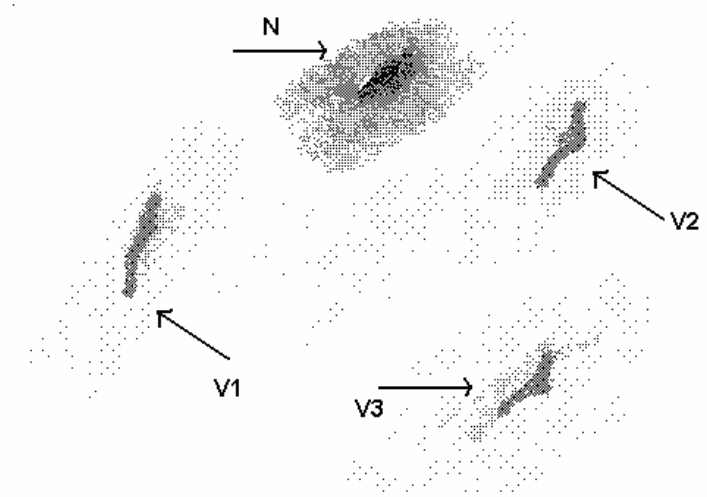

Fig. 2.11. Representation of various beat forms: the normal QRS beats are represented by N, and three different ventricular extra beats are represented by V1, V2 and V3 in plain representation (the calculation space of the regressive model had 32 dimensions and among them the two most significant were selected).

2.5.12. Optimal filtering using general QRS wave pattern database

The optimal filter is based on the pre-processed signal and the template bank. Let

$$\overline{X}(n) = \sum_{k=0}^{nr-1} \left(s_k \cdot \sum_{i=-q}^{q} a_{F,i} \cdot f_k(X(n-i)) \right), \tag{2.24}$$

and

$$\widetilde{X}(n) = p_{F,X-\widetilde{X}}(n) \cdot \overline{X}(n) + (1 - p_{F,X-\widetilde{X}}(n)) \cdot \sum_{i=-q}^{q} b_i B(m,i), \tag{2.25}$$

be the processed data. The low value of p_F ($p_F < 0.2$) justifies the need of the collection B, whose m-th element has the maximal correlation value with $\overline{X}(n)$. The characteristic point localizer algorithm is performed in a similar way to the template bank building method. An important difference consists in the appliance manner of pre-filtered data. Firstly, the template bank is created for every recognizable event. With the aid of pre-filtered data, we could minimize the isoelectric line movement caused problem. In the case of fast isoelectric line movement the shape of the waves can be deteriorated. The separation in clusters can hide low level deformations the deteriorated samples are correctly included in the template bank. In case of high electric line movement velocity, we will re-estimate the isoelectric line and we will not include the recognized waves into the template bank.

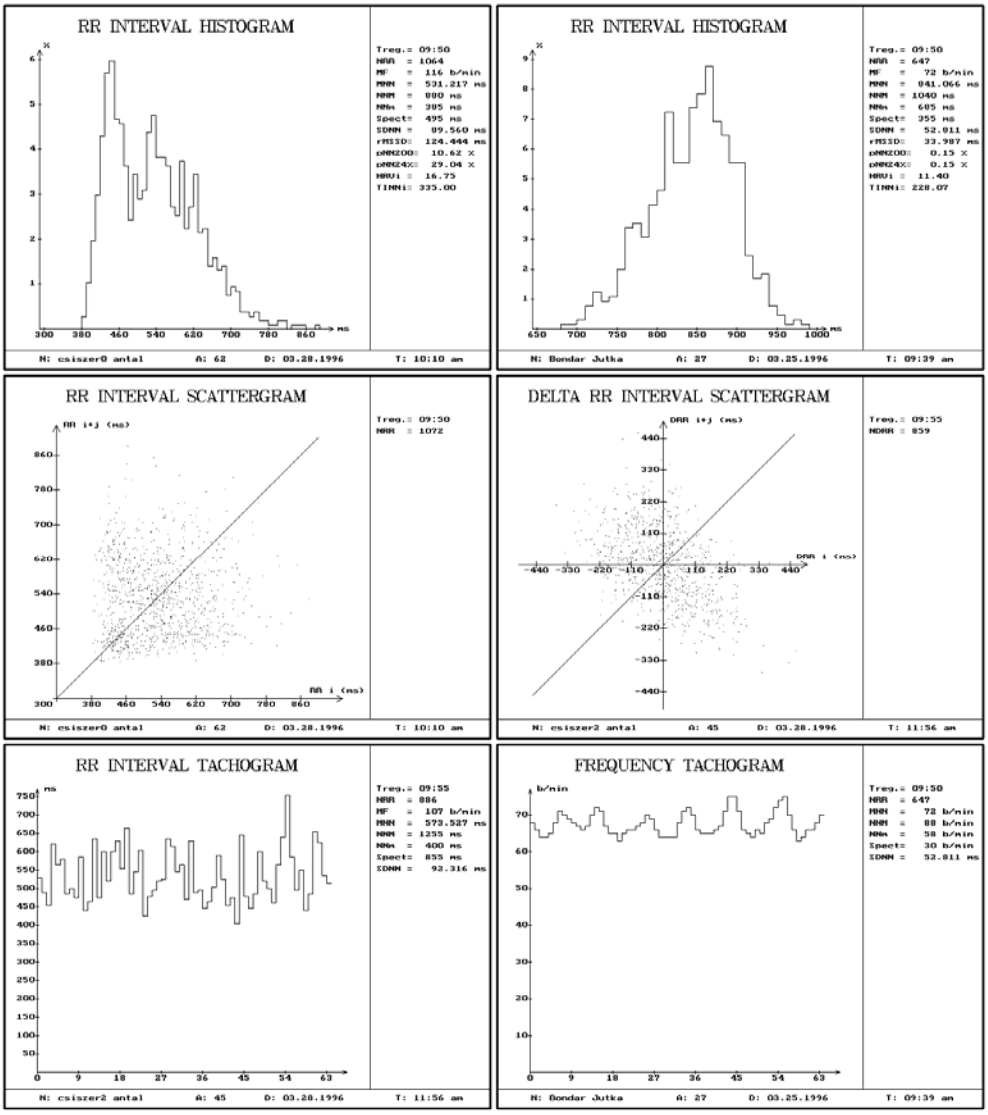

Fig. 2.12. These extracted parameters and graphic representations can help physicians to determine a treatment

2.5.13. Determine all recognizable characteristic points

The determination algorithm of the characteristic points (R, T and T waves) is similar to the template bank building method. The major difference consists in the fact that this step is applied for the pre-filtered data. In first step the template bank is realized for every recognizable event. The pre-filtered data eliminates the problem of isoelectric line movement. This fact enlightens the application of the wave recognition algorithm. The mathematical description of the problem was presented before.

2.5.14. Adaptive filtering and model parameters calculation

In this stage all inspected characteristic point is known. This additional information allows to perform a more precise filtering. This step is important, because all parametrical estimation models are heavily noise sensitive. As the model's parameters grow, the model itself become sensible. A low quality filtering decreases the number of useful parameters that establish the peak performance of the model. This study uses regressive models to estimate the signal values. Higher order estimation allows extra performance only if the recorded artifacts and noises are properly eliminated.

2.5.15. Biological parameter calculation

There are more than 100 important parameters (statistical, spectral, etc.) which can be studied during the analysis of the signal. The determination of these parameters usually need simple mathematical algorithms (statistical analysis).

The resulting values help physicians build up a diagnosis and determine the correct treatment for the patient. These parameters can reflect the effect of different medicines. Most parameters can be seen in Figure 2.12.

2.5.16. Perform a post-filter using pattern database and the model-based estimation

Such a pre-filtered and de-noised signal consist the entrance of a SVM trained ANN. This kind of formulation of learning leads to quadratic programming with linear constraints. The problem of learning SVM (Vapnik, 1998) is presented at point *A* of the materials and methods section.

After the ANN is trained, we used it to estimate the ECG as an output of a whitening filter (see Fig. 2.13.). The measured ECG near the useful signal contains various noises. For example in case of QRS detection is considered useful signal only the R wave. All artifacts and waveforms other than QRS have to be eliminated. Due to the colored nature of the usefulness signal it is necessary to proceed a whitening process using the ANN. In the presented AAN only the intermediate level in non-linear, where we used the normalized Gauss function. The input values are considered both the left and right sided values, so the output of the ANN has a *j* sample period delay.

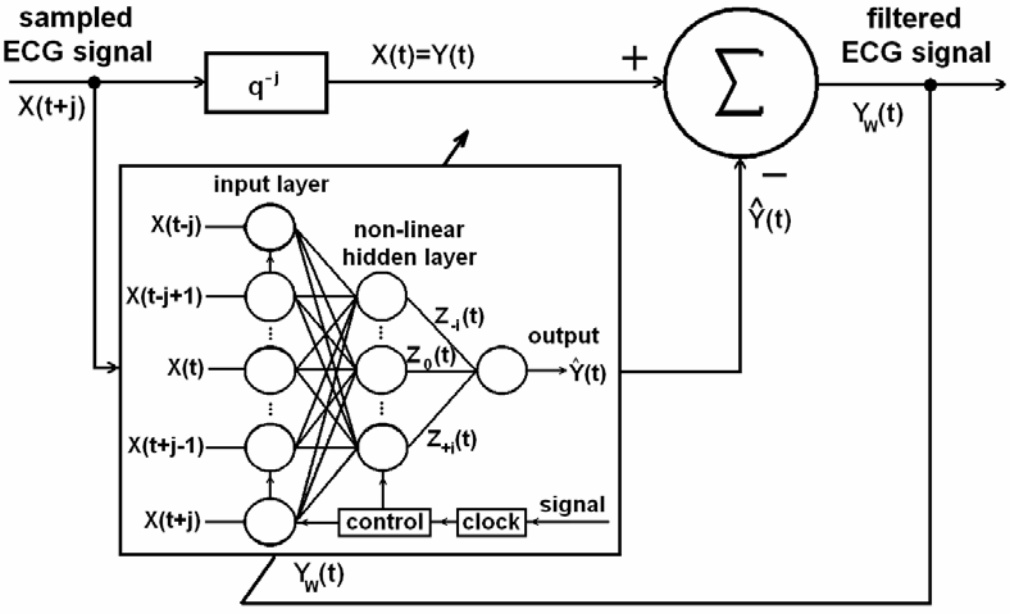

Fig. 2.13. The structure of the ANN-based adaptive filter

The non-linear intermediate result is:

$$Z_p(t) = f\left(\sum_{k=-j}^{j} c_{pk}(t) \cdot X(t+k) \right), \tag{2.26}$$

where $X_k(t) = Y(t+k)$, and $f()$ is a normalized Gauss function. The c_{pq} weight coefficients connect the input and the hidden layers. The output of the filter is:

$$Y_w(t) = Y(t) - \hat{Y}(t) = Y(t) - \sum_{p=-i}^{i} c_p(t) \cdot Z_p(t). \tag{2.27}$$

The adaptive behavior of the filter (Nave *et al.*, 1993) is assured by the permanent variance of the genetic search method based upon least mean square (LMS) algorithm computed coefficients. Both the input signal and the selected template are processed through the main filter. During this process the template bank is changing adaptively. The whitened template is:

$$T_{w,r}(t) = T(r) - \sum_{p=-i}^{i} c_p(t) \cdot f\left(\sum_{k=-j}^{j} c_{pk}(t) \cdot T(r+k) \right). \tag{2.28}$$

where *r=j,...L-j*, and *L* is the size of the template. The output of the matched filter will be:

$$Y_w(t) = \sum_{r=j}^{L-j} T_{w,r}(t) \cdot Y_w(t-L+r). \tag{2.29}$$

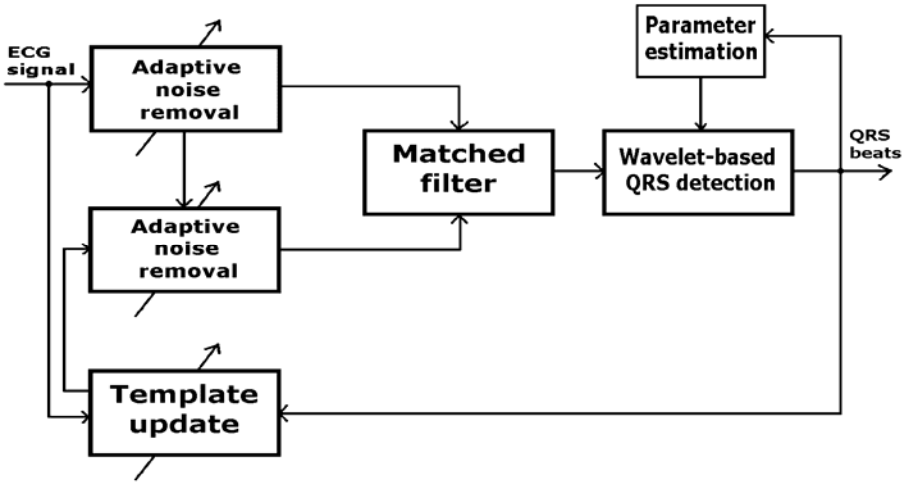

Fig. 2.14. The block diagram of ANN-based adaptive matched filter detection for QRS complexes

Finally, the $Y_m(t)$ signal is the input data for a wavelet-transform-based QRS detection algorithm. As Fig. 2.14. present, the input signal goes through an adaptive whitening filter. In each sample the input vector and template is shifted one step forward. The weights of the model are also updated by the generalized data rule. The template bank is updated only when a new QRS complex is identified. This complex has passed to the recognition part. The average template is filtered by the same adaptive noise removal filter from the neural net model synchronously with the input ECG signal. Finally, the data from the matched filter is sent to the parameterized wavelet-based QRS detection process.

2.5.17. Advanced estimation of the ECG

An ordinary ECG signal contains highly correlated periods. However all healthy patients generates a fluctuating R-R period size due to breath, sympathetic and parasympathetic stimulus. This event

encumbers the precise ECG sample estimation. An advanced signal processing method must handle properly the following cases:

- Estimate the a priori recorded samples
- On-line estimation and filtering of the measured signal
- Real time signal coding

2.5.17.1. Estimation of the a priori recorded samples

In case of a delayed processing or compacting of the signal all available resources are:

- The samples of the general codebook
- The samples of the patient specific codebook
- The whole studied record

However the signal compression step may use only prior information to the estimated sample, otherwise the signal cannot be reconstructed. Such estimation can be described by the formula:

$$\widetilde{X}(n) = p_{Sample} \cdot \hat{X}(n) + p_{GenCode} \cdot \hat{X}(n) + p_{PatientCode} \cdot \hat{X}(n) + p_{RecBeat} \cdot \hat{X}(n). \quad (2.30)$$

In Eq. (2.30) the sum of the probabilistic parameters p is equal with one: $p_{Sample} + p_{GenCode} + p_{PatientCode} + p_{RecBeat} = 1$, where p_{Sample} represents the weight of the close vicinity, $p_{GenCode}$ the weight of the general codebook, $p_{PatientCode}$ the weight of the a priori patient specific data and $p_{RecBeat}$ the weight of the highly correlating beats extracted from the whole studied measurement (excluded the studied one). The estimation of values $\hat{X}(n)$ is realized by the formula (2.20). It can be realized that from $\widetilde{X}(n)$ values the original signal cannot be reproduced, so this formula inhibit the coding of the signal, but allow the filtering of it. To realize a properly working signal coding method we must "forget" the whole studied record, and instead of it extract information from only prior $X(n)$ sample segment. The equation (2.30) can be rewritten as:

$$\widetilde{X}(n) = p_{Sample} \cdot \hat{X}(n) + p_{GenCode} \cdot \hat{X}(n) + p_{PatientCode} \cdot \hat{X}(n) + p_{EarlierBeat} \cdot \hat{X}(n). \quad (2.31)$$

The sum of parameters p obeys the relation: $p_{Sample} + p_{GenCode} + p_{PatientCode} + p_{EarlierBeat} = 1$.

2.5.17.2. On-line estimation and filtering of the measured signal

In case of an on-line processing or compacting of the signal all available resources are:

- The samples of the general codebook
- The samples of the patient specific codebook
- Earlier recorded beats

In this situation the filtering step may be delayed shortly (less than 100ms), so the filtering step may use both left and right situated adjacent samples (the signal compression must use only left-sided samples). According to prior mentioned facts the formula (2.30) will have the form:

$$\widetilde{X}(n) = p_{Sample} \cdot \hat{X}(n) + p_{GenCode} \cdot \hat{X}(n) + p_{PatientCode} \cdot \hat{X}(n) + p_{EarlierBeat+Delay} \cdot \hat{X}(n). \quad (2.32)$$

If we want to compress the signal we must use the sample estimation formula (2.32).

2.5.17.3. Real time signal coding

As mentioned earlier, Eq. (2.32) describes the calculation of the estimated signal. The above mentioned "earlier beats" can be separated into two data sets. The first one represent the collected

periods that can be used for long term prediction. These beats are analyzed with the current beat fragment, and the most correlated one is dynamically selected. The second set of data contains the "just recorded samples" that precedes the last time measured one. If we want to represent such estimation, we obtain the following formula:

$$\tilde{X}(n) = p_{Sample} \cdot \hat{X}(n) + p_{GenCode} \cdot \hat{X}(n) + p_{PatCode} \cdot \hat{X}(n) + p_{LTBeat} \cdot \hat{X}(n) + p_{STP} \cdot \sum_{i=1}^{q} p_q \cdot X(n-q). \quad (2.33)$$

The sum of parameters p and p_q fulfil: $p_{Sample} + p_{GenCode} + p_{PatCode} + p_{LTBeat} + p_{STP} = 1$ and $\sum_{i=1}^{q} p_q = 1$. The expression "LTBeat" means long-term-beat and the term "STP" represent short term prediction.

2.5.17.4. The importance of right-sided adjacent beats

As mentioned earlier the on-line filtering step may use right sided adjacent values if it is delayed with at least q samples (considering q the power of short term estimation). These left and right sided samples may have their contribution to realize a more adequate filtering. During a normal QRS beat estimation the benefic effect of the right situated samples is somehow hidden by the general and the patient specific codebook. However in a pathological case the proper estimation of a measured sample cannot be realized from general codebook elements. Moreover the patient specific codebook resolves the estimation problem partially.

2.5.18. Long term prediction of the ECG

A proper long-term estimation must take into consideration the shape of the QRS beat and the R-R period. These parameters establish a good criterion to select the most relevant periods for each new segment. This step of the processing may be effectuated real time, if the correlation among ECG segments allows it (nowadays computers admits this kind of real-time study).

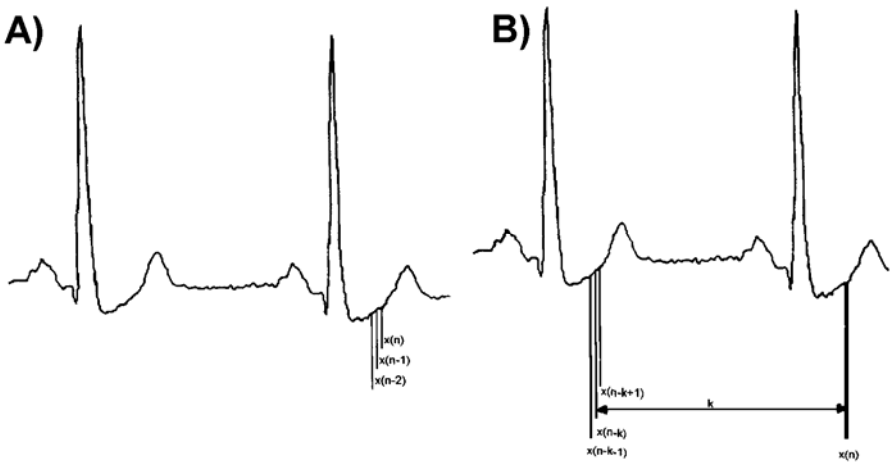

Fig. 2.15. The illustration of a short term (A) and long term (B) prediction of the ECG signal

The shape of an ECG period is determined by the shapes and timing of the constitutive waves. It is known that the R-R period influences the timing and the shape of the P and T waves (the distance from the R peak of the QRS beat). To select a mostly alike R-R period from the patient specific codebook to the measured one we applied the following criteria function:

$$J = a \cdot \Delta(RR_{Period}) + b \cdot \sum_{i=1}^{q} (X_{meas}(q) - X_{PatientCod}(q_{reg}))^2 . \quad (2.34)$$

As the size of the two periods may differ, the samples must be regularized using formula: $q_{reg} = \{q \cdot RR_{sample} / RR_{meas}\}$.

The real-time selection of the most alike period from a large measured signal may become an impossible task as the problem complexity is proportional with the square of measured periods. To handle this problem each period is approximated by a 64-bit size hash table value that can allow a fast comparison of the recorded periods and a proper elimination of the wrong solutions. In some circumstances may happen to select a good, but sub-optimal period to perform the long term prediction. Figure 2.15. illustrates the difference from short term and long term prediction, assuming that the most alike period precedes the measured one.

2.5.19. Characteristic points of the ECG

In our consideration the most important ECG period parameters (see Fig. 2.16.) can be divided into amplitudes and periods (durations). The most important amplitudes are:

- The positive size of the QRS, noted QRS^+
- The negative size of the QRS, noted QRS^-
- The amplitude of the T wave

The most important segments or wave durations are:

- Duration of the P, T, QRS wave
- The size of QRS, QT, TQ and ST segment
- Complex STU

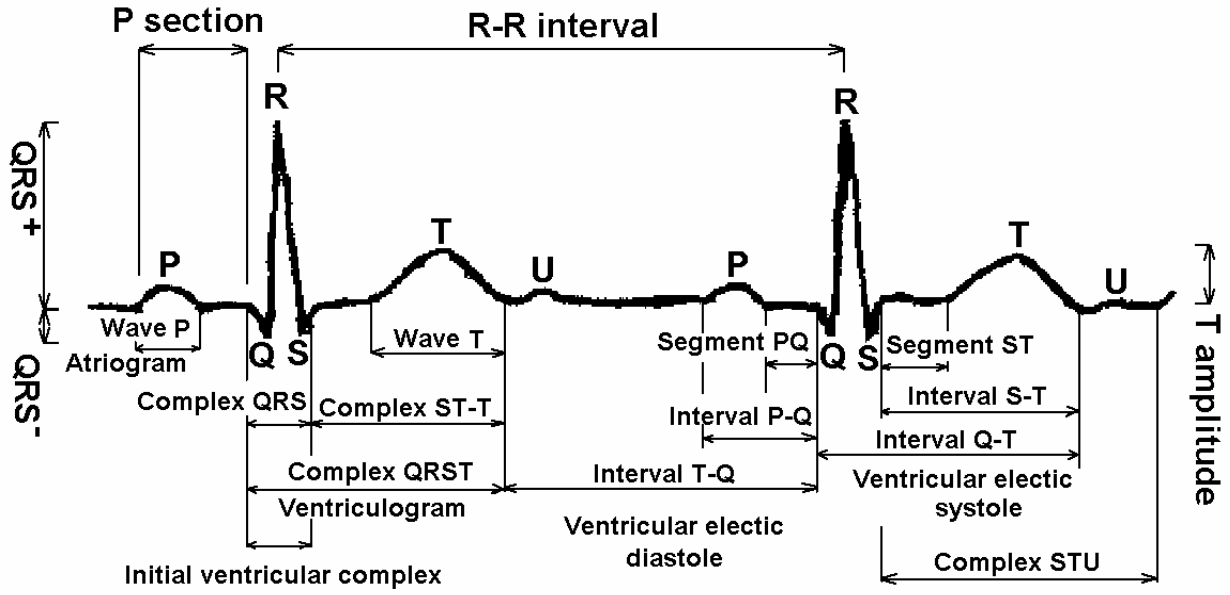

Fig. 2.16. The most important characteristic parameters of the ECG

2.5.20. Calculation of the hash value of an R-R period

A properly determined hash value must correspond to various biological restrictions. The most important task is to avoid the misprediction of the ECG period type. For example a ventricular extra beat period may have the same duration as a normal one, but has totally different characteristic, so the generated hash value must differ significantly. We suppose that the studied signal in this stage must obey the regularity rule, so the signal must be separable into periods with certain duration. The shape of the various waves, such as R, T or P may alter.

The generation of the hash value is realized with respect to the following considerations:

- Each segment is clustered, so the major type of the signal is the most important criteria
- The proper segment duration test is the second restricted criteria (for example each passing R-R period must have a duration between 0.3-2.0 seconds)
- The following values are extracted from the studied characteristic parameters. The importance of these parameters is determined by a genetic algorithm.

2.5.20.1. R-R period clustering

Ordinary one lead ECG signals are measured with 500-2000Hz frequency. Forasmuch an R-R period has about 700-800ms duration each period is represented by about 350-1600 samples. If a clustering is based on measured samples the obtained representation space has an equal dimension size with the number of samples. The high number of dimensions inhibits the appliance of such clustering for practical purposes. An easily realizable simplification way would be the selection of only 100 points from each measured periods. In this case the dimension number is still too high for practical usage and the un-proper selection of the points may cause the modification of the signal characteristics. Altered signal characteristics may cause wrong diagnosis.

A second clustering way may base on characteristic biological values that can be determined by conventional ECG analyzer algorithms. The most important values were described in Section 2.5.19. A higher measuring frequency and bit rate allow a better description of the biological parameters that may permit better clustering performance. Moreover the proper selection of important aspects can reduce significantly the dimension of the clustering space. A lower dimension means a faster processing and robust solution.

Each patient has specific waveforms that characterize the measured ECG. For example physiologists determinate the rules to identify a normal QRS beat, but the measured parameters (such as slope, amplitude, duration) may vary in a relatively large interval. This identification allows an almost infinite normal QRS waveform. However each patient that manifest normal QRS beats holds specific characteristics. This kind of approximation of the problem implies the determination of patient specific parameters that may allow a finer clustering. A finer clustering means better ordering of the signal that permits a more efficient long term prediction.

The patient specific behavior of the ECG signal is more relevant in pathological cases. For example the shape of a ventricular extra beat may vary in a really wide interval. However each patient that manifests extra beats has a specific QRS shape. Quite often a patient has few (more than one) type of extra beat. These beats can ordered into groups, and the inner-group correlation for extra beats is almost as high as for normal ones.

2.5.20.2. R-R period analysis

The normal human heart rate is about 70-80 beats per second. This rate may vary in an interval of 40-220 in function of the state of the patient and its activity. For example an athletic person may have a 40 heart rate and a fat person 90. The state may vary in months or years but the activity in few seconds. Various biological phenomena like breath vary the hearth rate during every aspiration and expiration. From these considerations rely that the consecutive R-R periods may vary in normal case not more than 20-25%.

To separate the normal and pathological cases the investigation of the ECG's shape is not enough. The abrupt variation or an almost constant value of the heart rate present pathological cases albeit that the measured R-R sequences are normal. The recognition of the dangerous pathological cases the heart rate turbulence method is applied.

In our consideration the studied ECG interval is considered correct and hashable as ordinary period if both the shape of the QRS wave and the heart rate is normal. The pathological cases are also hashable, but in the clustering phase these beats must be separated and marked properly.

2.5.20.3. Genetic algorithm based hash structure determination

Each earlier defined biological parameter, such as R-R period or T wave amplitude could be introduced in the hash structure. However the most important properties mean higher difference between R-R periods and should be introduced as early as possible. The principal role of the genetic algorithm (GA) is to define the most important parameters. The GA contains multiple parallel populations with varied population number. From each R-R period of the studied signal is generated a hash value. The aim is to realize a low hash value difference when the periods are almost the same and in case of lower likeness to increase the hash difference.

The likeness criteria function is determined in the following way:

- Normalize the P-R, R-"Tend" and "Tend"-P differences separately, where the "Tend" represent the end moment of the T wave
- Calculate the correlation values among the normalized segments
- Create the weighted sum of the determined correlation values

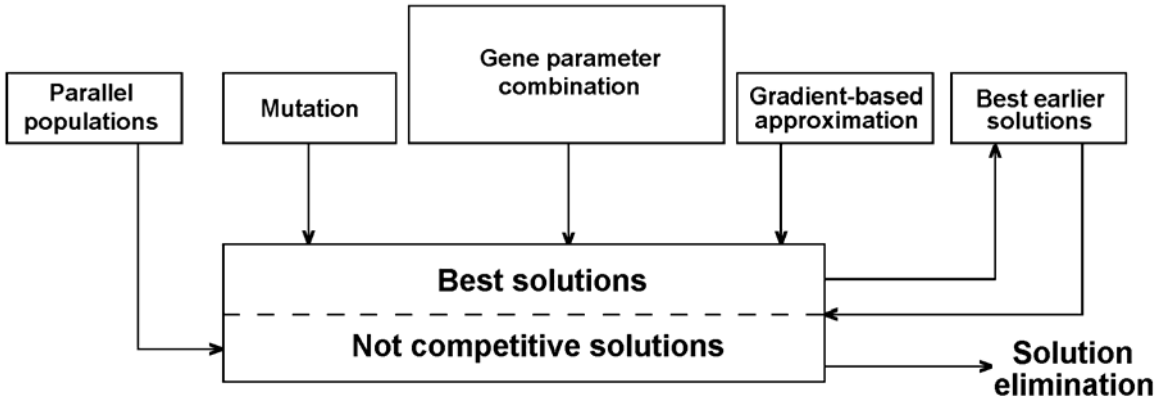

Fig. 2.17. The schematic representation of the genetic algorithm

Figure 2.17. shows the functioning of the GA. Each algorithmic parameter, such as the number of parallel populations is freely adjustable. The proposed GA uses multiple parallel populations (usually in order of tenth) with numerous populations (in order of hundreds). The gene combination, mutation and gradient-based approximation (in case of multi level genes) are applied during the new population creation. After each entity is evaluated the most performing ones are stored and the others are discarded. The best solution storage unit may introduce in the populations performing entities to avoid worse local minimal solutions if it is necessary. The most important parameters are: the genes structure, parameter representation, combination rules, mutation incidence, number of populations and entities, prevalence of gradient-based approximation, best solution selection rule and local solutions managing rules. Using this kind of hash values we realize a transformation from the multidimensional segments to a mono-dimensional value. This mono-dimensional representation of the ECG signal allows a fast search capability for likeness of the R-R periods.

2.5.21. Complete the general template bank for all recognized waves

The general template bank contains the main characteristic shapes of an ECG signal, the R-R period segments and the R, T and P waves. In learning phase new pre-filtered samples may be included in the database. These elements are included in the existing clusters or in case of a special waveform a

new cluster is created. The inner cluster searching mechanism is based on an n-tree search, where the branches represent a combination of biological parameters. These parameters are determined by a GA that works like the GA presented at the hash generation step.

In the filtering step, when the elements of the general template bank are used to improve the estimation performance of the investigated samples the proper selection of the most likeness waveform is performed by the pre-determined n-tree. If the obtained results cannot accomplish the aimed performance level, the pre-filtering step must be repeated (the best obtained results are permanently saved).

2.5.22. Complete the patient specific template bank for all recognized waves

To avoid the uncertain result obtained by the usage of general codebook in special pathological cases a patient dependent codebook is created. Each patient's pathologic ECG holds an individual dependent characteristic that cannot be correctly estimated by the general codebook due to the almost infinite number of the possible waveforms. These individual dependent characteristics are involved in the patient codebook.

The learning and data storage mechanism is the same as presented in the case of general codebook. The selection of patient specific characteristics is realized by a Hermitian function based clustering method. A special waveform manifest low correlation with the elements of the general codebook, but strong relation with the earlier recorded individual specific beats of waveforms.

2.5.23. Multi-channel ECG analysis

The earlier presented single channel processing method can be applied to any measuring lead. However these leads present different waveforms, so for each lead a separate general and patient specific codebook is needed. If we use the measured channels individually and create a result from each channel we cannot extract the extra-channel information. The importance of this extra-channel information can be enormous and is increasing with the number of measured leads. The principal aspect of this kind of mixed processing is the increased certainty. An ordinal ECG signal may be disturbed by various artifacts and abrupt baseline movement. These annoying elements can inhibit the processing of various ECG segments and can enforce false results. Using more than one lead these artifacts can be easily eliminated. Fortunately the measured artifacts and the baseline movement is channel dependent, so the processing method has to estimate the clearest channels and to determine the studied parameters from these results. This channel viewing and processing method can be adaptively realized, so it can select dynamically the best channel for each QRS beat.

The 12 lead measurements contain a 2 lead redundancy, so the values of the perturbed channels may be correctly estimated. However some empiric diagnostic algorithms that are used by physicians are related to pre-determined channels, so a heavily perturbed signal cannot be used in all circumstances for diagnostic purposes (Cohen *et. al.*, 1998). With numeric processing the missing information sometimes can be determined from the other correctly measured leads, but this kind of reconstruction may have only verification purposes and not diagnostic one (due to the decreased reliability).

2.5.24. Multi-channel signal estimation

In multi-lead ECG signal estimation and processing the extraction of the inter-channel information increases significantly the obtained performance. For each QRS beat the most creditable lead is determined (that contains the less amount of artifact). The selected guider lead is responsible to estimate the characteristic points from the investigated period. After the searched variables are

determined for the guider lead, the artifact level and credibility of each leads is determined. From the determined creditability levels for each lead represented by cr_{lead} values, the optimal signal estimation can be determined using formula:

$$\widetilde{X}_{multilead}(n) = \sum_{lead=D1}^{V6} cr_{lead} \cdot \widetilde{X}(n), \tag{2.35}$$

where $\widetilde{X}(n)$ is determined by the formula:

$$\widetilde{X}(n) = p_{Sample} \cdot \hat{X}(n) + p_{GenCode} \cdot \hat{X}(n) + p_{PatCode} \cdot \hat{X}(n) + p_{LTBeat} \cdot \hat{X}(n) + p_{STP} \cdot \sum_{i=1}^{q} p_q \cdot X(n-q). \tag{2.36}$$

2.5.25. Adaptive smoothing and encoding

The adaptive smoothing and encoding phase is performed after a properly effectuated post-filtering of a single or multi-lead ECG signal. In this stage only the estimated values are used, the inter-channel information was extracted in the estimation phase and is no longer needed.

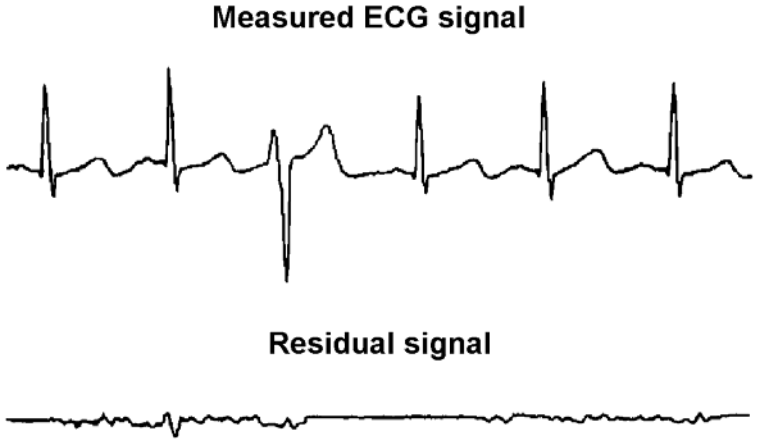

Fig. 2.18. Representation of a measured ECG signal segment and the obtained residual signal using a one lead registration

After the signal is post-filtered, a smoothing operation should be performed to reduce the size of the compacted data. The compression strength should be selected in accordance with the diagnosis performance decrease from the recovered signal. A too high compression rate can deteriorate the useful information from the signal that will contribute to a lower diagnostic precision. The main aim of this algorithm is to decrease the length of the compressed signal and to keep the data quality as high as possible. Let be:

$$\widetilde{X}_{[sm.]}(n) = \frac{1}{k}\left(\sum_{i=1}^{k-1} \widetilde{X}_{[sm.]}(n - i \cdot \tau) + \widetilde{X}(n) \right), \tag{2.37}$$

where $k = 2^j; (j \in N)$, τ in a positive integer and $\widetilde{X}(n) = Y_w(n)$. Normally, the adjacent samples are highly correlated, and we select the positive integer τ that minimizes the auto-correlation function of the ECG signal. Usually the sampling delay τ is about half a QRS complex duration. The inverse transform is given by:

$$\widetilde{X}(n) = k \cdot \widetilde{X}_{[sm.]} - \sum_{i=1}^{k-1} \widetilde{X}_{[sm.]}(n - i \cdot \tau). \tag{2.38}$$

In the meantime of the transform, the values of $\widetilde{X}(n)$ and $\widetilde{X}_{[sm.]}(n)$ can be modified with $k/2$ in order to reduce the reconstruction error or the dispersion of the smoothed signal. The efficiency of

this algorithm highly depends on the chosen values for k and τ. Because the scatter of the filtered and optionally smoothed signal $\sigma_{\widetilde{X}_{[sm.]}}(n,l)$ is too high to allow sufficient compression rate, a linear prediction transform is needed. This method eliminates the redundancy due to correlation between adjacent samples and beats. The resulting data:

$$Y(n) = p_{E,\widetilde{X}_{[sm.]}-B(m)}(n) \cdot \sum_{i=1}^{q} a_{E,i}\widetilde{X}(n-i) + (1 - p_{E,\widetilde{X}_{[sm.]}-B(m)}(n)) \cdot \sum_{i=-q}^{q} b_{E,i}B(m,i), \tag{2.39}$$

allows the calculation of the residual signal

$$r(n) = Y(n) - \widetilde{X}_{[sm.]}(n). \tag{2.40}$$

Verifying processes determine the compression operation caused diagnostic performance decrease in accordance to square error and diagnostic robustness. More iteration should be calculated to determine the optimal set of parameters. In most cases the estimation errors have nearly normal distribution. In order to reduce the length of the residual data, an adaptive method-based entropy coding is needed. For every moment we determine the dispersion $\sigma_r(n,l)$ and the probability $p_{\sigma_r(n,l)}(r(n,l))$ of the errors. If the quantum $q = 2^u$ and u is the length in bits of the word, the output value is obtained by:

$$N_{[act.]}(n,k) = I_1(n-k+1) + p_1(n-k+1) \cdot I_2(n-k+2) + \prod_{i=1}^{k-1} p_i(n-k+i) \cdot I_k(n). \tag{2.41}$$

using $p_i(n-k+i) = p(r(n-k+i),l)$ and $I_{k-i}(n-i) = \int_{-\infty}^{r(n-i)} p_{k-i}(n-i) \cdot dr$.

2.5.26. Distortion analysis of the encoded ECG

The ECG signal compression uses an advanced estimation based on multi-channel information, general and patient specific codebook and long- and short-term prediction. In conventional methods (Nave *et. al.*, 1993) the level of signal distortion is estimated by a percentage root mean square difference (PRMSD) method, given by the relation:

$$PRMSD = \sqrt{\frac{\sum_{n=1}^{N}(x(n) - \widetilde{x}(n))^2}{\sum_{n=1}^{N}(x(n) - \bar{x}(n))^2}} \cdot 100. \tag{2.42}$$

In Eq. (2.42) $x(n)$ represents the original signal, $\widetilde{x}(n)$ the reconstructed signal and $\bar{x}(n)$ the mean value of $x(n)$. The number N represents the studied window's length where the PRMSD was calculated. Unfortunately the varying baseline level may alter the calculated PRMSD level that can produce mediocre diagnostic relevance (Ishijima, 1993). The presented distortion analyser method uses instead of PRMSD a weighted diagnostic distorsion (WDD). Likeness WDD-s were presented by Zigel (Zigel *et. al.*, 2000b), but this method uses different parameters. The WDD is based on comparing the PQRST complex features of the measured and the reconstructed ECG signal. This measuring method reflect the relative preservation of the diagnostic information in the reconstructed signal. These parameters were enumerated in the Section 2.5.19. and are illustrated by Figure 2.16.

There are two major difference compared to WDD-calculation described by Zigel (Zigel *et. al.*, 2000b). The first difference consists in introduction of a low pass filter to the reconstructed signal. This kind of filter may eliminate the white noise caused by the rounding errors ocurred during reconstruction. The second difference consists in an adaptive weighting of the studied parameters in function of clinical relevance. The construction of feature vectors is the same as in paper (Zigel *et. al.*, 2000b), but the included parameters and the adaptive weighting of them makes the difference.

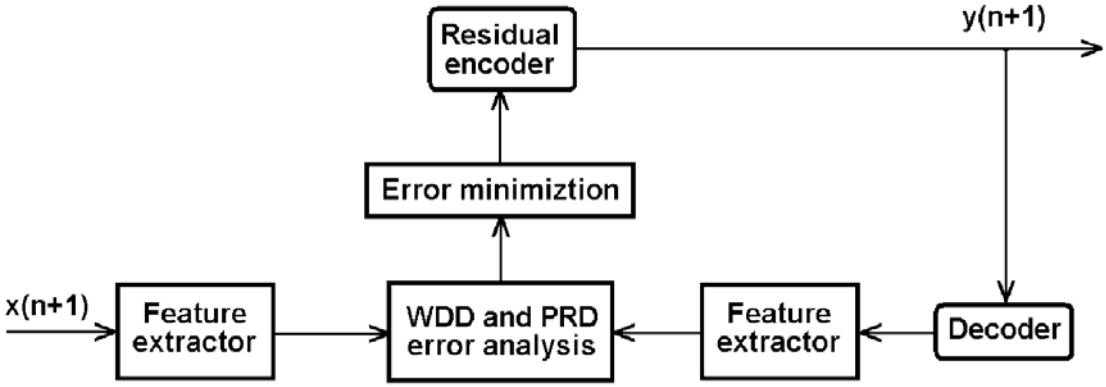

Fig. 2.19. Representation of the distortion analysis using WDD or PRD (PRMSD) between a post-filtered signal X and the reconstructed signal Y

Let be $\beta^T = [\beta_1,...,\beta_n]$ the feature vector with n elements of the original signal (after post-filtering). The vector $\beta_{rec}{}^T = [\beta_{rec,1},...,\beta_{rec,n}]$ that contains the same amount of characteristic elements of the reconstructed and low-pass filtered signal can be compared with the original one to determine the clinical relevance difference among the measured and reconstructed signals. The level of relevance difference (the level of WDD) can be determined by the formula: $WDD(\beta^T, \beta^T{}_{rec}) = \sum_{i=1}^{n} clr_i \cdot (\beta - \beta_{rec})^2$. The weights clr_i represent the importance of a parameter in function of the studied pathological cases. The adaptive weighting is based on empirical information, given by cardiologists. For example the level of ST segment is quite important to detect heart attack, but has lower relevance during a conventional rhythm analysis.

2.6. Results

The recognition of the totally irregular ECG segments was realized with a 99.98% performance. However in case of heavily disturbed, un-reparable signal segments the realized recognition rate was processing aim dependent. For example in case of R-R period analysis the obtained recognition performance was higher than is case of complex processing. Considering a 90% recognition rate we determined the noise tolerance of the method. The obtained data is summarized in Table II.2.

The role of the pre-filtering step is to eliminate the disturbing noise from the measured signal in cases where the irregularity test consider the studied segment adequate for further processing. Taking into consideration that the irregularity test eliminates only the heavily disturbed signal segments, the remaining artifacts in the measured signal can more or less alter the obtained results in function of processing style. From Table II.2. relies that the obtained performance for various processing type can be determined by dividing the results with the performance obtained in case of noisy environment. So in case of T wave detection the obtained result is 9890/99.98 = 98.9198 percent.

Table II.2. The obtained recognition rate and determined noise tolerance for yielding 90% correct results of the irregularity detection method

Processing type	Recognition rate	Noise tolerance for 90% rate
Noisy	99.98	over 100%
R-R segments	99.98	over 100%
T waves	98.9	55%
QT analysis	96.2	23%
P waves	96.1	17%
QRS duration	95.9	14%
Complex	92.9	6%

The segmentation of an ECG segment is much easier than to determine the nature of each QRS waveform. The segmentation has a 99.98% performance, but the nature of the QRS waveforms was determined by a 98.73% dependability (considering correct answer only the successful clustered beat using about 200 clusters). After the ECG signal is segmented, the filtering can be realized more preciously. In our case significant progress has acquired especially in case of recognition of low amplitude elements, such as P wave, S or J point position.

Table II.3. The obtained recognition rate with and without using irregularity detection method

Processing type	Recognition rate	Recognition rate without irregularity test
R-R segments	99.98	97.43
T waves	98.9	92.18
QT analysis	96.2	87.19
P waves	96.1	85.42
QRS duration	95.9	90.18
J point	93.7	78.34
Complex	92.9	75.81

The ECG signal may contain pathological waveforms. These waveforms may be patient dependent (especially in case of ectopic beats) or general. Using general and patient dependent database can significantly improve the obtained recognition rate. Our method was tested on various pathological registrations and the obtained results were collected in Table II.4.

Table II.4. The obtained recognition rate using general and patient dependent codebooks

Processing type	Recognition rate	Recognition using only general codebook	Recognition using both codebooks
R-R segments	99.98	98.11	98.89
T waves	98.9	95.63	97.28
QT analysis	96.2	92.22	94.58
P waves	96.1	91.10	94.85
QRS duration	95.9	92.35	94.98
J point	93.7	85.20	88.93
Complex	92.9	84.00	87.19

An important aspect of the processing method is the codebook uploading procedure. In our case the most relevant thing is to use only the most representative waveforms that can enhance the recognition rate without increasing the codebook size too much. In our experiment we used various codebook size in order to determine how affect the size the recognition rate. The obtained results are represented in Table II.5. In some cases the used codebook size cannot reach the implied maximal barrier. In this case the whole general codebook was used, so the real impact of the database size has greater effect than reported in Table II.5.

Table II.5. The obtained recognition rate in function of general database codebook size

Processing Type	Codebook size 1000 samples	Codebook size 10000 samples	Codebook size 100000 samples
R-R segments	97,99	98,11	98,11
T waves	93,83	94,58	95,63
QT analysis	88,82	90,03	92,22
P waves	87,18	89,33	91,10
QRS duration	91,48	91,92	92,35
J point	81,42	83,28	85,20
Complex	80,57	82,64	84,00

Table II.6. The obtained possible compression rate in function of parameter number and resolution (without using long term prediction and codebook samples)

Number of parameters	Possible compression rate	Resolution
2	4.808	1/16
4	5.009	1/16
4	5.031	1/64
7	5.131	1/64
7	5.162	1/256
11	5.375	1/64
11	5.402	1/256

Table II.7. The obtained possible compression rate and RMS error in function of resolution (without using long term prediction and codebook samples)

Resolution	RMS estimation error	Possible compression rate
1	10688136	4.95
1/2	6685124	5.89
1/4	6578311	6.02
1/8	6472824	6.15
1/16	6392158	6.22
1/32	6351966	6.24
1/64	6295062	6.25
1/128	6289744	6.26
1/256	6276328	6.26
1/512	6272225	6.26
1/1024	6271859	6.26

The consecutive samples of the ECG registration are estimated by the regressive model parameters. However the size of the model constitutes an important issue. As the size of the parameter vector grows the obtained results are better as presented in Table II.6. The resolution represents the number of possible parameter levels between two consecutive numbers. Greater resolution means a lower granularity, more possible values, better performance and more computation. From the averaged estimation error was determined the possible compression rate. Better estimation mean higher possible compression rate. The studied sample had 12 bit resolution sampled at 500 Hz rate. A more detailed representation of the resolution is presented in Table II.7. In this table the average values from 50 measurements were used. The records were realized with 11 bit resolution at 360 Hz (MIT-BIH database, second edition). Results were determined using 12 parameters.

Table II.8. The obtained possible compression rate and RMS error in case of normal and zero-level parameter study (without using long term prediction and codebook samples)

Number of parameters	RMS estimation error	Possible compression rate	RMS estimation error using zero-level	Possible compression rate using zero-level
1	1817646	3.31	1761534	3.34
2	907701	4.18	726497	4.56
3	676450	4.70	619483	4.89
4	647790	4.79	561483	5.10
5	609283	4.92	552125	5.15
6	608930	4.92	551012	5.16
7	603598	4.94	550602	5.16
8	603598	4.94	548605	5.16

The estimation performance depends not only from the number and resolution of the parameters. In Table II.8. is presented the importance of parameter quality. In this case a special "zero-level" parameter is introduced that significantly improves the estimation quality. The studied samples had 12 bit resolution and 360 Hz sampling rate.

The usage of both left- and right- handed parameters drastically reduces the estimation error. Unfortunately this approximation cannot be used in compression but improves the filtering performance. The estimation error in function of parameter number is presented in Table II.9.

Table II.9. The RMS error in case of normal and zero-level parameter study using 1/256 resolution (without using long term prediction and codebook samples)

Number of parameters	RMS error	RMS error using zero-level
2×1	265348	265192
2×2	81889	81875
2×3	56581	56579
2×4	50877	50876
2×5	49456	49456
2×6	49249	49249
2×7	49061	49061
2×8	49061	49061

Table II.10. The RMS error in case of one- and two- sided estimation. We used zero-level parameter and 1/256 resolution (without using long term prediction and codebook samples)

Number of parameters	RMS error one sided estimation	RMS error two sided estimation	RMS error one sided adaptive estimation	RMS error two sided adptive estimation
(1 or 2)×1	1761534	265192	1423976	192355
(1 or 2)×2	726497	81875	448292	54923
(1 or 2)×3	619483	56579	394556	39567
(1 or 2)×4	561483	50876	371232	35626
(1 or 2)×5	552125	49456	360448	34983
(1 or 2)×6	551012	49249	358934	34671
(1 or 2)×7	550602	49061	358231	34610
(1 or 2)×8	548605	49061	357449	34602

Table II.11. The RMS error in case of one- and two- sided, normal and adaptive estimation. We used zero-level parameter and 1/256 resolution (without using long term prediction and codebook samples)

The parameter's serial number	RMS error one-sided estimation	RMS error two-sided estimation	RMS error one-sided adaptive estimation	RMS error two-sided adaptive estimation
1.	1643218	265192	1423976	192355
2.	5829187	793477	5092118	559403
3.	11058545	1412668	10076427	1101488
4.	16060207	1983011	14479233	1569040
5.	20164794	2512990	18000552	1995327
6.	23244105	2965578	20815767	2288405
7.	25504879	3266778	22904631	2505893
8.	27208925	3405921	24209457	2641108
Zero-value	12586228	12586228	12586228	12586228

Adaptivity may have an important role in estimation. If the parameter levels may change in function of earlier experience the overall estimation performance is increased. The significance of adaptivity in one- and two- sided estimation is presented by Table II.10.

It could be important to determine the relevance of each parameter separately. This kind of study may enlighten the individual role of each parameter. The obtained RMS error values that are inverse proportional with relevance are summarized by Table II.11.

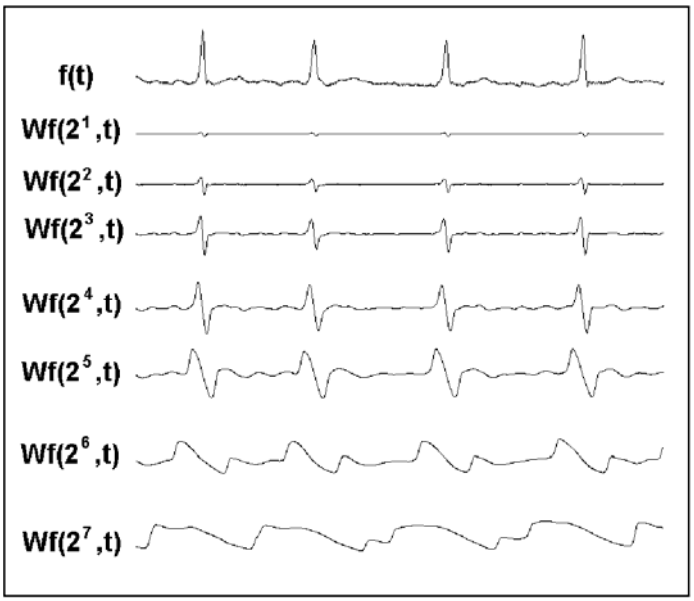

Fig. 2.20. The ECG signal and its wavelet transforms at scale $s=2^1,\ 2^2, ..., 2^7$

One important segment of the wavelets is considered the dyadic wavelets, where the transformation is performed using a scale $s=2^1,\ 2^2, ..., 2^n$. Each dyadic wavelet is sensible for a given spectra segment. The various ECG waveforms manifest diverse spectra, so each waveform has an optimal scale. Using this optimal scale that can vary for each waveform or pathological shape we can detect the investigated events more easily. Using the dyadic wavelet for the MIT 201 data we obtained the transformed waveforms according to Fig. 2.20.

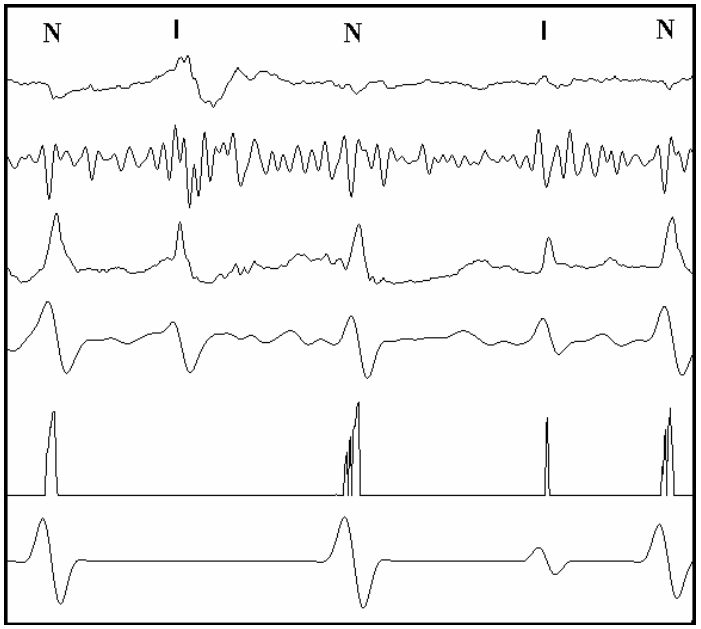

Fig. 2.21. The separation of normal beats from isolated QRS-like artifacts using mixed (genetic-parametrical transformation algorithm)

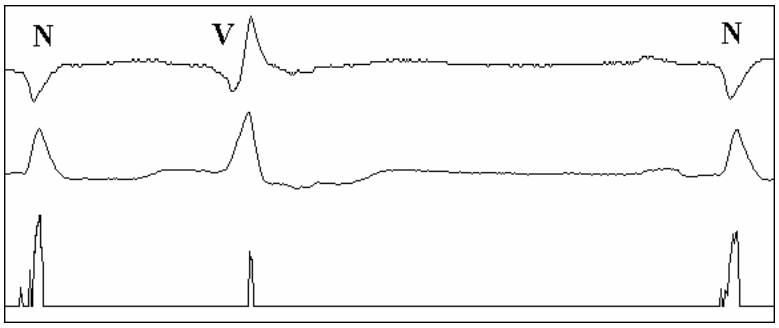

Fig. 2.22. The separation of normal QRS beats (N) from abnormal ventricular beats (V)

As mentioned earlier, the mixed processing methods can yield better recognition results than transformation algorithms. In the following image (Fig. 2.21.) we can see a separation problem of a heavily deteriorated ECG segment. In this image the first and third line is the two lead of the investigated ECG segment and the second and fourth line is their wavelet transformed form. The *N* mark means a normal beat and *I* represent a pathologic beat. The studied sample is from the MIT-BIH database and the evaluation was realized by physicians (file number 228). In the fifth line we can observe the results of a genetic waveform estimator and the last line represents its wavelet transformed form.

The genetic estimator can be used to separate ventricular beats from normal ones. This process is illustrated in Fig. 2.22., where the first two lines represent the two leads of the studied signal. In the last line we can observe the output of the genetic estimator method. The separation can be realized by further processing of the yielded result.

Figure 2.23. presents the importance of the adaptive filtering. The first line is a heavily deteriorated ECG segment and the lost one is its filtered version. In this experiment a 200Hz sampling rate was used with 8 bit resolution. Better resolution and higher sampling rate increase the performance of the filter method.

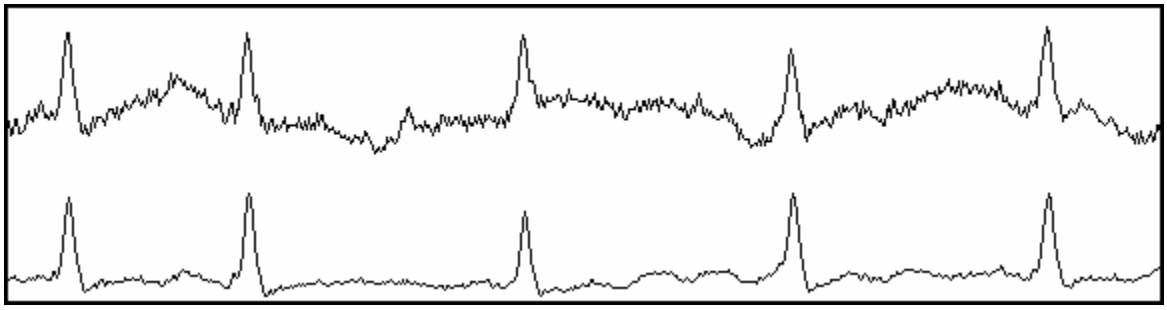

Fig. 2.23. The bulk of the perturbation is eliminated from the ECG signal by the adaptive filter. The main characteristics of the signal are kept successfully

An important aspect of the medical data storage represents the efficiency of entropy coding. In our case a special SVM-based entropy coding mechanism is used that performs significantly better than conventional algorithms (see Table II.12.). The performance is determined by the number of estimation parameters, smoothing strength, resolution and sampling rate. The entropy coding can decrease at least 12 times the theoretical 'waste', compared with Huffman coding, during signal compacting.

Table II.13. presents the recognition rate of QRS beats for the noisiest MIT-BIH registrations. Both genetic-parametric and mixed models performances are presented. The records selected from the database manifests the lowest recognition rate from the whole dataset. From the number of total beast and failed decisions can be determined the obtained a 99.77% recognition rate for the mixed method. The obtained results from other records was slightly higher, the processing method yielded a global recognition rate as high as 99.84%.

Table II.12. Representation of the entropy coder's performance using 32 parameters

Record number	Theoretic entropy	Huffman code size	SVM-based coding
104	170889	202158	172823
105	167021	197384	168882
108	172093	204214	174734
201	156878	185962	158004
203	185872	218977	187322
222	168126	199880	169634
228	181774	214708	183019

Table II.13. Representation of the QRS detection rates for the noisiest MIT-BIH registrations

Records number	Total beats	Failed detection genetic-parametric	Failed detection mixed
104	2230	6	3
105	2572	9	5
108	1763	16	11
201	1963	8	5
203	2982	16	10
222	2484	4	2
228	2053	4	1
Total	16047	63	37

The characteristic wave recognition performance heavily depends on the level of allowed root mean square error during signal compression. Figure 2.24.(a) represents the level of detection error of P, T and R waves when the relative RMSE varies from 0 to 20%. We investigated the detection error in function of the nature of R wave. The ventricular ectopic beats QV1 and QV2 included in this study were treated patient specific. Figure 2.24.(b) illustrates the separation problem of various QRS waveforms in a 32-dimensional parameter space.

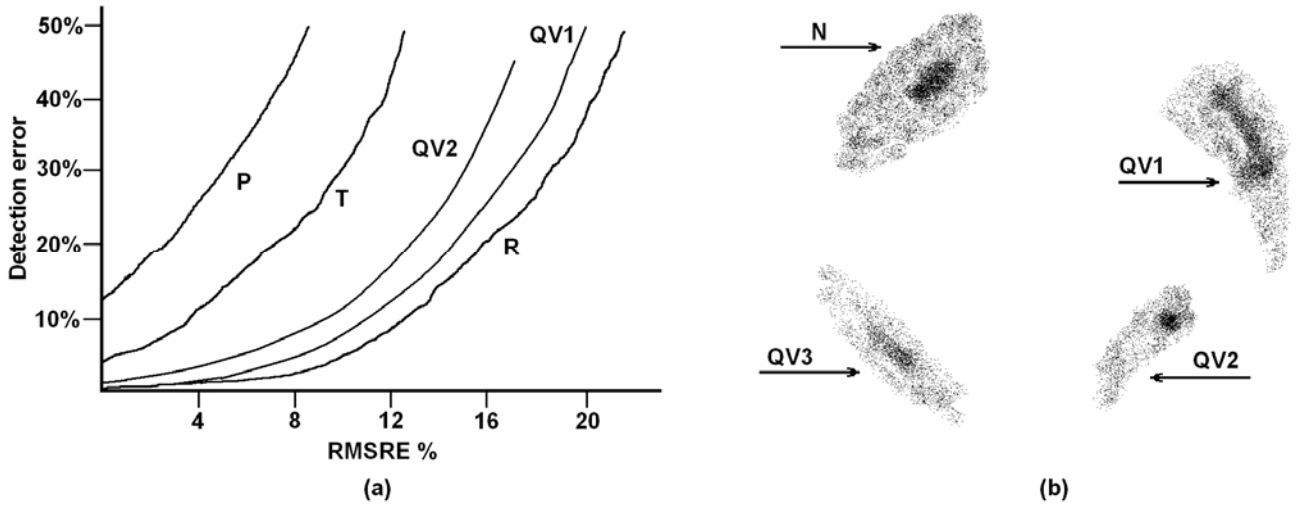

Fig. 2.24. (a) The recognition ratio of R, T, P and QV1, QV2 waves plotted against RMSRE; (b) Representation of various beat forms: the normal QRS beats are represented by N, and three different ventricular extra beats are represented by QV1, QV2 and QV3 in plain representation (the calculation space has 32 dimensions, and the two most significant orthogonal combinations were selected for planar representation)

Table II.14. The probability of a detection error of various waveforms using 8% RMSRE and multi-channel configurations

Lead number	P wave	T wave	QRS beat	QV1 beats	QV2 beats
1	44.3%	23.4%	3.2%	5.1%	8.3%
3	31.9%	12.5%	1.8%	3.3%	5.1%
6	23.8%	9.7%	1.2%	2.1%	3.8%
12	21.1%	7.7%	0.8%	1.6%	2.9%

2.7. Discussion

The irregular ECG may contain such shaped waveforms that can be mistakable with ordinary waveforms. To avoid such situations the irregularity testing and ECG segmentation is necessary. The importance of irregularity test is direct proportional with processing complexity. For example the noise tolerance of recognition for QRS beat is much higher than for P waves. The data involved in Table II.2. mention that the complex analysis method has a 92.9% recognition rate that decreases to 90% in presence of a noise with 6% signal's amplitude power.

A segmentation problem is by far easier than a wholse beat classification. For example the presence of a QRS beat can be detected by several ways, but a complex classification among various clusters (at least 200 types) is much harder. Each QRS complex must be parametrized and the separation in clusters is taken on in a multi-dimensional hyperspace. In our experiment using 32 dimension we could reach 98.73%. The further increase of the parameters number can not increase significantly the recognition rate as the genetic solution searcher method become saturated. Table II.3. presents the importance of irregularity test. As the wrong data segments are eliminated the segmentation and recognition process is enlightened significantly. For example the segmentation process can be seriously disturbed by abrupt iso-line movements. The separation of the un-usable data creates the possibility that the adaptive method focus on the real problem.

The majority of QRS waves can be properly handled using general databases. However the signal may contain patient specific waveforms that can manifest in such a various way that cannot be included in general codebooks. The most common pathological case that cannot be properly handled using general codebooks is the presence of ectopic beats. These beats are generated mostly from a patient specific ventricular location. The presence of these generator points is so sparse that cannot be generalized a proper localizing rule. However these points are strongly patient dependent. As the patient's heart is depolarized in two different moments from the same location, the generated QRS waveforms will be quite close. This fact can be exploited to generate a relatively small patient specific codebook. As Table II.4. presents, the recognition rate of all studied waveforms was increased by a proper patient specific database.

Both the classifying speed and accuracy is codebook size dependent. The importance of the general codebook was tested using various size of it. As Table II.5. presents, the size of the general codebook can influence significantly the recognition rate of the waves. At a higher level we could observe a saturation of recognition performance, so an almost infinite size of the codebook cannot yield 100% reconstruction. Depending of the processing time a balance should be established between the codebook's sizes and processing speed.

The estimation performance of the consecutive ECG samples from weighted adjacent values depends from the number of parameters. From Table II.6. we can observe a slightly higher possible compression rate that is inverse proportional with squared estimation error. The resolution of the parameters has lower impact in estimation performance. From the realized measurements we deducted that the performance increase is maintained until at least 10-15 parameters using a

resolution at least 1/256. The optimal parameter number depends from data sampling rate and resolution. A higher sampling rate and resolution makes useful a higher parameter number of the estimation model. From Table II.7. can be determined that the resolution of the model's parameters has lower impact than the number of them. As Table II.8. elucidates, the quality of the parameters is more important than itself the number of them. The introduced zero-level parameter has greater impact than the fourth regressive component (see Table II.11.). A sampled value can be much better estimated from both adjacent samples than from only the prior ones. If all adjacent samples are involved in estimation process, a drastic estimation error decrement happens that can be observed from Table II.9. Due to the non-a priori behavior of the estimation process (in estimation of a given value are involved samples that are recorded later) these estimation results cannot be used directly in a compression process, because the reconstruction of the signal cannot be proceeded.

A proper estimation should use the temporal modifications in signal's characteristics. To perform it we used an adaptive parameterization of the estimation process. The overall performance of the estimation process was increased significantly, as presented in Table II.10. The performance increment phenomena can be observed in case of both one- and two- sided estimations.

The estimation performance of the ECG signal can be increased by involving medical information in the process. The used ECG specific data is the morphology of a whole ECG period, long term semi-periodic behavior and the shape of the studied waves. In our case the proper estimation of the normal QRS beats can be used to decrease from the estimated signal. Doing so the estimation error is reduced, but the places and types of the subtracted waves must be stored.

From Table II.13. can be deducted that both QRS detection algorithms are slightly more efficient than Li's WT (Li *et. al.*, 1995). According to the power spectra of the ECG signal, noise and artifacts, it is evident, that QRS complex are rather reflected at scale $s = 2^3$ and $s = 2^4$ (see Fig. 2.20.). The QRS complex corresponds to two local extremes with opposite sign. The onset (Q or R point) and offset (S or J point) of the QRS complex contains higher frequency components, so it can be easily studied at finer scales.

The major advantage of this method is the ability to change its behavior in time, if necessary. Table II.13. demonstrates the superiority of the iteratively filtering mixed methods. Although the forward method ensures good results and no better transformation algorithm is known, the iterative algorithm easily overtakes its performance. This is because the post-filtering is much more complex, and can base on all until that moment obtained information.

Normally the P and T wave's power spectrum is between 0.5-10 Hz. According to this, it can be investigated at scale $s = 2^4$ or $s = 2^5$. Although the baseline movement is dominant between 0.5-6 Hz, P and T waves can be detected. Then PR, ST and QT intervals can be simply calculated. The J point introduces a 'break' into the signal, it's detectable at scale $s = 2^4$. The noise caused by the electrical network is integrally filtered from the signal at all scale $s \geq 2^3$.

In case of QRS detection the whitening filter of the network removes baseline movement, suppresses the P and T waves and increases the R wave. The QRS complex can be easily recognized from the output of the adaptive matched filter. The P and T waves can't be accurately detected without additional processing steps (squaring, moving average).

In Fig. 2.22. the separation and waveform recognition was performed, but in more complex situation the optimal classification is not possible yet. Because of the discontinuities in the parameter sets solved by the genetic method the filtered output often contains spikes. The elimination of these spikes is the major difficulty caused by this method.

In Fig. 2.21. it is clearly demonstrated, that the combined method can solve much nasty situations. The isolated QRS-like artifacts represent a much more difficult task for a correct classification. In the

first lead the separation with wavelet transform seems to be quite difficult. Although each normal beat has a specific waveform the separation seems to be a hard task. The problem is totally different, when we see the wavelet transform of the genetic estimator. Because this estimator works in different way for every detectable waveform in order to perform a correct classification we must separate first all the well-recognizable waveform. The scale of the wavelet transform highly depends on the current task. In the case of the ECG signal the scale was 6 and 22, for the estimators output was 19. Figure 2.23. shows us how performing could be a classification-based filtering. To reach such-a performance we should identify as much as possible fix characteristic point from the signal.

Table II.12. illustrates the compaction effectiveness for some of the most perturbed files, whose noise level and missed R wave detection rate was almost maximal. The new coding formula (2.41) has far better results than the adaptive Huffman coding. The elements distribution is close to normal and its change is not recommended without further knowledge. The smoothing strength should be adjusted by k and τ (see (2.37), (2.38)).

The ANN-based adaptive matched filter (Szilágyi *et. al.*, 1997a, 1997b) and the wavelet-transform-based QRS detection algorithm were applied for the noisiest ECG signals. The distinct features of these methods are:

- A multi-layer neural network structure can better model the inherently non-linear ECG signal, than linear model-based filtering methods;
- The QRS templates used for filtering is updated by a parameterized wavelet-based algorithm, which provides better adaptation to the signal changes than any other static structure technique;
- Wavelet-based analysis could be more robust than parameter extraction methods;
- With the parametrical estimator it is possible to permanently choose the optimal size of the neural network for real-time processing. It is able to remove the redundancy introduced by the increased number of the hidden units,
- The network learning step may vary in time in order to adapt in time to the eventually changes in the measured signals structure.

Experiments show that (Fig. 2.24.(a)) the R wave can be accurately recognized even if RMSRE is about 10%. For T and P wave detection the root mean square error must not exceed 3-5% of the signal's power. S (J), Q points and U wave cannot be recognized in most of the cases if RMSRE is higher than 1%. The lower amplitude of the T and P waves is the main reason of the lower detection rate. The amplitude of the QV1 and QV2 ectopic beats is about the same as in case of R waves, but the uncommon patient-specific shape of them inhibit the usage of a priori waveforms (we considered new patients, so the database had not any information about them). It can be observed a smoother shape of the performance graph for the studied QV1 and QV2 ectopic beats caused by the much lower available occurrence (almost 100 times less). The separation of the normal QRS beats from ventricular extra beats is realized in a 32 dimensional calculation space. The separation process consists in selection of the most relevant orthogonal parameter combination and clustering problem in a lowered dimensional hyperspace. A classic two dimensional presentation can be observed in Fig. 2.24.(b).

Multi-channel ECG has several advantages over one-lead registration. Not only the acquired data contains redundant information that can be used to increase reliability, but diverse phenomena can be monitored much better. The estimation of diverse waveforms despite the necessary higher databases (the computer has no opportunity to determine directly from one-channel data the other one) is much better (see Table II.14.) due the higher reliability. Not only the detection of diverse waveforms is more adequate, but the signal estimation is also performed. For example the unbalanced two-sided estimation can be performed for all channels without the first one (all estimations may use the preliminary determined partial results).

2.8. Conclusions

The post-filter algorithm for beat recognition is efficient. For other waves, the detection rate is also higher than the earlier developed wavelet and neural-network-based recognition methods. Normally the Wavelet could solve the recognition task, because P and T wave power spectra are between 0.5-10Hz. According to this, it can be investigated at scale between 15 and 35.

Although the baseline movement is dominant between 0.4-8Hz, the P and T waves can be detected. Then PR, ST and QT intervals can be simply calculated. In case of QRS detection the filter of the genetic estimator removes baseline movement and the bulk of the artifacts, suppresses the P and T waves and increases the R wave. The QRS complex can be easily recognized from the output of the adaptive estimator. The P and T waves cannot be accurately detected without additional processing steps based on wavelet transform.

The major advantages of post-filtering method usually rise in trouble, when the patient has unique behavior. In clinical healthcare, these situations are the most dangerous. A better malfunction recognition during real-time measurements and diagnosis could save human lives. Experiments show this adaptive filter can model the non-linear ECG signal better, than linear algorithms. The combination of the recognition, separation and classification methods allow new perspectives in the field of reliable fully automated ECG signal classification.

An experimental real-time processing using this method needs a powerful computer able to perform massively parallel algorithms. In Holter telemetry and diagnostic systems, where a vast amount of data is acquired and transmitted by radio wave, the compression is an unavoidable step of the computerization. Sophisticated long computation and lingering unpack of the signal could be the major disadvantages of this process. Although quite often the calculation term doesn't admit on-line computerization (in multitasking mode), the rapid evolution of the computers will shortly change this fact.

3. Parallalized Dynamic Heart Modelling

***Abstract*:** This paper presents a new way to solve the inverse problem of electrocardiography in terms of heart model parameters. The developed event estimation and recognition method uses a unified neural network (UNN)-based optimization system to determine the most relevant heart model parameters. A UNN-based preliminary ECG analyzer system has been created to reduce the searching space of the optimization algorithm. A relation between objective function minimization and robustness of the solution determined the optimal model parameters. The patient specific deformable heart model that involves the known electric and mechanic properties of the cardiac cells and tissue. The accuracy and efficiency of the algorithm was tested for anisotropic and inhomogeneous 3D domains using ten Tusscher's and Nygen's cardiac cell models. During propagation of depolarisation wave, the kinetic, compositional and rotational anisotropy is included in the tissue, organ and torso model. The connection between electrical and mechanical properties was realized at the cell model level using the calcium channel properties. An intensive parameter reduction was performed by the abstract formulation of the searching space. This patient specific parameter representation enables the adjustment of deformable model parameters in real-time. The validation process was performed using measured ECG and ultrasound image records that were compared with simulated signals and shapes using an abstract, parameterised evaluation criterion. The final evaluation results, validated by physicians, were about 96% correct. Starting from the fact that input ECGs contained various malfunction cases, such as Wolff-Parkinson-White (WPW) syndrome, atrial and ventricular fibrillation, these results suggest this approach provides a robust inverse solution, circumventing most of the difficulties of the ECG inverse problem. The optimised dynamic heart modelling is based on a parallelized space–time adaptive mesh refinement algorithm (AMRA). The spatial and temporal simulation method of the anisotropic excitable media has to achieve great performance in distributed processing environment. The generated inverse ECG with conventional and parallelized algorithm has the same quality, but a speedup of factor 200 can be reached using AMRA modeling and single instruction multiple data (SIMD) programming of the video cards. These results suggest that a powerful personal computer will be able to perform a one-second long simulation of the spatial electrical dynamics of the heart in approximately five minutes.

Keywords: spatial visualization, heart wall movement analysis, parallel processing, electro-mechanical model, active appearance model.

3.1. Introduction

Nowadays the health problems related to the malfunction of the heart affects large groups of people and have become the most important mortality factor (Haider *et al.*, 1998). These malfunctions are usually caused by heart attack, rhythm disturbances and pathological degenerations. Modern health study is focusing on predicting these kinds of tragic events, and identifying the endangered patients, to make it possible to apply a preventing therapy.

Despite decades of research, the mechanisms responsible for ventricular fibrillation are not yet well understood. It would be important to understand how the onset of arrhythmias that cause fibrillation depends on details such as heart's size (Winfree, 1994), geometry (Panfilov, 1999), mechanical and electrical state, anisotropic fibre structure and inhomogeneities (Antzelevitch *et al.*, 1999). The main difficulty in development of a quantitatively accurate simulation of an entire three-dimensional human heart is that the human heart muscle is a strongly excitable medium whose electrical dynamics involve rapidly varying, highly localized fronts (Cherry *et al.*, 2000).

Traditional computerized electrocardiogram (ECG) analyzer systems used the collected signal as an input to suggest an empiric-information-based evaluation of the ECG (Noble, 2004). These systems

may recognize various waveforms, but the leakage of information about the inner functioning of the heart inhibits to understand the producing phenomena (Sermesant *et al.*, 2006b).

The construction of a heart model (Thaker *et al.*, 1998) may allow computers to recognize the origin and the evolvement process of the ECG signal (Lagerholm *et al.*, 2000). These systems may unify the vast empiric information applied in traditional systems with model-based-recognition, creating hybrid processing structures (Szilágyi *et al.*, 2003a). These hybrid systems may activate the model-based-approach at any moment to handle correctly almost all unrecognizable waveform. The strange waveforms may appear in case of unknown patients or uncommon states, such as ventricular fibrillation (Szilágyi, 1998). In these cases the model-based approach estimates the causes of the encountered phenomenon.

In this paper we present a new spatial (3-D) electro-mechanical model of the heart that can be used for simulation purposes and analysis of various pathologic cases such as ectopic beats or ventricular fibrillation. The overall principle of the model is presented by Fig. 3.1. that includes knowledge from several disciplines, such as anatomy, electrophysiology and biomechanics. The measured ECG signal and ultrasound image record constitutes the biological data obtained directly from the patient in clinical environment. Using several processing methods, such as adaptive ECG processing (Szilágyi, 1998), QRS wave clustering (Szilágyi, 1998), ultrasound image segmentation (Dumoulin *et al.*, 2003) or active appearance models (Cootes *et al.*, 2001) our method can yield the necessary engineering parameters that can be used to adjust the pre-determined general model to latest patient information. The a priori patient specific data relieves the formulation of patient specific model.

At the basis of a dynamic heart modeling stands a performing ECG signal processing (Szilágyi, 1998) and an efficient electrocardiograph image sequence segmentation method (Dumoulin *et al.*, 2003). The main challenge in modern ECG processing is the correct clustering of the obtained waveforms that reflects the electric property of the heart.

The mechanic properties can be visualized by using an ultrasound imaging method. The obtained images must be filtered, to separate the useful image from disturbing elements like speckle noise (Evans *et al.*, 1996). In order to properly deal with the numerous deficiencies of echocardiographic imaging techniques several automated segmentation methods have been developed and reported. Geiser *et al.* (Geiser *et al.*, 1998) proposed arc filtering for boundary detection, while Brotherton et al. (1994) gave a hierarchical fuzzy neural network solution. Dias *et al.* (1996) introduced an iterative multi-grid dynamic programming technique based on Rayleigh distributed random variables and a probabilistic model formulated within Bayesian framework. Belohlavek *et al.* (1996) proposed the automated segmentation using a modified self-organizing map. Chalana *et al.* (1996) traced the epi- and endocardial border using active contour models. In spite of their significant merits, these methods still neglect the following aspects:

- Sought boundaries are not always represented by the strongest edges.
- They use no a priori information concerning the allowable shapes and ranges of the segmented object.
- Segmented boundaries should be consistent with the cardiac cycle.

In the last decade, advances have been made in the content-based retrieval of medical images, such as extraction of boundaries of cardiac objects from echocardiography image sequences (Duncan *et al.*, 2000). Montagnat *et al.* (1999) used a two-simplex mesh-based cylindrical deformable surface to produce time continuous segmentation of 3-D sequences. Angelini *et al.* (2001) proposed a feature enhancement and noise suppression using a wavelet-like decomposition of the spatial frequency domain. A snake-based segmentation is carried out later on the de-noised data.

Active appearance models (AAM), introduced by Cootes *et al.* (2001), are promising image segmentation tools that may provide solutions to most pending problems of echocardiography, as

they rely on both shape and appearance (intensity and/or texture) information. Bosch et al. proposed a robust and time-continuous delineation of 2-D endocardial contours along a full cardiac cycle, using an extended AAM, trained on phase-normalized four-chamber sequences (Bosch *et al.*, 2002).

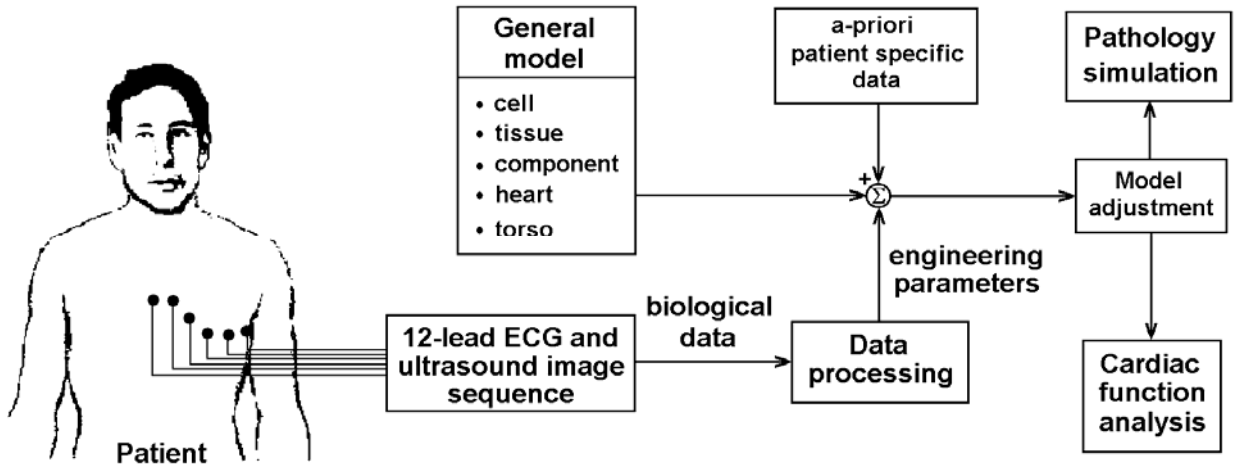

Fig. 3.1. General overview of the problem is presented. From patient data the biological and engineering parameters are determined. Using the general model, a priori patient specific data and the determined engineering parameters, the general electro-mechanic heart model is adjusted to cover patient specificity. The obtained model can be used to realize a cardiac function analysis or a pathology case simulation.

The spatio-temporal extension of the active shape models (ASM) in (Hamarneh *et al.*, 2004) is realized by introduction of spatio-temporal shapes (ST-shapes). The AAM framework is extended to both planar and time representation in (Lelieveldt *et al.*, 2001) by considering the image sequence as a single shape/intensity sample, realizing in this way the active appearance motion model (AAMM).

The functional modeling of the heart has a vast literature (Noble, 2004). A general model of the patient can be separated to many levels including genetic DNS sequence organization (for example the cause of Bruggada syndrome), protein structures, cardiac cell composition (Nygren *et al.*, 1998; ten Tusscher *et al.* 2004, 2006), tissue branching (Masood *et al.,* 2000), atria (Harrild *et al.*, 2000) and ventricles anatomy (Winslow *et al.*, 2000), heart functioning (Courtemanche, 1996) and heart-torso positioning.

The construction of a heart model (Thaker *et al.*, 1998) may allow computers to recognize the origin and the evolvement process of the ECG signal (Lagerholm *et al.*, 2000). These systems may unify the vast empiric information applied in traditional systems with model-based- recognition, creating hybrid processing structures (Szilágyi *et al.*, 2003a, 2006). These hybrid systems may activate the model-based-approach at any moment to handle correctly almost all unrecognizable waveform. The strange waveforms may appear in case of unknown patients or uncommon states, such as ventricular fibrillation (Szilágyi, 1998). In these cases the model-based approach estimates the causes of the encountered phenomenon.

A dynamic organ such as the heart places special demands on modeling techniques. To understand its physiology and patho-physiology, not only the electrical activity and spatial distribution of its structures is important, but also their movement during cardiac cycles (Noble, 2004). The shape of the measured ECG signal is influenced during repolarization by the mechanical contraction of the heart (Moreau-Villéger *et al.*, 2006). The main problem of inverse ECG processing consists in reconstruction of cardiac electrical events from measurements (Sermesant *et al.*, 2006a). In contrast to the forward problem of electrocardiography, the inverse problem does not possess a mathematically unique solution (MacLeod *et al.*, 1998) and in order to improve stability, it needs to adopt regularization techniques (Shahidi *et al.*, 1994; MacLeod *et al.*, 1998).

The problem of multiple solutions of the inverse models enforced the development of several approaches such as equivalent cardiac generators (e. g. equivalent dipole and multi-pole) (Moreau-Villéger *et al.*, 2006), heart surface isochrones (Cuppen *et al.*, 1984), or epicardial potential (Guanglin *et al.*, 2001). These methods led to a significant progress, but the different uncertainty elements of the processing method hinder the potentially beneficial ECG inverse solutions from becoming a routine clinical tool.

An almost complete ECG data acquisition from the human torso is accomplished by the body surface potential mapping (BSPM) technique (Mirvis, 1988). BSPM may have a great advantage over the standard 12-lead system in different situations due to deeper accessible information. Mirvis has shown some cases of BSPM recordings that clearly demonstrate the inadequacies of the standard ECG lead sets in a variety of pathologies (Mirvis, 1988). The better understanding of the depolarization-repolarization mechanism may enlighten the origin of diverse pathological events.

In the area of data processing, numerous interesting biomedical applications of artificial neural networks are included (Minami *et al.*, 1999). The best known neural solutions involve multilayer perceptrons (Thaker *et al.*, 1998), Kohonen self-organizing networks (Szilágyi *et al.*, 2003a), fuzzy or neuro-fuzzy systems (Smola *et al.*, 1998), genetic algorithms (Szilágyi *et al.*, 1998) and the combination of various solutions within a hybrid system (Osowski *et al.*, 2001).

Earlier heart modeling systems applied many neural networks and chose the best one, while the others were discarded. After a deep investigation of the obtained results, it was recognized that the most efficient approaches should rely on the combination of many classifiers utilizing either different classifier network structures or different data preprocessing methods (Osowski *et al.*, 2001).

The conventional artificial neural networks (ANNs) suffer from diverse drawbacks that can be handled by the support vector machines (SVMs) pioneered by (Vapnik, 1998), which had to face to following problems:

- Modern biological problems are high-dimensional, and if the underlying mapping is not very smooth, the linear paradigm needs an exponentially increasing number of terms with an increasing dimensionality of the input space, that implies an increase in the number of independent variables. This is known as 'the curse of dimensionality';
- The real-life data generation laws may typically be far from the normal distribution and a model-builder must handle any kind of distribution in order to construct an efficient learning algorithm;
- The maximum likelihood estimator (consequently the sum-of-error-squares cost function, too) should be replaced by a new induction paradigm that is uniformly better. This indicator may accomplish the properly modeling of non-Gaussian distributions.

SVM classifiers have become quite popular due to their robustness and stability (Osowski *et al.*, 2004). A SVM used in a heart modeling system is rigorously based on statistical learning theory and simultaneously minimizes the training and test errors. Apart from that, they produce a unique globally optimal solution and hence are extensively used in diverse applications including medical diagnosis (Smola *et al.*, 1998).

Volumetric heart models have been introduced in cardiac function analysis (Park *et al.*, 2003) as they yield richer mechanical parameters. They were involved in deformation analysis of the organ. An important idea has been introduced by the „ProActive Deformable Models" (Sermesant *et al.*, 2006b) that integrates the a priori knowledge on the organ's motion in the whole segmentation process and simulation (Winslow *et al.*, 2005).

Ectopic heartbeats are arrhythmias involving variations in a normal heartbeat. Sometimes they may occur without obvious cause and are not harmful. However, they are often associated with electrolyte abnormalities in the blood that should be treated. Many times ectopic beats can be associated with ischemia, or local reduction in blood supply to the heart. Once an ectopic beat appears, the underlying reversible reasons should be investigated, even if no further treatment is needed.

An important aspect of ectopic beats caused by the altered depolarization of cardiac tissue is the significantly altered displacement of the heart during the whole beat. This special movement is easily visible in echocardiography image sequences. Each ectopic beat has a patient dependent special waveform caused by the irregular depolarization order of the cardiac tissue. The formulation of an ectopic beat and the generated mechanical movement can be simulated with computers.

In ventricular tissues the width of a depolarization front is usually less than half mm. A simulation approximating the dynamics of such a front requires a spatial resolution of $\Delta x \leq 0.1$ mm. Forasmuch the muscle in an adult heart has a volume of 250 cm^3, and so a uniform spatial representation require at least $2.5 \cdot 10^8$ nodes. Taking into account that each node's state is described with at least 50 floating numbers, the necessary storage space rises higher than 50GB, which exceeds by far the available memory of personal computers. The rapid depolarization of the cell membrane is the fastest event in the heart; it blows over in few hundred microseconds, which implies a time step $\Delta t \leq 25$ μs. Since dangerous arrhythmias may require several seconds to become established, the 10^{10} floating point numbers associated with the spatial representation would have to be evolved over 10^5-10^6 time steps. Such a huge uniform mesh calculation currently exceeds all existing computational resources (Cherry *et al.*, 2003).

The spatiotemporal structure of wave dynamics in excitable media suggests an automatically adjustable resolution in time and space. The basic idea of this improvement (Cherry *et al.*, 2000, 2003) is deducted from experiments and simulations (Courtemanche, 1996), which recommend that the function of electrical membrane potential of a ventricular cell $f_V(t, x, y, z)$ in the fibrillating state consists of many spirals or of many scroll waves. An interesting property of these spatiotemporal disordered states is that the dynamics is sparse: at any given moment, only a small volume fraction of the excitable medium is depolarized by the fronts, and away from them, the dynamics is slowly varying in space and time. This idea permits the decrement of necessary computational effort and storage space for regular beats but the total front volume can greatly increase with fibrillating state. By varying the spatiotemporal resolution to concentrate computational effort primarily along the areas with large spatial and temporal gradients, it is possible to reduce the computational load and memory needs by orders of magnitude.

This paper presents an event recognition study performed with ECG signal analysis and 3D heart model using unified neural networks (UNNs). These UNNs are based both on conventional ANNs and SVMs. The main purpose is to evaluate the strength and weakness of the method, and to analyze the cooperation efficiency in malfunction diagnosis.

The rest of the chapter describes the organization of general heart model, the details of the deformable organ representation, the construction of 4D heart model from ultrasound images using AAM applied human cell and tissue model, the time and spatial position dependent heart and torso model, the position of the ectopic beat generators, the adaptively variable resolution wave-propagation method and the parallel processing of these algorithms aided by graphic cards. Using this algorithm, we can simulate the electric and mechanic formulation of ectopic beats on a parallel functioning platform.

3.2. Materials and Methods

3.2.1. Study records

The BSPM signal resource contains 192-channels sampled at 1000 Hz with 12- bit resolution, obtained from the Research Institute for Technical Physics and Materials Science (MTA-MFA) of Budapest. These registrations, which were separated in two independent series, hold various malfunction cases, such as WPW syndrome, atrial and ventricular fibrillation, flutter. Our 12-lead

ECG registrations were recorded at the County Medical Clinic Nr. 4 of Târgu Mureş. These signals were sampled at 500-1000 Hz with 12-bit resolution.

The coarse calibration of the implemented models, such as cell model, tissue model, torso model and spatial heart model was realized using the Series 1 BSPM measurements. The preliminary ECG analyzer system (PAS) uses both the Series 2 of the BSPM records and our 12-lead registrations.

3.2.2. The approach of ECG inverse problem

Most fundamental problems in theoretical ECG can be described by an inverse solution. Their goal is to describe bioelectric cardiac sources based on knowledge of the ECG and the volume conductor properties that surrounds the sources. As mentioned earlier, the most cumbersome point of the inverse solutions consists in its stability. In order to decrease the sensibility of our solution, in our approach the heart model parameters are obtained indirectly. This approximation of the inverse problem is in contrast to methods that directly solve the matrix equation linking electrical sources with electrical potential fields to estimate the inverse ECG solution.

We constructed the PAS based on detailed, a priori knowledge of human anatomy and physiology. It was developed using an ANN, tested and validated by physicians in clinical environment (see Fig. 3.2.). The most important parameter that describes a whole cardiac cycle is related to the site of origin of cardiac activation. This information was obtained using the PAS module, where the output of the ANN provides the initial heart model parameters.

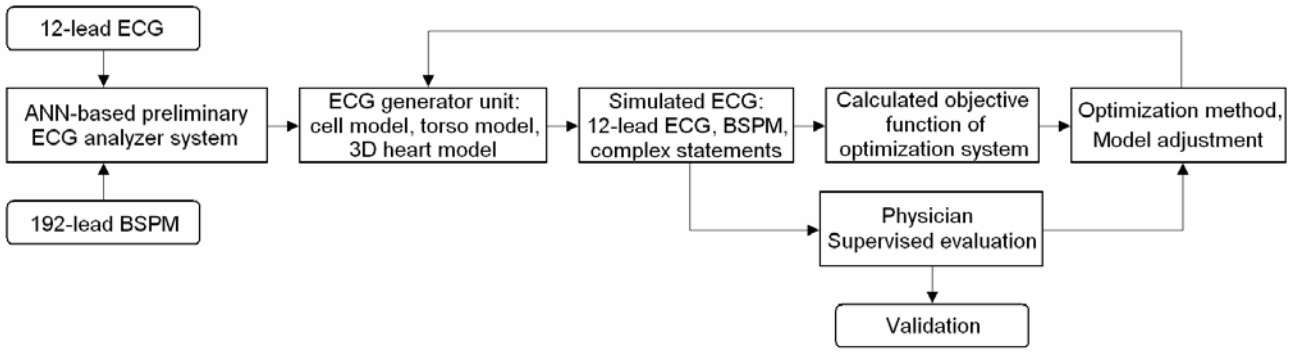

Fig. 3.2. The schematic diagram of the heart analyzer and modeling method

The ECG generator unit uses the cell, tissue and torso model to simulate a BSPM or 12-lead ECG. The objective functions that assess the similarity between the measured and simulated signals were also determined. As the structure of the used models was determined by the anticipative general model creation unit (AGMCU), only the proper parameter values have to be established. These heart model parameters were determined and adjusted with the aid of optimization algorithms or in certain cases by physicians. The simulation procedure is performed until the objective functions satisfy the a priori given convergence criteria. Finally physicians validate the parameters.

3.2.3. ANN-based preliminary ECG analyser system

The high number of heart model parameters implies a high dimensional searching problem. The a priori biological knowledge must be used to drastically reduce the number of necessary dimensions of the parameter space of heart model. The role of PAS unit consists in a rough determination of the cardiac status and state, that is used to initialize the model parameters and to simplify the searching problem for the optimization system.

In the present study, the PAS was developed using a three-layer UNN. This network is capable of mapping the non-linear input-output relationship, with the desired degree of accuracy. An adaptively

weighted coefficient calculation method was used to train the ANN. The input layer incorporates 192 neurons, corresponding to the number of body surface electrodes used in the present simulation study. In case of 12-lead records, the unused channels' signals were estimated. From heuristic considerations, the number of hidden layer neurons was selected to 125. The output layer had 512 neurons, which corresponded to 32 ventricular myocardial segments of computer heart model. Sixteen cardiac cellular units were selected for each of the 32 myocardial segments in the ventricles, and each of these 16×32 = 512 sites was then paced in the forward simulation using the computer heart-torso model, generating the data set for training the ANN.

3.2.4. The chosen cell, tissue, component, heart and torso models

We used the ten Tusscher heart cell model (ten Tuscher *et al.*, 2004) for ventricular and Nygren's model (Nygren *et al.*, 1998) for atrial cells, to investigate the accuracy and efficiency of the simulation algorithm. These models are based on recent experimental data on most of the major ionic currents, such as the fast sodium, L-type calcium, transient outward, rapid and slow delayed rectifier, and inward rectifier currents. With the inclusion of basic calcium dynamics, the contraction and restitution mechanism of the muscle cells can be investigated. The model is able to reproduce human epicardial, endocardial and M cell action potentials, to modify the internal state of the cells and to show that differences can be explained by differences in the transient outward and slow delayed rectifier currents. These properties allow us to study the evolution of re-entrant arrhythmias. The conduction velocity restitution of this model is broader than in other models and agrees better with the available data. We conclude that the applied model can reproduce a variety of electrophysiological behaviours and provides a basis for studies of re-entrant arrhythmias in human heart tissue.

As described in (ten Tuscher *et al.*, 2004), the cell membrane can be modelled as a capacitor connected in parallel with variable resistances and batteries representing the different ionic currents and pumps. The electrophysiological behaviour of a single cell is described as:

$$\frac{dV}{dt} = -\frac{I_{ion} + I_{stim}}{C_{memb}}, \tag{3.1}$$

where V is the voltage, t is the time, I_{ion} is the sum of all trans-membrane ionic currents, I_{stim} is the externally applied stimulus current, and C_{memb} is the cell capacitance per unit surface area. The ionic current is given as the following sum:

$$I_{ion} = I_{Na} + I_{K1} + I_{to} + I_{Kr} + I_{Ks} + I_{CaL} + I_{NaCa} + I_{NaK} + I_{pCa} + I_{pK} + I_{bCa} + I_{bNa} \tag{3.2}$$

where I_{NaCa} is Na^+/Ca^{2+} exchanger current, I_{NaK} is Na^+/K^+ pump current, I_{pCa} and I_{pK} are plateau-, I_{bCa} and I_{bK} are background- Ca^{2+} and K^+ currents. The fast Na^+ current that is responsible for the fast depolarization of the cardiac cells is given by:

$$I_{Na} = G_{Na} \cdot m^3 \cdot h \cdot j \cdot (V - E_{Na}), \tag{3.3}$$

where G_{Na} is the sodium conductance, m represents the activation gate, h the fast- and j the slow-inactivation gate. All detailed equations are described in (Harrild *et al.*, 2000). These gates have mainly a voltage dependent behaviour. The maximal value of the first derivative of the L-type calcium current I_{CaL}, transient outward current I_{to}, slow delayed rectifier current I_{Ks}, rapid delayed rectifier current I_{Kr} and inward rectifier K^+ current I_{K1} and all other described currents are lower with at least two orders of magnitudes than for the fast Na^+ current I_{Na}.

A homogenous spatial cardiac tissue can be modelled in space as a continuous system, using the following partial differential equation:

$$\frac{dV}{dt} = \frac{1}{C_{memb}}\left(- I_{ion} - I_{stim} + \frac{1}{\rho_x S_x} \cdot \frac{\partial^2 V}{\partial x^2} + \frac{1}{\rho_y S_y} \cdot \frac{\partial^2 V}{\partial y^2} + \frac{1}{\rho_z S_z} \cdot \frac{\partial^2 V}{\partial z^2} \right), \tag{3.4}$$

where ρ_x, ρ_y, ρ_z, are the cellular resistivity and S_x, S_y, S_z are the surface-to-volume ratio in the *x*, *y* and *z* directions.

Computational modelling of the cardiac tissue is a useful tool for developing mechanistic insights into cardiac dynamics. The most important parts of human cardiac analysis are atria and ventricular tissue modelling. In this study, the tissue-level excitation mechanism is based on Fast's work (Fast *et al.*, 1998). In this stage, each tissue element works as a secondary generator element. These elements can generate a depolarization wave if the adjacent elements are repolarized; otherwise, the wave propagation is swooned.

Our study uses Harrild's atria model (Harrild *et al.*, 2000) that is the first membrane-based description of spatial conduction in a realistic human atrial geometry. This model includes both the left and right atria, including representations of the major atrial bundles and a right-sided endocardial network of pectinate muscle. The membrane's kinetics is governed by the Nygren (Nygren *et al.*, 1998) formulation for the human atrial cell. An advantage of this model is that it provides an easy perceptibility of atrial activation, particularly in regions that cannot be easily recorded in patients.

It has long been appreciated that cardiac ventricular fibres are arranged as counter-wound helices encircling the ventricular cavities, and that the orientation of these fibres depends on transmural location. Fibres tend to lie in planes parallel to the epicardium, approaching a longitudinal orientation on the ventricular surfaces, and rotating toward the horizontal near the mid-wall. The direct anatomical reconstructions are labor-intensive and time-consuming tasks. In our study, we applied Winslow's ventricular tissue model (Winslow *et al.*, 2000).

As mentioned earlier, the developed heart model has cell, tissue and organ levels. We used the ten Tusscher heart cell model (ten Tusscher *et al.*, 2004) for ventricular and Nygren's model (Nygren *et al.*, 1998) for atrial cells, to investigate the accuracy and efficiency of the simulation algorithm. These models are based on recent experimental data on most of the major ionic currents, such as the fast sodium, L-type calcium, transient outward, rapid and slow delayed rectifier, and inward rectifier currents. With the inclusion of basic calcium dynamics, the contraction and restitution mechanism of the muscle cells can be investigated. The model is able to reproduce human epicardial, endocardial and M cell action potentials, to modify the internal state of the cells and to show that differences can be explained by differences in the transient outward and slow delayed rectifier currents. These properties allow us to study the evolution of reentrant arrhythmias. The conduction velocity restitution of this model is broader than in other models and agrees better with the available data. We conclude that the applied model can reproduce a variety of electrophysiological behaviors and provides a basis for studies of reentrant arrhythmias in human heart tissue.

Our study uses Harrild's atria model (Harrild *et al.*, 2000) that is the first membrane-based description of spatial conduction in a realistic human atrial geometry. This model includes both the left and right atria, including representations of the major atrial bundles and a right-sided endocardial network of pectinate muscle. The membrane's kinetics is governed by the Nygren (1998) formulation for the human atrial cell. An advantage of this model is that it provides an easy perceptibility of atrial activation, particularly in regions that cannot be easily recorded in patients.

It has long been appreciated that cardiac ventricular fibers are arranged as counter-wound helices encircling the ventricular cavities, and that the orientation of these fibers depends on transmural location. Fibers tend to lie in planes parallel to the epicardium, approaching a longitudinal orientation

on the ventricular surfaces, and rotating toward the horizontal near the mid-wall. The direct anatomical reconstructions are labor-intensive and time-consuming tasks. In our study, we applied Winslow's ventricular tissue model (Winslow *et al.*, 2000).

There are several possible different heart structures. To describe various representative cases, we studied our breast MRI records (42 examples) and numerous CT images. These samples lead us to construct a morphological heart structure for simulation, using a segmentation method presented in (Dumoulin *et al.*, 2003). The obtained results were classified by physiologists and used to identify each atrial and ventricular region. The identification process uses as a base Harrild's atria model (Harrild *et al.*, 2000) and Winslow's ventricular tissue model (Winslow *et al.*, 2000).

From the correctly segmented images, we constructed a spatial representation of the heart, using an averaging technique. Such a prototype heart representation must be adjusted taking into consideration the ECG data. The ECG has an important role, as it may describe the electric property of the heart. For example, the mechanic related data obtained from MRI and CT images cannot give us any information about some malfunctions, such as the presence of numerous ectopic beats. An ultrasound image sequence, due to the relation between electric and mechanic properties of the heart, may hold some mechanic information that can be used to identify diverse electric dysfunctions. The obtained heart model prototype contains most mechanic characteristics of the heart, such as tissue mass, wall thickness, internal structure of atria and ventricles. Some electric properties, such as conduction speed of the depolarization wave, are not deductible from captured images and the unique information sources are the parameters determined from the ECG signal. For example, the activation delay between atria and ventricles can be determined from P and R wave distance. The increment speed of the R wave determines the conduction speed on the ventricular tissue. This information was used to construct the electric-mechanic heart model (Szilágyi *et al.*, 2007a).

The anatomical structure of the atria (Harrild *et al.*, 2000) and ventricles (ten Tusscher *et al.*, 2006) was involved in the geometrical model of the heart and torso. The torso, lung, endo- and epicardial surfaces were initially divided into 23647, 38844, 78809 and 89723 sub-units. For each of the units, the constant properties were determined (mass, tissue type but not the tissue state). During an ordinary simulation, the number of these sub-units can vary by demand. The only restriction relies on preserving the ratio among the numbers of sub-units pre-determined for each heart region. Such a heart model could have a maximal spatial resolution of 0.025mm (restricted by the size of computer main memory) that means more than ten billion individual compartments at highest decomposition. To allow a flexible simulation, we may choose the minimal time-slice between 0.01ms and 2ms. Each of these units may contain diverse variable properties, such as tissue state, ionic concentrations or diverse malfunction information such as ischemia. Starting from anatomical information and selected resolution for both time and space, the heart is constructed using tetra meshes. During a simulation with selected spatial resolution, the number of meshes remains constant. However, the mechanical displacement of the heart modifies the shape of each created mesh structure.

The structure of the torso, its spatial position, the relative position and distance of the compartments with respect to the electrodes, and the electrical behaviour of the torso's contents are necessary to be known. As the model has to count with extremely numerous parameter values, the problem cannot be solved in a deterministic way (we have much more unknown values than known equations). That is why a stochastic method (genetic algorithm, adaptive neural networks and fuzzy systems) should be applied to determine the values of the parameters. The search space of the optimization problem was reduced using the genetic algorithm (GA) presented in (Godefroid *et al.*, 2002).

3.2.5. The mechanical functioning of the heart

The cardiac myocardium is an active, anisotropic and elastic tissue. A great presentation of its properties, as well as most problems of the active model of the heart, especially ventricles, is

presented in (Sermesant *et al.*, 2006b). The description law of the tissue is quite complex and contains an active part controlled by trans-membrane potential and a passive element that represents the mechanical elasticity and controlled by blood-flow (Caillerie *et al.*, 2002; Häfner *et al.*, 2002). In this paper we used the simplified mechanical model presented in (Sermesant *et al.*, 2006b). However this model was developed to model the mechanic properties of the ventricular tissue, the model equations assures to use them for atria tissue, too.

The interaction of the myocardium with blood has an important role during a whole cardiac cycle simulation. To treat all phases properly the whole cardiac cycle is divided in the following phases (starting from the end of repolarization of ventricles).

- Filling: the mean atrial pressure becomes higher than ventricular pressure. The blood flow from atria to ventricles. Its intensity is equal with the difference of mean atrial and ventricular pressures. In the first moment a larger quantity of blood is flowing than the flow speed is decreasing to the venal flowing level. The blood is flowing directly from vena to ventricles through atria, without any resistance. It is augmented during the P wave, when the atria are contracted, its volume is reduced, and the pressure difference between atria and ventricles is maximal.
- Ventricular contraction: in contrast to many scientific papers the ventricular contraction is not totally isovolumetric (Sermesant *et al.*, 2006b). In the first stage of ventricular contraction the atrial pressure is still higher, so a low amount of blood in still entering in ventricles. In the second phase of ventricular contraction, when the ventricular pressure is higher than atrial pressure but lower than aortal pressure, the ventricular compression is isovolumetric. In this time the blood is flowing from vena to atria, so the volume of atria is augmented. The last moment of the isovolumetric ventricular contraction consists the maximal heart volume due the filling atria region.
- Ventricular ejection: the ventricular pressure become higher than aortic pressure (the diastolic value of the measure pressure) and the blow is ejected from ventricles to aorta (or to the pulmonary artery, in case of right ventricle). In this time the atria is filling slowly.
- Ventricular relaxation: the ejection is happened and the ventricular pressure is decreasing. Until the ventricular pressure remains higher than atrial pressure, the ventricular relaxation can be considered isovolumetric after that moment the ventricular filling process is started.

We used the penalty constraints for ventricles form (Sermesant *et al.*, 2006b). The used time step for a proper simulation must be less than 1ms. In our consideration, the aortic and pulmonary artery diastolic pressure and the venal pressure is constant. The atrial pressure may vary in function of its state (filling, contracting). To determine to shape of the atria and ventricles under a given internal pressure it is important to know the constituting fiber orientation and volume. In the filling phase the strongest stretching force is applied to the endocardial tissue. This tissue has more longitudinal than circular orientation. In the contraction phase due the special electric properties of the epicardial cells (they have shorter repolarization period) the contraction starts from epicardium. In the middle is situated a high quantity of M cells, that have longest depolarization period. These cells are mostly situated in circular orientated fibers. The highest quantity of blood is ejected when these M cells are contracted.

The left and right parts of atria and ventricles in normal case are separated (in case of a healthy person older than three month). The atria and ventricles are not only electrically but also mechanically linked. In our simulation, the right and left side of the heart is considered linked electrically (the depolarization wave propagation is not obscured in barrier surface between the left and right side), mechanically (each tissue from right side is rigorously linked to the left sided tissues) but not volumetric way (they did not exchange blood).

Between the electric and mechanic properties of the heart, the connection is realized by a special property of the cardiac muscle cells. These cells, in their inner structure, construct (using a

significant amount of Ca^{2+}) and destruct (in repolarization phase) in each heartbeat some mechanical connections that cause the mechanical contraction of the cell. In the fast depolarization phase of these cells (fast Na^{+} channels are opened) the necessary quantity of Ca^{2+} to start mechanical contraction is not available. A massive quantity of Ca^{2+} will be available only after opening of the much slower Ca^{2+} channels. These calcium channels are opened at 10-20ms after depolarization, and the maximal contraction follows in about 80ms (Winslow *et al.*, 2005).

3.2.6. Mathematical description of the compartments

The heart is represented as a set of finite homogenous elements, called compartments. Since their size is obviously much larger than that of actual biological cells, these units effectively represent small tetrahedron-shaped groups of biological cells, and must capture their macroscopic behaviour rather than the microscopic behaviour of individual cells. Microscopic inter/intracellular interactions, such as ionic flow across membrane boundaries, were described in the cell model presentation. Compartment connectedness was defined as the set of rules that establish which units are considered directly connected to a given one, for the purposes of electrophysiological simulation, such that myocardial activation may be directly propagated between them. These rules are based on atria and ventricles anatomy; they define the neighbourhood for each unit.

Each compartment was considered homogenous, constructed by only one type of tissue with well-defined properties, such as cell type, cell state, cell activation potential (AP) function. The type of cells determines the electrical propagation properties, but no additional considerations were taken in, such as tissue fibre torsion and so on. The environmental parameters such as 4D position (x, y, z spatial coordinates and time), conduction speed of stimulus, weight and connection with neighbour structures, localize each unit.

The heart behaviour is characterized by the following parameters:

1. Type of cells: T; (such as ventricular muscle cell or Purkinje fibre cell)
2. State (time varying): S; (normal, ischemia)
3. Function of activation potential variation: $AP(T,S,t)$; (each compartment has a specific activation potential function that depends from cell type and state)
4. Space position in time: $Pos_C(x,y,z,t)$; (in every moment a given compartment has a spatial position)
5. Conduction speed of the stimulus: $CS(T,S)$; (it is type and state dependent)
6. Weight of the contents of the compartment: M;
7. Connections with other compartments;
8. The position of the electrode: $Pos_E(x,y,z,t)$; (the measuring electrode has a time dependent spatial position)
9. The relative resistance of the electrode: $R_{E,C}(Pos_C, Pos_E)$ (the time dependent electric resistance of the human tissue from the studied compartment to a given electrode).

Because the main ion channels situated inside the cells have a quite complicated behaviour (with lots of unknown parameters), the activation potential function of the compartment was considered as basic input parameter (we determine an AP function – based on cell model - with static shape for each cell type and state). Due to contractions of the heart, respiration, and other disturbing phenomena, the position of compartments was considered time varying. The mathematical expressions presented in the followings, that describe compartment behaviour are time variant.

Let V_C be the potential of an arbitrary compartment C: $V_C(t) = AP(T,S,t-\tau_C)$, where τ_C is the time the stimulus needs to reach compartment C. The activation potential function that varies from cell type T and state S, has a short delay τ_C due to activation propagation until compartment C.

The measured potential E_j, generated by compartment C_i is:

$$E_{j,C_i}(t) = V_{C_i}(t) \cdot R_{E_j,C_i}(t) - E_{GND,C_i}(t), \tag{3.5}$$

where $R_{E_j,C_i}(t)$ represents the time varying resistance from compartment C_i to electrode E_j. Using bipolar electrodes, the value measured on the reference electrode E_{GND} will be subtracted. As all compartments have an accession to the measured potential on each electrode, the measured voltage on electrode E_j will become the sum of each $E_{j,C_i}(t)$ generated by compartment C_i:

$$E_t(t) = \sum_{i=0}^{N-1} [V_C(t) \cdot R_{E_j,C_i}(t) - E_{GND,C_i}(t)], \tag{3.6}$$

where N is the number of compartments. These equations determine the measured electrical potentials and the inner mechanism in the heart. During the simulation, these voltages were determined for each compartment and electrode for every time-slice (mostly between 0.1ms and 2ms depending from the phase of AP function).

3.2.7. Anatomical model construction of the heart

The spatial representation of the myocardium is based on three main aspects: fiber orientation, functional separation and shape. The shape of the organ and its volumetric analysis was performed using ultrasound registrations. The complex measuring, processing and shape construction method uses AAM and the detailed description can be found in (Szilágyi *et al.*, 2007b). The fiber orientation cannot be obtained from ultrasound images, so their determination by clinical way was not possible. To solve this task we used the descriptions from (Quan *et al.*, 1998; Hsu *et al.*, 2001).

To increase the performance of the model it is necessary to mark each anatomical region of the heart. The labeling was performed in (Pommert *et al.*, 2001) using atlas description and segmented images from the Visible Human Project. We used the labeling described in (Pommert *et al.*, 2001).

The basic geometry of the heart can be extracted from various medical imaging modalities. From these images we obtained the volumetric representation of the heart (Szilágyi *et al.*, 2007b), but the functional labeling was realized using information according to (Pommert *et al.*, 2001). The obtained functional elements, such as ventricle walls, have to be triangulated in function of selected resolution.

3.2.8. Connections between electric and mechanic properties

The time-varying evolution of the cardiac volume is determined by the interconnection of electrical and mechanical phenomena. In a whole cardiac cycle there are two extremity values. The maximal volume can be coupled with the starting moment of ventricular contraction. The depolarization wave normally starts from the sino-atrial node (SA) and propagates through the atrioventricular node (AV) and ventricles. The moment of minimal volume shortly precedes the termination of ventricular contraction, but is much more difficult to identify, due to the dead time of a normal cardiac cell. This delay is caused by the strange property of a regular cardiac cell, whose electric response is most directly caused by the depolarization wave (fast Na+ channels), but the mechanical contraction is controlled by the much slower Ca^{2+} channels. The calcium channel opens at 10−20ms after depolarization, and the maximal contraction follows in about 80ms (Winslow *et al.*, 2005).

3.2.9. Deformable heart models

A deformable model must have the necessary elasticity to comprise diverse information referring to the same thing. This parameter selection and adaptation must be realized in a robust way, otherwise the model will be quickly polluted with un-adequate solutions. In our consideration the dynamic handling of a pre-determined triangulated heart is computationally costly and has not the adequate precision. The main reason of it is the superfluity of the processed parameters that describes the heart's shape. A more intelligent way is the reduction of parameters to a reasonable level. Although many algorithms were developed to decrease a search space in a multi dimensional hyperspace (Godefroid *et al.*, 2002), the yielded result from such algorithms may not succeed most cases. The main reason of this consideration is the general formulation of the searching problem that obscures to reduce significantly the searching space. A more clever way is the usage of the known a priori information that can be used to generate a simpler description of the studied organ, and to formulate the aim of the study more generally. Decreasing drastically the initial parameters, general space reduction method can be more useful. The representation of this idea can be seen in Fig. 3.3. The triangulated form of the organ may describe the surface (inner and outer) of the object. Considering a pre-defined spatial resolution *r*, and temporal resolution *t* the necessary elements to describe a whole beat can be determined as: $n = \sum_{i=0}^{[t_{beat}/t]} S_{organ,t_i} \cdot r^{-2}$. For example, using a spatial resolution of 1 mm and a temporal resolution of 0.1 ms, having an estimated average surface of 250 square mm and simulating a 1 second duration period, the necessary element n will be approximately $n = 2.5 \cdot 10^8$. Moreover, if the patient manifests different types of heartbeats that can be easily determined from the clustered ECG waveforms, the necessary parameter number will increase by *c* times, *c* representing the necessary number of clusters and could be in order of hundreds. If we want to realize a spatial representation using volume tetrahedrons and not triangles, the estimated number of necessary basic elements will be: $n = c \cdot \sum_{i=0}^{[t_{beat}/t]} V_{organ,t_i} \cdot r^{-3}$. Using the same resolution and considering the number of clusters 200 we obtain a result as high as $n = 5 \cdot 10^{12}$. It becomes clear that such a representation cannot be handled in real time. Moreover, the resolution has a great impact on the necessary elements number, being on the third power harmonic to it.

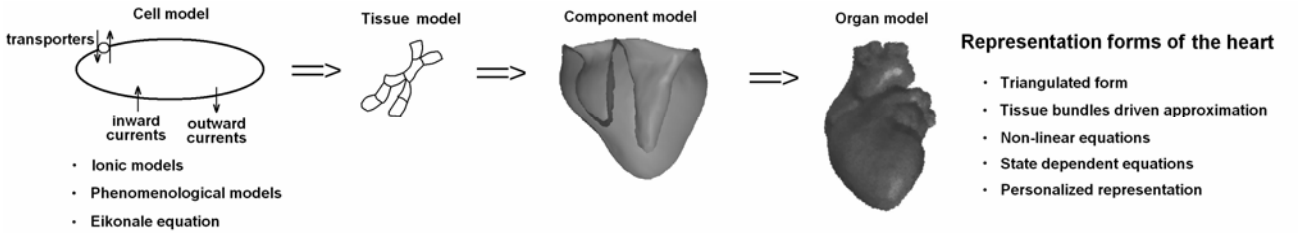

Fig. 3.3. The hierarchical structure of the heart model is presented here. In the right side of the image the main representation forms of the heart is enumerated. Each representation form has a more complex and abstract structure than its predecessor and enables a more general formulation of the personalized dynamic shape of the heart.

To overcome the above-mentioned problem of necessary elements, we introduced a tissue driven approximation. If we describe each involved tissue with a parameter array that contains its orientation, mass, size, elasticity and connections (as restrictions) the number of necessary parameters will decrease drastically. Using a mathematical equation that describes the state of the cells in the studied tissue the electrical properties can be represented using $n_{tissue} = r_{tissue} \cdot n_{descr}$ parameters. The used tissue resolution can be described by mathematical equations, so a proper approximation can be realized using a logarithmically harmonic relation between resolution and equation coefficient number.

The necessary parameter number for a tissue will be in order of hundreds. The atria and ventricles can be approximated almost correctly using about 200 tissue branches. The week point of this approximation is the time resolution that can be handled as efficient as in case of triangular (or tetrahedral) representation. The obtained number of parameters $n = c \cdot \sum_{i=0}^{\lceil t_{beat}/t \rceil} n_{tissue} \cdot \ln(r) \approx 3 \cdot 10^5$ (using the above mentioned resolutions).

Using non-linear equations to describe the smooth transitions between successive states, the time resolution problem will become much more manageable. The estimated state series of the studied organ may form a Markov chain. Using this approximation only the latest estimated state value is important, so the necessary parameter number is drastically decreased. The obtained parameter number is: $n = c \cdot \ln(t_{beat}/t) \cdot n_{tissue} \cdot \ln(r)$. In this case the obtained result was just higher than ten thousand. All described approximation was not able to threat the global state dependent event. For example a normal heart beat duration may wary between half and two seconds. Investigating each period it can be observed that the principal elements are just delayed, but the most important characteristics are almost the same. For example the QRS shape or T shape is almost the same in case of normal beats with different duration. The amount of parameter reduction cannot be described using a simple formula, due to the different similarity coefficients for different beat types. A good approximation of the necessary parameters can be determined as: $n = n_{non-linear} \cdot \sum_{i=1}^{c} \lambda_i$. The coefficient λ_i describes the amount of similarity for each clustered waveform. From experimental measurements we obtained a parameter decrement in order of 10 using 200 clusters.

The most advanced patient specific description uses the patient data to enhance the model accuracy. Special waveforms can be handled much easier, but significant parameter decrement cannot be obtained at low resolution. Obtaining a reduction in order of 2 we obtained about 500-850 parameters. This number is heavily patient dependent.

3.2.10. Adaptively varied resolution

As presented earlier, the simulation of each compartment at each small time slice needs a powerful computer. To enhance the simulation performance we can increase the computational power of the simulation platform and modify the algorithm such a way, that it determines the most important data more accurately. Anyway, due to the limited computational power of the computer, the simulation must contain approximations. In our formulation, the simulation task can be performed in the following manners:

1. determine a pre-defined time and space resolution (not adaptive);
2. guarantee an estimation error that is lower than a pre-defined threshold value (adaptive);
3. guarantee a pre-defined processing speed (adaptive).

In the first case nothing is known about the simulation speed and estimation error. The simulation algorithm uses pre-defined time and space resolution and the result's performance (speed and accuracy) can only be estimated. The second processing manner has an adaptive behaviour. Resolution is not important, but the estimation error is. This approximation of the problem leads to low estimation error, but we have no guaranteed processing speed. The processing speed may highly depend on the heart's state (see Section 3.4. for details). The third approximation of the problem is useful to create an on-line processing system. However, in this situation, we have the pre-defined simulation speed, but we do not have any control regarding simulation accuracy. In both adaptive approximations of the problem, the scalability of the simulation is realized in the same manner.

During the simulation problem, the key element is the compartment. Each compartment has a time dependent voltage that is increased by depolarization waves and decreased due the self-repolarization

process. Both high voltage increment and a high diversity of the compartments (adjacent compartments can have significantly different voltage levels) increases estimation error. This error is estimated by the following formula:

$$err(C,t) = \lambda_d \cdot \frac{dV_C}{dt} + \lambda_v \cdot \sum_{i=0}^{N-1} \{\lambda_{C,C_i}(t) \cdot [V_{C_i}(t) - V_C(t)]\}^2 . \quad (3.7)$$

The estimation error is weighted by λ_d (derivative weight) and λ_v (voltage weight). The derivative term contains the voltage's increment caused by the fast Na^+ ionic current during depolarization and by Ca^{2+} and K^+ currents during repolarization phase. In the second term, λ_{C,C_i} represents a weight between compartments C and C_i. This weight is considered time dependent, as the distance among compartments may vary during simulation. A high voltage difference may increase estimation errors dramatically. From this formula emerges, that the most sensitive moments are the moment of depolarization especially in presence of multiple depolarizing fronts. From the determined estimation error, its variance in time, and the initial settings referring to error threshold or simulation speed, the necessary time and space resolutions are determined. However, during a whole heartbeat the estimation error may vary, that implies the spatial and temporal modification of the used resolution. In order to assure a good alignment among diversely selected resolution slices, each high-resolution value must be selected 2^i times shorter than the initial reference resolution (this is the coarsest resolution in both time and space). To assure proper resolution values, each determined variable is rounded down to the closest allowed level. Data on all resolution levels are synchronized only after one full time step on the coarsest grid level is completed.

The efficiency of the method arises from its ability to refine or to coarsen the spatial and temporal representations of sub-units automatically and locally. The approximation errors are estimated on each sub-units to determinate the lowest necessary resolution to keep under a pre-defined tolerance value.

The most important factor that demands a finer temporal and spatial resolution to keep the estimation errors under the pre-determined tolerance level, is the fast depolarization wave of the atrial and ventricular tissue cells. The simulation program varies the resolution in concordance with the first derivative of the activation potential.

3.2.11. Parallel processing

The implementation of the method allows high parallelization. As sub-unit potential values are determined independently from each other at all possible resolution levels, these tasks can be processed on separate processors with reduced communication needs. The hardware accelerated programmability of graphical processing units (GPUs) (that may contain up to 320 individual processor units) admits the development of programs called shaders vertex and fragment shaders, which are loaded into the graphics card memory for replacing the fixed functionality. The fragment shaders are used in our method to perform the SIMD commands for each sub-unit. From architectural concepts results that the GPUs are most efficient in case of more than 1000 similar tasks, which is caused by the relatively long video memory delay.

3.2.12. Validation of the model

Our model validation was performed by the comparison of the simulated ECG signals and generated ultrasound contour images with measured data. At every moment from the spatial position of the heart and of the measuring ultrasound electrode the observable plan can be determined. Performing

an image filtering and segmentation, the observable contours can be determined. The simulated object intersected with a visualizing plan generates an intersection. If the obtained data is transformed to fit with ultrasound images, the simulated and measured contours can be compared. To evaluate the obtained results a better evaluation relation is needed than a simple root mean square error (RMSE). The obtained result (contour) may be displaced or rotated that seriously disturbs a simple comparison method. In our consideration a proper estimation uses AAM, and evaluates the obtained parameter differences between simulated and measured contour.

This approximation eliminates the displacement or rotational errors, the image can be magnified (Procoust alignment), and only the main characteristics, such as shape is took into consideration. The steps of AAM were presented in (Szilágyi *et al.*, 2007b). The simulated ECG signal is compared with the measured signal. However the correct comparison of the signals needs a transformation. In estimation error calculation the directly determined RMSE cannot be taken into consideration due to some perturbing phenomena such as baseline displacement.

To realize a proper comparison the measured signal must be filtered. The role of the used filter is to eliminate various artifacts such as abrupt baseline movement and various noises. There are other perturbing phenomena that are patient dependent, for example the baseline elevation or depression caused by the inspiration-expiration process. These displacements are not caused by artifacts, but the perturbing phenomena are not included in the simulation model, so the impact of these events cannot be simulated. The best way in our consideration is to determine the most important patient and ECG wave dependent parameters, such as QRS duration, R and T wave's positions and amplitudes and to calculate a weighted error among these parameters. This approximation is not only easier to apply, but has significantly much robustness.

3.2.13. Simulation platforms and environment

Experiments were performed on four platforms with different configuration shown in Table III.1. The size of memory has limited the maximal spatial resolution to 0.01mm for normal beats and 0.1mm for ventricular fibrillation. The lowest temporal resolution was selected to 1μs. The simulation program was developed in C++ programming environment and the shader programs were developed using ATI's graph library (shader model 3.0).

Table III.1. Configuration of the simulation platforms involved in this study

Configuration	CPU	GPU	RAM
1st	Athlon 3000+	nVidia 6600	1GB DDR
2nd	Core2 Duo 6400	ATI 1950 Pro	1GB DDR2
3rd	Core2 Duo 6400	2 × ATI 1950 Pro	1GB DDR2
4th	Pentium D805	nVidia 7600GT	1GB DDR2

3.3. Results

A parameter classification algorithm was applied to distinguish normal QRS complexes from abnormal ones, in order to determine the specific differences between the normal and abnormal parameter values. For normal cases the detection ratio is practically 100%. The signals presented in Fig. 3.7. were obtained via simulation using the initial parameter set for a normal and abnormal (bypass tract) situation.

Figure 3.5. presents a series of cell activation simulations. In Fig. 3.5(a) and (b) the simulation of the cell depolarization mechanism is presented. The excitation rises at the sino-atrial node. The state of

the cells is illustrated with a 200ms delay from the excitation moment. Figures 3.5.(c) and (d) show the activation moment of the cardiac cells. The neighbor slices have 10mm distance from each other, so a totally 5cm wide ventricular tissue is visualized. The position of the slices is considered at a repolarized moment. Table III.1. shows the efficiency of simulation for different cases. The evaluation of the simulated results was made by physicians. The performance was determined as the ratio of correct and total decisions.

Table III.2. informs about the parameter reduction using various formulation of the simulation problem. The used spatial and temporal resolution was 1mm and 0.1ms. The simulated results were averaged for normal and ectopic beats. The results were determined from the single available ventricular fibrillation record.

Table III.2. The whole simulation and visualization time of a one second duration event performed on involved platforms using two spatial and temporal resolutions

Used Model Formulation	Normal beat (19 samples)	Ectopic beat (7 samples)	Ventricular fibrillation
Triangulated description	4.97×10^{12}	6.77×10^{12}	9.21×10^{12}
Tissue bundle parameters	297005	311784	693445
Non-linear equations	11894	19534	514993
State dependent equations	1510	6112	502997
Personalized representation	548	2945	492885

Table III.3. The whole simulation and visualization time of a one second duration event performed on involved platforms using two spatial and temporal resolutions

Configuration and resolution	Normal beat	Ectopic beat	Ventricular fibrillation
1st – (1 mm, 0.2 ms)	11.3 sec	37.15 sec	4 min 2 sec
2nd – (1 mm, 0.2 ms)	1.32 sec	5.21 sec	33.11 sec
3rd – (1 mm, 0.2 ms)	0.7 sec	2.68 sec	17.13 sec
4th – (1 mm, 0.2 ms)	2.37 sec	9.03 sec	57.48 sec
1st – (0.1 mm, 0.05 ms)	1h 11 min	4h 22 min	1d 5h 11 min
2nd – (0.1 mm, 0.05 ms)	9 min 20 sec	37 min 10 sec	3h 53 min
3rd – (0.1 mm, 0.05 ms)	5 min 3 sec	19 min 17 sec	1h 59 min
4th – (0.1 mm, 0.05 ms)	15 min 40 sec	1h 6 min	6h 42 min

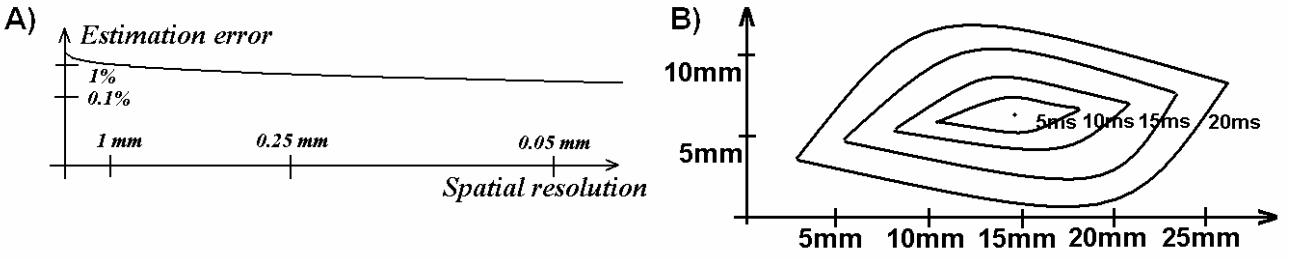

Fig. 3.4. (A) The relation between the applied spatial resolution and resulting estimation error simulating a normal beat, (B) The simulated depolarization wave in anisotropic ventricular tissue: from the pace origin, the wave front propagation is plotted with 5ms resolution

Table III.3. informs about simulation times using various configurations. All simulation tasks were performed with adaptive time and spatial resolution, and Table III.3. show the finest ones among them. The simulated normal and pathological cases have one second duration. In all cases, the number of simultaneously performable tasks has the order of thousands. The conventional simulation (constant resolution) was performed only for 1mm spatial and 0.2ms temporal units, and was slower about 200 times in normal and 35 times in fibrillating case.

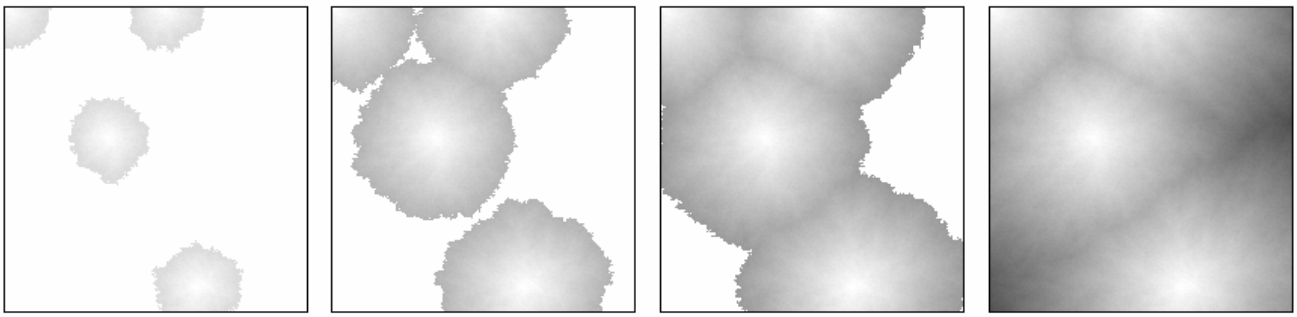

Fig. 3.5. Propagation of the depolarization wave in a ventricular tissue area during ventricular fibrillation. The visualized area contains four ectopic points. The white excitable area is fast depolarized and the arisen wave fronts extinguish each other. The color of each point represents the voltage level for each individual cell

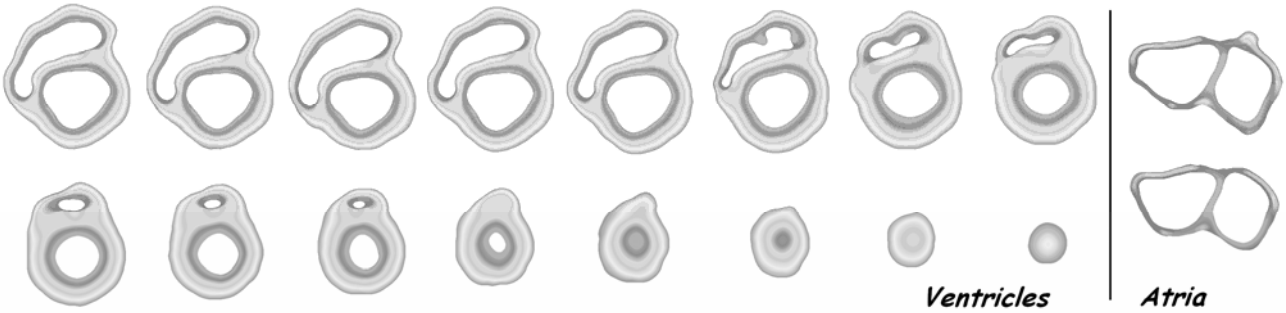

Fig. 3.6. The propagation of the depolarization wave in the ventricular and atrial tissue. In the left side of the image the consecutive ventricular slices are presented from the ventricular top region to apex (using 5mm inter-slice distance). The propagation of the depolarization wave is presented, simulating a normal heart beat. The right-sided two images present atrial slices (5mm distance)

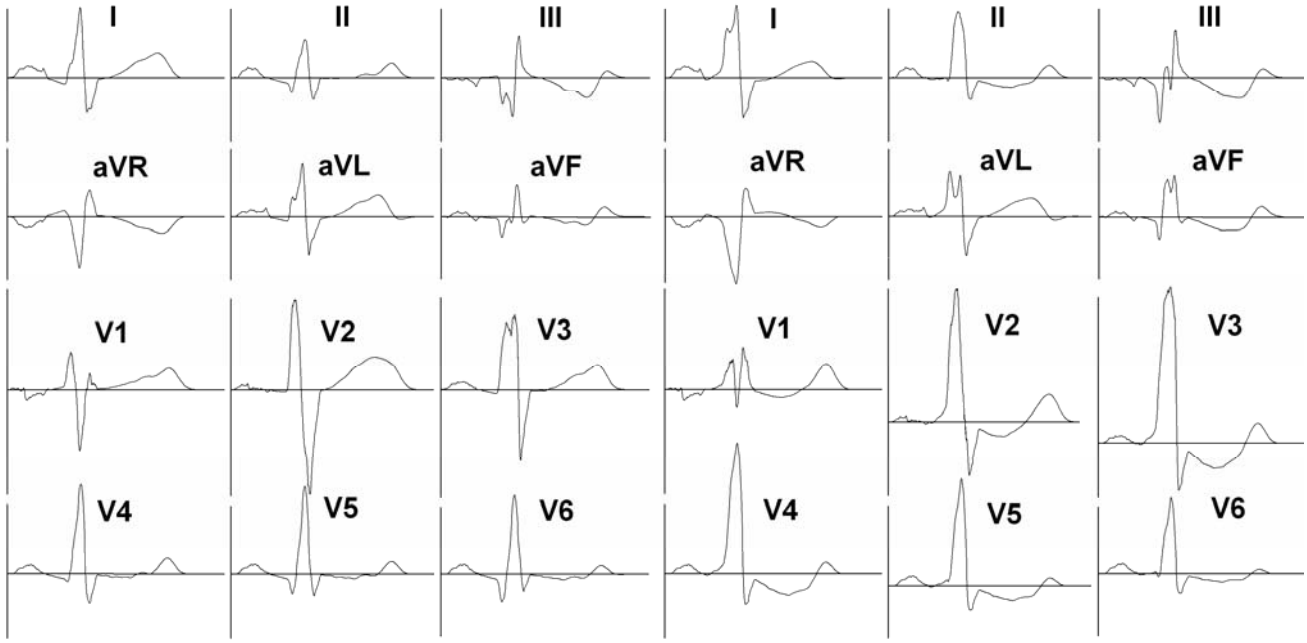

Fig. 3.7. Simulated ECG signal in normal and abnormal case (Wolff-Parkinson-White syndrome)

Figure 3.4.(A) elucidates the relation between estimation error and spatial resolution. The obtained results are almost similar for pathological cases. The propagation of the depolarization wave for a anisotropic tissue is presented in Fig. 3.4.(B). Figure 3.5. presents the collision of the depolarization waves.

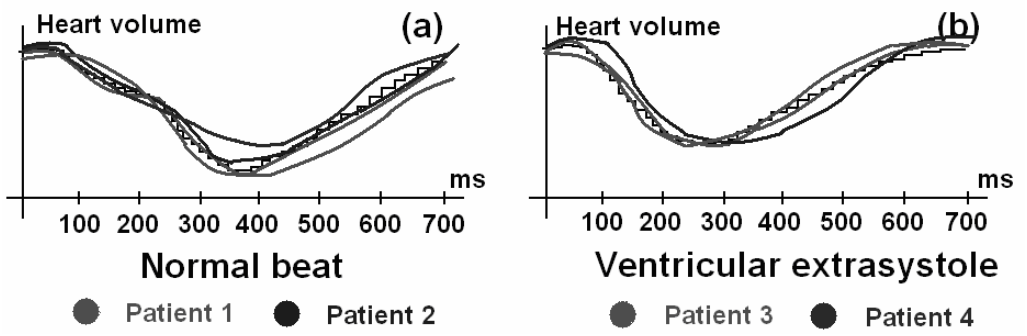

Fig. 3.8. Representation of the averaged heart volume for the most „typical" R-R beat (included shape and duration analysis) for the averaged patient. The volumetric variance of each patient is represented by the four colored continuous lines. The graph visualizes a normal cardiac cycle (a) and a patient specific ventricular extra-systolic cycle (b).

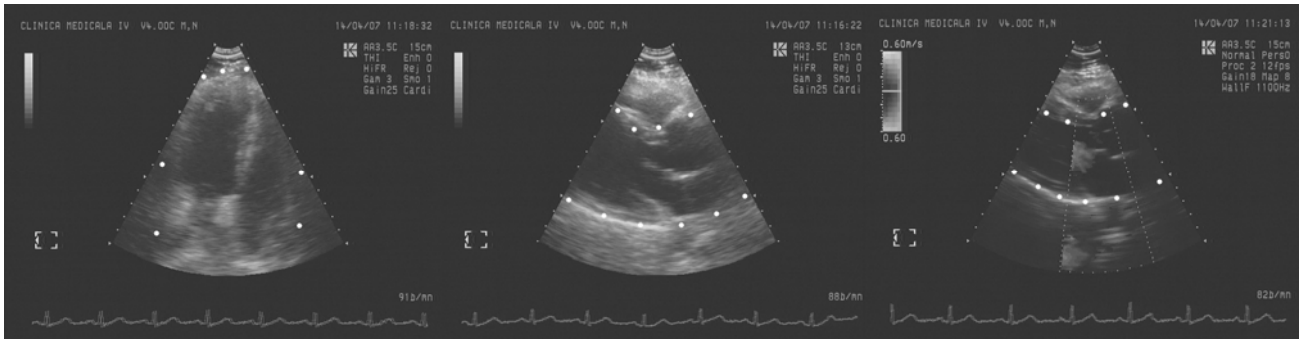

Fig. 3.9. The visualization of some selected control points from various echocardiographic images, represented by white dots. In the third image, the blood movement speed is represented by the upper light area. The light spot situated in the bottom is a measuring artifact.

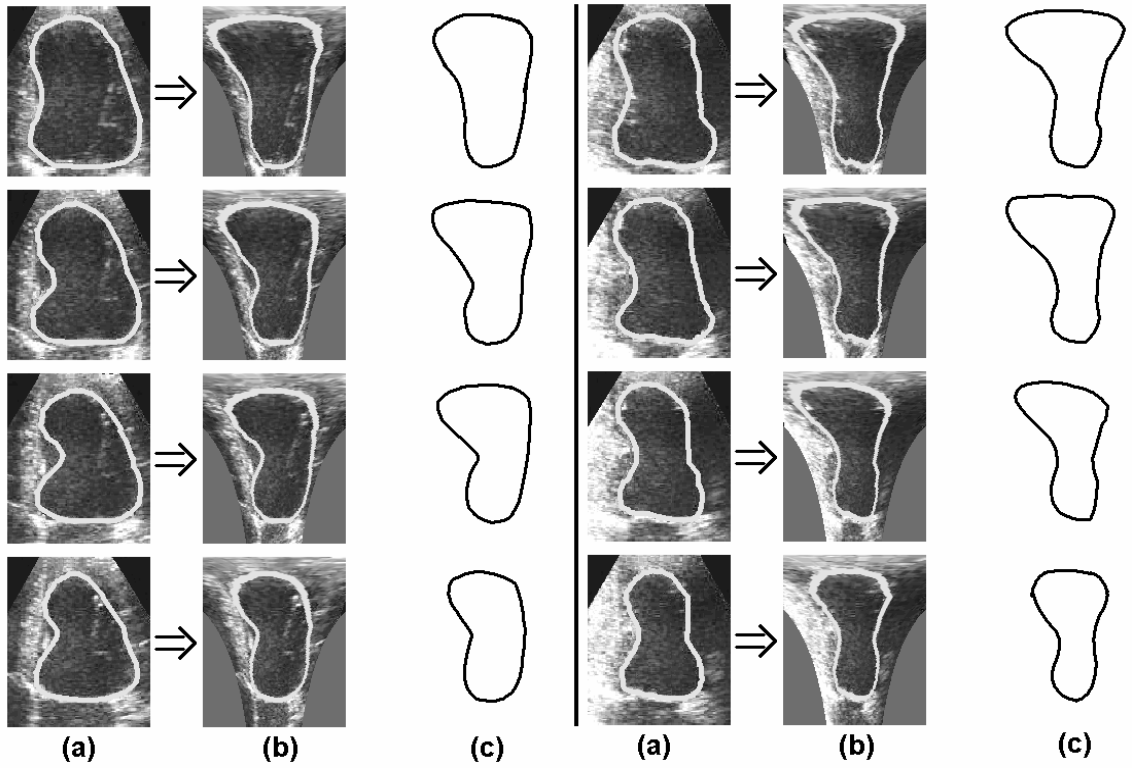

Fig. 3.10. Results of shape reconstruction: (a) and (b) time varying 2-D contour of the left ventricle before and after normalization, (c) the shape of the simulated left ventricle

The depolarization of various ventricular and two atria slices for normal case is presented in Fig. 3.6. The simulated ECG signal in normal and abnormal case (Wolff-Parkinson-White syndrome) can be seen in Fig. 3.7. The representation of the averaged heart volume for the most „typical" R-R beat (included shape and duration analysis) determined for four patients are presented in Fig. 3.8. In Fig. 3.9., the visualization of some selected control points (used by the AAM) from various echocardiographic images is observable. The Fig. 3.10. present the reconstructed and simulated 2-D contours of the left ventricle. The elapsed time among each consecutive slice is 20ms. The spatial representation of the ventricles during a normal heart beat is presented in Fig. 3.11. The resting and contracting tissue is visible in the first and second rows, respectively. In this simulation, a 0.2mm spatial resolution was used.

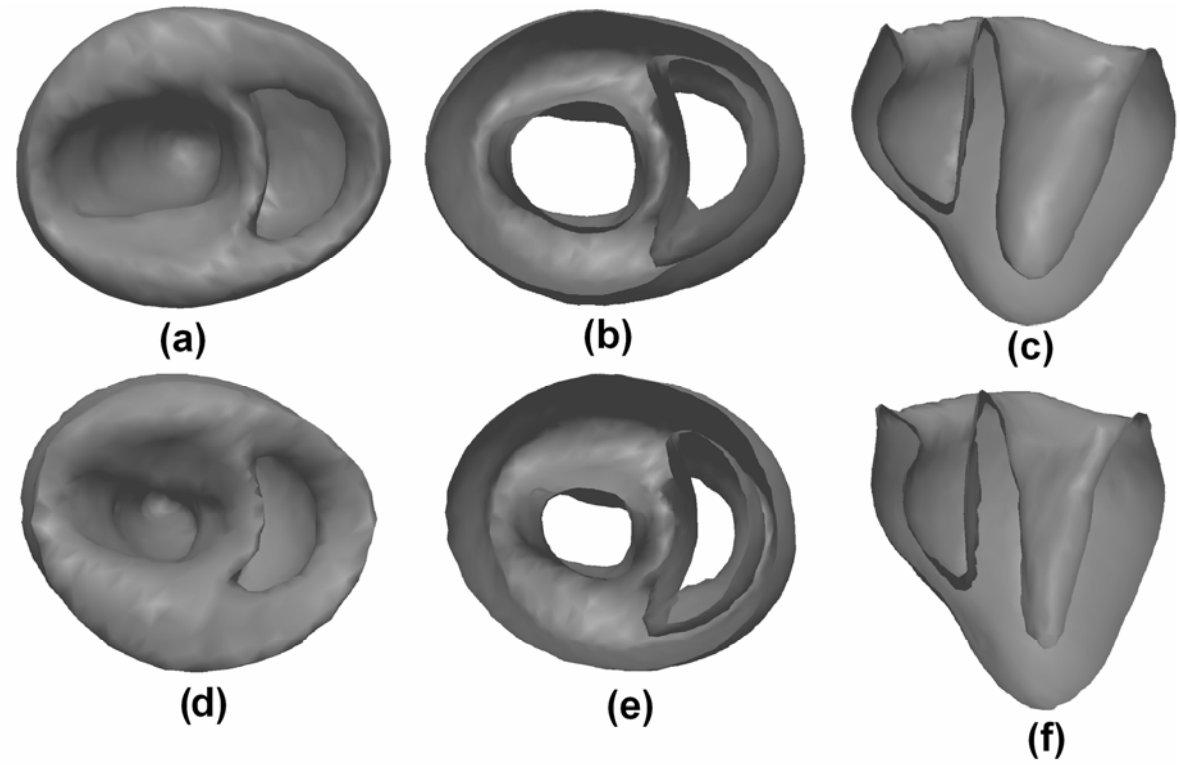

Fig. 3.11. The spatial representation of the ventricles in resting ((a), (b) and (c) images) and contracted ((d), (e) and (f) images) state during a normal beat as follows: (a) and (d) upper view, (b) and (e) sectioned bottom view, (c) and (f) sectioned frontal view

Table III.4. shows the efficiency of simulation for different cases. The evaluation of the simulated results was made by physicians. The performance was determined as the ratio of correct and total decisions.

Table III.4. Simulation performance for normal and pathological cases

Pathological case	Decision number	Failed decisions	Performance
Normal	44	0	100.00%
Ectopic beat	21	0	100.00%
WPW syndrome	14	1	92.86%
Atrial flutter	22	1	95.45%
Atrial fibrillation	18	1	94.44%
Ventricular fibrillation	19	1	94.73%
Re-entry mechanisms	19	2	89.47%
Triggered activity	36	2	94.44%
Aberrant ventricular conduction	21	1	95.24%

3.4. Discussion and Conclusions

Table III.1. presents four configurations with shader model (SM) 3.0 ready GPUs. The 3rd configuration is the most powerful one, due to the cross-fire connected ATI 1950 PROs. The type of CPU (Intel or AMD), the clock speed (1.86-2.66 GHz), the core number (solo or duo) and memory bandwidth (DDR or DDR2) did not play an important role because a powerful video card has a much higher floating-point calculation power (internally has 8-36 pixel shader units). In all cases, the size of memory was selected at 1GB that restricts the applicable maximal resolution.

From Table III.2. can be concluded that the performance of various parameter reduction methods may differ significantly from the studied phenomena. We could observe in all presented cases the decrement of necessary parameters in case of tissue bundle representation. However, the impact of the representation is highest in normal case and lowest in case of ventricular fibrillation. Moreover this tendency is observable indifferently from the used formulation method. The response of this manifestation can be deducted from the nature of the presented phenomena. For example the ventricular fibrillation has no general or patient specific manifestation, so the estimated organ shape could be estimated using the measured ECG and the recorded ultrasound images, but not from a priori data. The ectopic beats have a strong patient specific behaviour.

Table III.3. summarizes a simulation for normal beat, ectopic beat and ventricular fibrillation state. The finest spatial and temporal resolution was 16 times greater in case of normal beat, 32 times greater in case of ectopic beat and 64 times greater in case of ventricular fibrillation. This result is in perfect concordance with the complexity of the studied events. A more complex event implies longer depolarization waveform that enforces the processing algorithm to choose smaller spatial and temporal steps.

From the data of Table III.3. we could observe the clear dominance of GPUs. Although the spatial and temporal resolution limit the necessary simulation time, in all cases a massive parallelization could be performed. All shader programs were created using a low-level programming environment. We could observe that in normal cases, the active depolarization wave front has a much lower size than in case of ventricular beat of ventricular fibrillation. In a complex biological situation, as the wave front size grows, the parallelization becomes harder. This assumption is reflected by the simulation times from Table III.3. It is observable that a normal heart has at least 20 times lower front area than a fibrillating one. As a cardiac muscle (especially left ventricular), become less homogeneous, the relative simulating speed decreases. Some basic characteristics of the heart such as size, maximal tissue volume and left wall width, significantly influence the maximal performance.

Figure 3.4.(A) represents the estimation error in function of spatial resolution. The temporal resolution has almost similar effect, but with lower impact. From measurements, we could deduct that estimation error is free from physiological state. In normal and pathological cases, we measured almost the same error values.

In this paper, we have discussed new features and new capabilities of a space-time adaptive heart-modeling algorithm. We have shown the algorithm's ability to simulate inhomogeneous and strongly anisotropic tissue regions (see Fig. 3.4.(B)).

This method can provide a variety of advances in addition to reductions in time and memory requirements. For example, the algorithm allows a more complex ionic model, higher spatial resolution of a non-linear tissue model. Similarly, it allows the use of higher spatial and temporal resolution to reduce the angle dependence of propagation patterns in spatial domains with rotational anisotropy or to verify that a calculation is sufficiently resolved, so that an increase in resolution does not affect the results (see Fig. 3.4.).

From Fig. 3.5. we can conclude that the diverse depolarizing wave fronts are unifying and the arisen wave fronts extinguish each other. The simulation was done on a simple ventricular tissue surface to be able to verify the obtained results and to compare with other simulation methods, such as presented in (Cherry *et al.*, 2000). We can affirm that the obtained front shapes were almost the same.

The propagation of the depolarization wave in the ventricular and atrial tissue is presented in Fig. 3.6. The propagation of the depolarization wave can be seen in the consecutive slices. Using this view, we can supervise the propagation of the depolarizing waves in various circumstances, such as normal beat, ectopic beat, Wolff-Parkinson-White (WPW) syndrome and ventricular fibrillation.

Besides the wave propagation, the simulated ECG can be visualized (see Fig. 3.7.). The simulation model combined with a forward heart model presented in (Szilágyi *et al.*, 2007a) can yield a simulated ECG. For example in Fig. 3.7. the results obtained from simulation model combined with a forward heart model presented in (Harrild *et al.*, 2000) can yield a 12-lead ECG for many pathological cases (in Fig. 3.7. a normal beat and a pre-excitation beat is presented).

The evolution in time of the heart volume during a normal and an ectopic (ventricular extra-systole) RR period is presented by Fig. 3.8.(a) and (b). Four different patient data was averaged in normal case, but the fourth patient did not produce ventricular extra-systolic beats. As the depolarization wave in case of an ectopic beat starts from the ventricular area, the minimal volume is obtained earlier (the delay caused by the AV-node is skipped), and at a higher value compared to normal beats (the contraction of the heart is not optimally synchronized). The first moment of LV volumetric calculation (t = 0ms) was considered at the moment of maximal positive deflection of the ECG signal.

The proper selection of the landmark points to train AAM is an important step of spatial shape generation. The selected points from Fig. 3.9. must suffer a transformation in order to create the normalized shapes for AAM. The normalization is an un-avoidable step of ultrasound image process due the recording mechanism of the echocardiographic images (the magnification value at a given image pixel depend from the position of the measuring electrode).

From Fig. 3.10. we can observe that the generated slices from the created deformable model have quite similar shapes (only after Procoust alignment process). From the generated and recognized shapes and ECG waveforms the deformable model can be validated. These shapes were generated during a normal beat. The realized shapes for an ectopic beat may differ significantly from the segmented contour. To validate the method in all circumstances we need more clinical measurements.

It is important to study the shape of the heart during a whole cycle. Despite various perturbing phenomena, it was possible to realize the spatial representation of the heart or some segments of it (see Fig. 3.11.). Using this kind of approach, we can balance between performance and accuracy. The optimal solution may depend on the used platform, studied events and the available time.

Table III.4. reveals that the 3D heart simulation (Szilágyi *et al.,* 2003d) succeeds in most cases, such as WPW (Wolf Parkinson White) syndrome, pre-excitations, and tissue activation modeling. The performance in case of re-entry mechanisms and triggered events is slightly decreased due to the hazard nature of the events. The application in practice of the model has several obstacles, which can be classified into the following groups:

- Effects of internal and external perturbations (such as environment, sympathetic and parasympathetic despondence);
- Lack of information on different elements of the model;
- Lack of technical background.

Several problems could be found, but the most important limitations are:

- The processes performed inside the cells are not well known, the behavior of the studied components cannot be determined with an acceptable precision;
- In critical cases, if a group of cells does not get the necessary food, it changes its behavior. A model created to simulate the normal behavior of the cell will not simulate it correctly in abnormal case;
- Because the structure of the heart differs from patient to patient, this structure is not known a priori, it has to be determined in real-time, based on the available information;
- The structure of the torso introduces the same problem. It is hard to determine the electrical conductivity and precise position of its elements.

In case of human system identification the most important disturbing phenomena are:

- It is known, that respiration makes the heart change its shape and position. Although the motion of the heart can be tracked, it is not possible to determine from the ECG the amplitude of the motion;
- The continuous motion and displacement involves very hard problems. Because the motion has an effect on the behavior of all internal elements, the behavior of the heart will also be modified. The model has to follow the changes of the cell properties. For example: a resting man suddenly jumps out of the bed. The controlling mechanisms start their adjustment, the values of model parameters will change;
- Fever and respiration frequency can also cause alterations.

External events (the patient senses something annoying or pleasant) change the dependence between the previously measured signals, and the determined parameters. This is one of the causes why the perfect simulation of a human body is impossible.

At present, the performance of personal computers does not make possible the real-time determination of parameter values. The practical application is possible only in case of strongly parallel systems. The simplified model can be applied in real-time, but its efficiency is reduced because of the neglected parameters. The waveform of the simulated ECG in normal cases can be considered acceptable. The shape and duration of basic waves have realistic values. In case of abnormal cases the obtained waveform is not acceptable and more simulations are needed.

The proper connection between the electric and mechanic properties of the heart is a challenging task and demands a good understanding of the constituting models describing cells, tissue or various components. An efficient parameter reduction generated by a more abstract formulation of the information may enable the development of real-time deformable models for various pathological cases.

We have presented a massively parallelized flexible and efficient heart simulation method that uses almost all features of a modern processing hardware. After that, we have demonstrated that the processor of a modern graphics card can provide better performance than a modern CPU under certain conditions, in particular, allocating data in a regular and parallel manner. In these situations, the GPU should operate in a SIMD fashion to get the most performance hit. Experimental results show that the graphics card can be exploited in order to perform non-rendering tasks.

4. Volumetric Analysis and Modeling of the Heart Using Echocardiographic Image Sequence Compression

Abstract: The first part of this chapter presents a volumetric cardiac analysis and movement reconstruction algorithm from echocardiographic image sequences and electrocardiography (ECG) records. The method consists of two-dimensional (2-D) echocardiogram transformation, shape detection, heart wall movement identification, volumetric analysis and 4-D model construction. Although the semi-periodic behavior of the ECG and the breath caused heart rate variance disturbs spatial and temporal reconstruction, the presented algorithm is able to overcome these problems in most cases for normal and ventricular beats. The obtained model provides a tool to investigate volumetric variance of the heart and the phenomenon of normal and abnormal heart beating that makes possible to explore continuously the heart's inner structure. In the second part of this chapter an active appearance model based echocardiographic image sequence compression method is presented. The key element is the intensive usage of all kind of a priori medical information, such as electrocardiography records and heart anatomical data that can be processed to estimate the ongoing echocardiographic image sequences. Starting from the highly estimated images we could obtain lower amplitude residual signal and accordingly higher compression rate using a fixed image distortion. The realized spatial active appearance model provides a tool to investigate the long term variance of the heart's shape and its volumetric variance over time.

Keywords: echocardiography, sequence analysis, QRS clustering, volumetric analysis, 3-D active appearance model

4.1. Introduction

The most important health problem affecting large groups of people is related to the malfunction of the heart, usually manifested as heart attack, rhythm disturbances and pathological degenerations. One of the main goals of health study is to predict and avoid these kinds of tragic events, by identifying the most endangered patients and applying a preventing therapy.

Creating a heart model is important (Thaker *et al.*, 1998), as the computer, when applying traditional signal processing algorithms, recognizes lots of waves, but it does not really "understand" what is happening. To overcome this, the computer needs to know the origin and the evolvement process of the ECG signal (MacLeod *et al.*, 1998). During signal processing, if the traditional algorithm finds an unrecognizable waveform, the model-based approach is activated, which tries to estimate the causes of the encountered phenomenon (e.g. quick recognition of ventricular fibrillation) (Szilágyi, 1998).

The main goal of the inverse problem of ECG is to characterize and reconstruct cardiac electrical events from measurements. In contrast to the forward problem of electrocardiography, the inverse problem does not possess a mathematically unique solution and in order to improve stability, it needs to adopt regularization techniques.

The heart is a dynamic organ and places special demands on spatial techniques. To understand its physiology and patho-physiology, not only the electrical activity and spatial distribution of its structures is important, but also their movement during cardiac cycles. The measured ECG signal is influenced during repolarization by the mechanical movement of the heart.

Echocardiography is the fastest, least expensive and least invasive heart imaging method. Accordingly, it is one of the most commonly used techniques to quantify the ventricular systolic function in patients. The examination is based on visual analysis of myocardial wall motion and

deformation by an experienced and trained physiologist. This investigation is subjective, experience dependent and the obtained results are only partially quantitative. The segmentation of the measured image sequences focuses on finding the exact boundaries of particular objects of interest, but it usually requires manual assistance. Besides their several advantages, ultrasound images have the following drawbacks:

- They include not only the reflections from tissue transitions, but also several interference patterns (speckle noise). Consequently, tissues can hardly be distinguished by the intensity of their representing pixels.
- Image data highly depend on the position and angle of incidence of the ultrasound beam.
- A wide scale of imaging artifacts are frequently present, so still-frame images might contain only partial information.

In order to deal with these kinds of deficiencies, several automated segmentation techniques have been developed and reported. Geiser et al. (Geiser *et al.*, 1998) proposed arc filtering for boundary detection, while Brotherton et al. (Brotherton *et al.*, 1994) gave a hierarchical fuzzy neural network solution. Dias and Leitão (Dias *et al.*, 1996) introduced an iterative multigrid dynamic programming technique based on Rayleigh distributed random variables and a probabilistic model formulated within Bayesian framework. Belohlavek et al. (Belohlavek *et al.*, 1996) proposed the automated segmentation using a modified selforganizing map. Chalana et al. (Chalana *et al.*, 1996) traced the epi- and endocardial border using active contour models. In spite of their significant merits, these methods still neglect the following aspects:

- Sought boundaries are not always represented by the strongest edges.
- They use no a priori information concerning the allowable shapes and ranges of the segmented object.
- Segmented boundaries should be consistent with the cardiac cycle.

In the last decade, advances have been made in the content-based retrieval of medical images, such as extraction of boundaries of cardiac objects from echocardiography image sequences (Duncan *et al.*, 2000). Montagnat et al. (Montagnat *et al.*, 1999) used a two simplex meshbased cylindrical deformable surface to produce time-continuous segmentation of 3-D sequences. Angelini et al. (Angelini *et al.*, 2001) proposed a feature enhancement and noise suppression using a wavelet-like decomposition of the spatial frequency domain. A snake-based segmentation is carried out later on the denoised data.

Active appearance models (AAM), introduced by Cootes et al. (Cootes *et al.*, 2001), are promising image segmentation tools that may provide solutions to most pending problems of echocardiography, as they rely on both shape and appearance (intensity and/or texture) information. Bosch et al. proposed a robust and time-continuous delineation of 2-D endocardial contours along a full cardiac cycle, using an extended AAM, trained on phase-normalized four-chamber sequences.

To understand the physiology and patho-physiology of the heart, not only the electrical activity and spatial distribution of its structures is important, but also their movement during normal and abnormal cardiac cycles. The ECG signal is measured simultaneously with echocardiography sequence recording, in order to localize the investigated events.

Echocardiography is a popular medical imaging modality due to its noninvasive and versatile behavior. There are no known side effects, and the measuring equipment is small and inexpensive relative to other options, such as MRI or CT. Reducing storage requirements and making data access user friendly are two important motivations for applying compression to ultrasound images, with the retention of diagnostic information being critical (Chiu *et al.*, 2001).

A typical echocardiography image consists of a nonrectangular scanned area, and a passive background, which may contain patient related text or limited graphics (e.g. a single channel ECG signal). The resulting spatial variation in image statistics presents a hard task to coding methods that use a single partition strategy. For example, many modern image compression algorithms, such as zero-tree coding (Shapiro, 1993) and set partitioning in hierarchical trees (SPIHT) (Hang *et al.*, 2006; Said *et al.*, 1996) are based on the wavelet transform, which partitions the input images into frequency bands whose size decreases logarithmically from high frequencies to low ones. This kind of decomposition strategy works well when the input images are statistically homogeneous, but not in the case of echocardiography image sequences.

In paper (Erickson, 2002) is presented the investigation results of the improved transformation based lossy compression techniques for ultrasound and angiographic images. The goal of the study was to clear out where the compression process could be improved for the medical application. It was proved that wavelet transform outperforms discrete cosine transform applied for ultrasound image sequence.

The analysis of international image compression standards was carried out with special attention to the new still image compression standard: Joint Photographic Experts Group (JPEG) 2000. The JPEG2000 compression is better than ordinary JPEG at higher compression ratio levels. However, some findings revealed that this consideration is not necessary valid for lower compression levels. In study (Shiao *et al.*, 2007) the qualities of the compressed medical images such as computed radiography, computed tomography head and body, mammographic, and magnetic resonance T1 and T2 images were estimated using both a methods. The negative effect of blocking artifacts from JPEG was decreased using jump windows.

The impact of image information on compressibility and degradation in medical image compression was presented in paper (Fidler *et al.*, 2006). This study used axial computed tomography images of a head. Both (JPEG) and JPEG 2000 compression methods were evaluated using various compression ratios (CR) and minimal image quality factor (MIQF).

In pattern recognition research the dimensionality reduction techniques are widely used since it may be difficult to recognize multidimensional data when the number of samples in a data set is comparable with the dimensionality of data space. Locality pursuit embedding (LPE) is a recently proposed method for unsupervised linear dimensionality reduction. LPE seeks to preserve the local structure, which is usually more significant than the global structure preserved by principal component analysis (PCA) and linear discriminant analysis (LDA). In paper (Zhenga *et al.*, 2006) the supervised locality pursuit embedding (SLPE) is investigated. These dimensionality reduction methods can improve the understanding level of the medical information borrowed in the recorded image sequences (Yuan *et al.*, 2004).

Usually the medical applications do not tolerate much loss in fidelity, so the distortion free methods, such as context-based adaptive lossless image coding (CALIC) (Wu *et al.*, 1997) have been recently adapted to “near-lossless” situations (Wu *et al.*, 2000) with good results. Erickson et al. (Erickson *et al.*, 1998) have compared SPIHT and JPEG methods to compress magnetic resonance imaging (MRI) and ultrasound images. They concluded that wavelet-based methods are subjectively far superior to JPEG compressed at moderately high bit rates. Medical images are typically stored in databases, so it is possible for computers to extract patterns or semantic connections based on a large collection of annotated or classified images. Such automatically extracted patterns can improve the processing and classifying performance of the computers.

In the recent past, researchers in the image analysis community have successfully used statistical modeling techniques to segment, classify, annotate and compress images. Particularly, variations of hidden Markov models (HMMs) have been developed and successfully applied for image and video processing. The key issue in using such complex models is the estimation of system parameters,

which is usually a computationally expensive task. In practice, often a tradeoff is accepted between estimation accuracy and running time of the parameter estimation method (Joshi *et al.*, 2006).

Such a statistical information-based estimation highly depends on biological parameters. In our case, the most important task in efficient echocardiography image compression is the accurate detection of QRS complexes from the simultaneously measured ECG signal. Due to the semi-periodic behavior of the ECG signal and echocardiography image sequences, the parameters of the patient model can be more precisely estimated.

In this paper we present our algorithm that reconstructs the heart wall boundaries and motion in order to determine the spatial and temporal cardiac activity. The determined model parameters are used to estimate more precisely and efficiently compress the captured image sequences. Several papers in the literature have already reported the usage of spatial AAM (Mitchell *et al.*, 2002a; Stegmann *et al.*, 2005). The present work has the following contributions:

- Reported techniques classify ultrasound images only as belonging to systolic or diastolic interval. Our approach distinguishes normal and extra beats, and processes the corresponding images accordingly.
- ECG event classification makes possible the investigation of several pathological cases (e.g. volumetric effect of a given extra beat). Comparisons were made between normal and pathological cardiac cycles of the same patient.
- We developed a heart reconstruction algorithm including time dependent wall boundaries in order to estimate the image variances that allow a better compression rate at a fixed image quality than conventional methods.

4.2. Materials and Methods

4.2.1. Scanning procedure and motivation

Three-dimensional echocardiography (Fenster *et al.*, 2001) is not a magic tool, but with an optimal 2-D image quality, spatial reconstructions can be accomplished. The known limitations of various 2-D ultrasound techniques are also true for 3-D echocardiography. Extra-cardiac structures or cardiac structures hidden in part by lung tissue cannot be visualized. In addition, ultrasound artifacts such as shadowing and reverberations are still present, along with near and far field penetration problems. Further problems in 3-D echocardiographic imaging were also encountered, such as reduced resolution, a relatively low frame rate, limited frequency and a too large footprint for the intercostal space. Hopefully, the ongoing technical developments in 3D echocardiography will probably solve a lot of these problems in the near future.

Simultaneous echocardiography sequence recording and ECG signal measurement were carried out at the County Medical Clinic of Târgu-Mureş, using a 2-D echocardiograph that produces 30 frames per second, and a 12-lead ECG monitoring system that samples at 500 Hz frequency and 12-bit resolution. Each image frame received a time stamp, which served for synchronization with ECG events. Two different series of measurements were recorded. The first series, which served for AAM training, consisted of 35 patients (12 of whom having extraventricular beats), 20 ultrasound sequences for each patient, of 10-15 seconds length each sequence, with previously established transducer placements. Based on these data, an a priori information database was created, which organized the ultrasound images grouped by corresponding ECG events.

The second series of measurements, which involved 4 patients, consisted of two stages. In the first stage, the same measurements were performed, as in the first series, in order to provide patient-specific training data for the AAM. In the second stage, several measurements were performed using different placements and positions of the transducer. In this order, image sequences were recorded at

17 parallel cross sections in horizontal and rotated (45° to the left and to the right) positions (see Fig. 4.1.(a), (b), (c)), with a 1 cm inter-slice distance. We used 30 common axis planes that were placed at front, lateral and back side of the torso, as presented in Fig. 4.1.(d), (e). For each patient a total number of 30 × 17 × 3 = 1530, at least 2-3 second long image sequences were created.

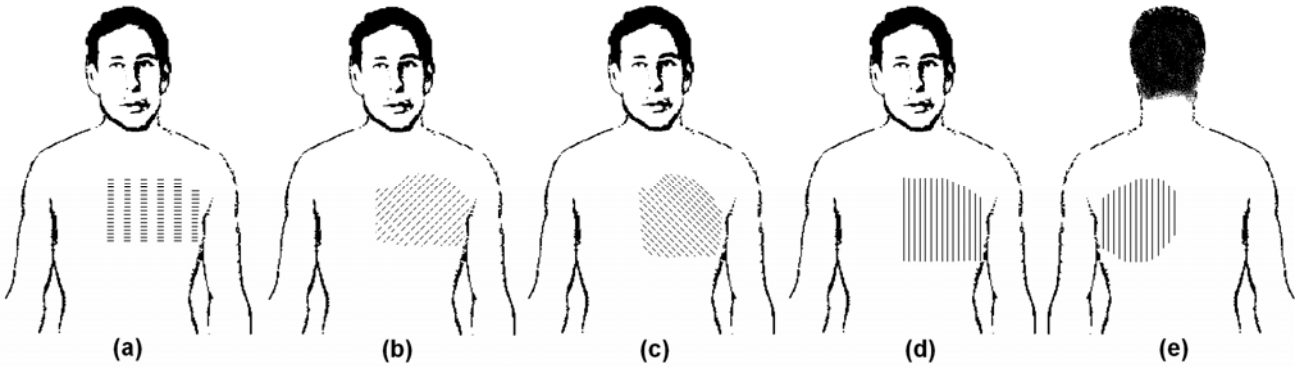

Fig. 4.1. Various positions of the parallel cross sections and the orientation of the transducer: (a) horizontal plane(s), (b) left rotated plane(s), (c) right rotated plane(s). Various positions of planes with common axis: (d) front view, (e) back view

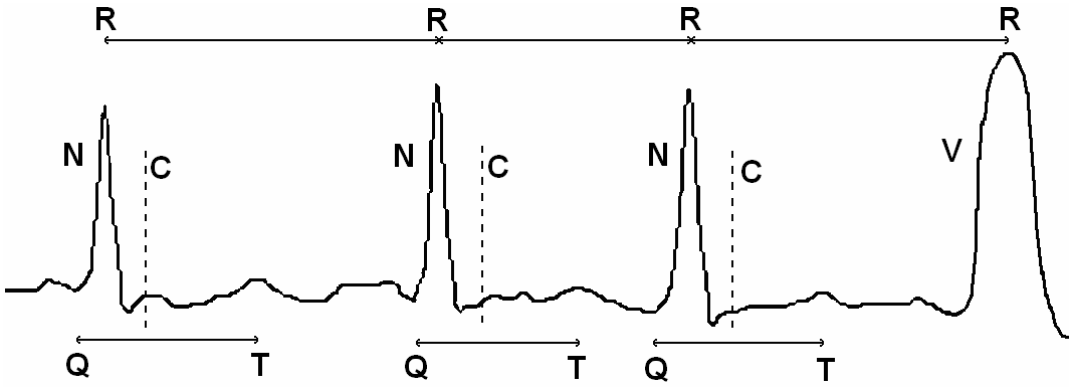

Fig. 4.2. Normal (N) QRS and extra ventricular QRS beat (V), with indicated RR and QT distances. Dotted lines denoted by C (maximal contraction) represent the minimal volume moment of heart during normal cardiac cycle

The duration of the recorded image sequences was restricted by the semiperiodic behavior of the ECG signal. The spatial movement of the heart is constrained by the course of the depolarization repolarization cycle (Szilágyi *et al.*, 2005). For example the ectopic beats has altered electrical activity compared to normal ones (modified QRS waveform) and therefore a different mechanical contraction procedure (the recorded ultrasound images show other movement shape of the ventricular walls in case of ectopic beats than in normal case). The studied ECG parameters, as presented in Fig. 4.2., were shape of QRS beat, QT and RR distances. These parameters characterize the nature of a QRS complex, and were determined as presented in (Szilágyi *et al.*, 2003b).

ECG event clustering was accomplished using Hermite functions and self-organizing maps (Lagerholm *et al.*, 2000; Szilágyi *et al.*, 2005). Two main event clusters were created: normal and ventricular extra beats. This latter group, because of the patient specific manifestation of ventricular extras, had to be dealt with separately patient by patient. An adequate parameter extraction from the recorded ECG signal segments and ultrasound image sequences needs a significant number of samples, otherwise the obtained values has a great dispersion that negates the possibility to obtain reliable results. To guarantee reliable parameter values the recorded data from all less probable events, such as long R-R period or sparse pathological depolarizations were not included in further processing. In our case this mean the exclusion from further processing of abnormal QRS beats

(those beats that not belong to any pre-defined cluster types) with their corresponding ultrasound sub sequences. To eliminate the sparsely occurring normal QRS beats we included the further conditions: RR distance between 700-800ms and QT distance between 350-400ms. A detailed presentation of ECG processing is presented in previous chapter.

There are several possible different heart structures. To describe various representative cases, we studied our breast MRI records (42 examples) and numerous CT images. These samples lead us to construct a morphological heart structure for simulation, using a segmentation method presented in (Dumoulin *et al.*, 2003). The obtained results were classified by physiologists and used to identify each atrial and ventricular region. The identification process uses as a base Harrild's atria model (Harrild *et al.*, 2000) and Winslow's ventricular tissue model (Winslow *et al.*, 2000).

From the correctly segmented images, we constructed a spatial representation of the heart, using an averaging technique. Such a prototype heart representation must be adjusted taking into consideration the ECG data. The ECG has an important role, as it may describe the electric property of the heart. For example, the mechanic related data obtained from MRI and CT images cannot give us any information about some malfunctions, such as the presence of numerous ectopic beats. An ultrasound image sequence, although the measurement process had a duration of about two hours, due to the relation between electric and mechanic properties of the heart, may hold some mechanic information that can be used to identify diverse electric dysfunctions. This information was used to construct the electric-mechanic heart model as described in (Szilágyi *et al.*, 2005).

Fig. 4.3. shows the short graphical abridgement of the wall detection algorithm. The spatial reconstruction method from planar image sequence information is based on a voxel-based 3D construction proposed by Sanches and Marques (Sanches *et al.*, 2000). The voxel's value is the weighted average of the pixel values of its nearest neighbours. However a certain piece of the heart at a defined moment of the depolarization-repolarization cycle figurates in more than one image sequence. To obtain the most realistic movement for that piece (wall segment) we selected all relevant images and developed a patient-dependent conversation algorithm.

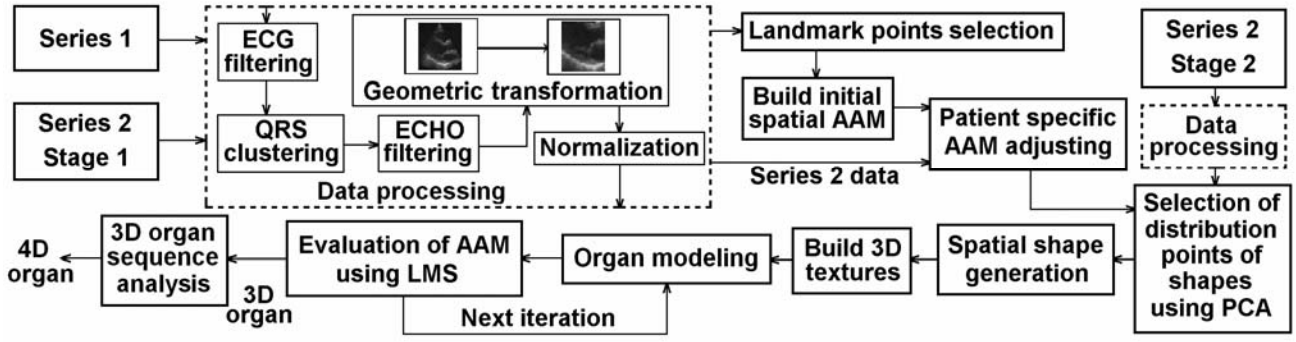

Fig. 4.3. The data recording and analyzing procedure: all echocardiography and ECG data go through the same processing module. The AAM is constructed from the measurements of series 1, and fine tuned afterward using the patient specific data resulting from series 2 stage 1. Stage 2 data serve for the detailed cardiac volumetric analysis. Reconstructed 3-D objects are finally aligned using an iterative LMS-based algorithm

As the measurements were made with known spatial coordinates x, y, z, time t and direction represented by angle α, the selected image sequences could be concomitantly processed with the measured ECG signal. All selected images that correspond to the same depolarization-repolarization phase and had almost the same ECG pattern (same QRS class, low QT and RR difference) were included into calculations. Let $c(cl,t)$ be the clustering function that determinates the appertainity coefficient to a cluster cl of a given ECG period measured at moment t. These clusters were determined with Hermite functions and self-organizing maps (Lagerholm *et al.*, 2000).

The strength of the relation between a given wall segment and cluster *cl* is determined by function *f* with form:

$$f(x,y,z,cl,t) = \frac{c(cl,t)}{dist(x,y,z,t)}, \tag{4.1}$$

where

$$dist(x,y,z,t) = \sqrt{(x_s(t)-x_w(t))^2 + (y_s(t)-y_w(t))^2 + (z_s(t)-z_w(t))^2}, \tag{4.2}$$

represents the spatial distance at moment *t* of the sensor *s* from the studied wall piece *w*. The angle α of the sensor and the wall place at the image measured at moment *t* determinates the spatial coordinates of the muscle segment. In this way, each wall movement was studied in time and the heart's spatial movement could be reconstructed.

4.2.2. The electrical and mechanical functioning of the heart

The detailed presentation of this problem is realized in Section 3.2.5. As presented in (Amano *et al.*, 2003) the cardiac cells have a mechanism which generates contraction force by a Ca^{2+} transient escalation triggered by an action potential (a depolarization of the cell membrane), which is called excitation-contraction coupling. As the contraction mechanism is essential component of cardiac cell, it is studied by many researchers and many theoretical models are proposed so far. A recent, contraction model was proposed by (Negroni *et al.*, 1996). In this four state model the transition among states is determined by Ca^{2+} concentration and cell length. The second studied model was proposed by (Campbell *et al.*, 2001), and contains two two-state models for *Ca* kinetics and RU on/off kinetics and a three state model for XB cycle kinetics.

4.2.3. Automated border and wall detection

The time-varying evolution of the cardiac volume is determined by the interconnection of electrical and mechanical phenomena. In a whole cardiac cycle there are two extremity values. The maximal volume can be coupled with the starting moment of ventricular contraction. The depolarization wave normally starts from the sino-atrial node (SA) and propagates through the atrioventricular node (AV) and ventricles. The moment of minimal volume shortly precedes the termination of ventricular contraction, but is much more difficult to identify, due to the dead time of a normal cardiac cell. This delay is caused by the strange property of a regular cardiac cell, whose electric response is most directly caused by the depolarization wave (fast Na^+ channels), but the mechanical contraction is controlled by the much slower Ca^{2+} channels. The calcium channel opens at 10-20 ms after depolarization, and the maximal contraction follows in about 80ms (Amano *et al.*, 2003; Winslow *et al.*, 2005). Figure 4.2. indicates the moment of minimal volume with a dotted line. The combination of the electrical and mechanical properties of the heart and the usage of knowledge-base allowed us to create a performance evaluation module that iteratively determines the most probable wall position, as shown in Fig. 4.3.

This image presents an overview of the image processing and volumetric reconstruction procedure. The first algorithmic step is noise elimination. Speckle noise represents a major difficulty to most ultrasound imaging applications (Dias *et al.*, 1996). In our case, the suppression of such phenomena was accomplished using the well-known motion-adaptive spatial technique presented in (Evans *et al.*, 1996).

Due to the measuring technique of traditional echocardiography, the obtained images are distorted. In order to become suitable input for 3-D processing, they need to go through a normalization transform. Every recorded ultrasound slice is represented by a plane, whose spatial alignment

depends on the position and rotational angle of the transducer. The normalization process also takes into consideration the distance of each image pixel from the transducer.

Ultrasound is a particularly harder imaging modality for interpretation than CT and MRI, because it suffers from several specific drawbacks, which impede automated analysis. The absence of a relation between pixel intensity and any physical property of the visualized tissue demand a deeper usage of the a priori information. The sensibility to noise and reflections implies an intelligent filtering. Even the definition of border position may be direction dependent (Vuille *et al.*, 1994).

Albeit these afore-named problems, the huge amount of recorded images demands the usage of automatic border detection (ABD) algorithms. We will refrain from a direct comparison of these methods, as there are no standard test data sets neither for this purpose nor standard test criteria (Sher *et al.*, 1992). The clinically most widespread algorithm is based on acoustic quantification (AQ) that is involved in several ultrasound machine models. However this method suffers from high sensitivity to image quality. A typical ABD algorithm contains the following steps:

- Preprocessing (smoothing, contrast checking)
- Edge or region detection (thresholds, edge detectors)
- Geometric object models (for example radial search)
- Anatomical structure model
- Interpretation (based on high-level knowledge).

An excellent example of a structure-based method was published by Geiser and Wilson (Geiser *et al.*, 1998; Sheehan *et al.*, 2000) for automatically detecting endocardial and epicardial borders in short-axis echocardiograms. This method is practically useful and it was validated on a large set of patients. In this method a great advantage over classic algorithms is the involvement of the a priori information and the usage of a feed-back between a high-level model of a short-axis cross section and a low-level feature data. The main weakness lies in its cascade dependent steps that can fail and cause the process to break down.

The enrolled disadvantages convinced us to use an Active Appearance Model that was developed by Edwards et al for facial recognition and medical image analysis (Edwards *et al.*, 1998) (see Fig. 4.3.). This technique can be considered as an extension of the Active Shape Model (ASM) and derives the typical shape and appearance of an echocardiogram from a large set of example images with expert-drawn contours (Bosch *et al.*, 2002). Its main steps are:

- Extract the average organ shape
- Extract the principal shape variations
- Create the appearance model
- Generate probable echocardiographic image
- Find the desired structure by error minimization technique.

This technique has some important advantages: it models average organ shape and variation, can model complete organ appearance including artefact cases.

The training data of the AAM is constructed based on the spatial position of each echocardiography slice recorded in the first measurement series, and on the positions of the heart wall pieces that correspond to the contours manually recognized by an expert. By averaging these spatial distributions, a mean base 4-D heart shape model is obtained, which will be the starting point of the AAM (Bosch *et al.*, 2002; Lelieveldt *et al.*, 2002). Landmark points are determined using the technique proposed by Mitchell et al (Mitchell *et al.*, 2002a). The sparse character of the obtained spatial description model doesn't allow the landmark points have 3-D texture information. That is why we restricted the texture to 2-D.

Subjects have their own specific, time dependent inner structure, which cannot be approximated properly from a population of few dozens of individuals. In order to make further adjustments to the AAM, the base structure was adjusted to the patient using the measurements made in the second series, first stage.

The landmark points determined on the images recorded during the second stage of the second measurement series allow us to create a 3-D distribution point model, which was established according to (Besl *et al.*, 1992; Mitchell *et al.*, 2002a). Having the distribution points established, the AAM will be enabled to adjust itself to a diversity of biological factors like the phase of ECG and breathing. A detailed description of the manifestation of these phenomena and the model adaptation is given in (Stegmann *et al.*, 2005). Our algorithm acts similarly, but it treats the cardiac cycle differently: not only systolic and diastolic phases are distinguished, but also a QRS complex clustering is performed to give different treatment to normal and ventricular cardiac cycles.

Spatial texture maps are determined via averaging (Stegmann *et al.*, 2005). The visual aspect of heart and its environment, because of their mutual motion, is changing in time. AAM models only include information on the texture situated within the model. The time dependent representation of the ultrasound slices obtained from the large stack of sequences enabled us to accurately determine the 4-D structure of the heart (Mitchell *et al.*, 2002a). The iterative algorithm of the AAM demands the comparison of measured and expected shapes. The AAM was adjusted using a quadratic cost function, until the desired accuracy was obtained (Mitchell *et al.*, 2002b).

4.2.4. Validation of the spatial construction procedure

Our model validation was performed by the comparison of the simulated ECG signals and generated ultrasound contour images with measured data. At every moment from the spatial position of the heart and of the measuring ultrasound electrode the observable plan can be determined. Performing an image filtering and segmentation, the observable contours can be determined. The simulated object intersected with a visualizing plan generates an intersection. If the obtained data is transformed to fit with ultrasound images, the simulated and measured contours can be compared. To evaluate the obtained results a better evaluation relation is needed than a simple root mean square error (RMSE). The obtained result (contour) may be displaced or rotated that seriously disturbs a simple comparison method. In our consideration a proper estimation uses AAM, and evaluates the obtained parameter differences between simulated and measured contour.

This approximation eliminates the displacement or rotational errors, the image can be magnified (Procoust alignment), and only the main characteristics, such as shape is took into consideration. The simulated ECG signal is compared with the measured signal. However the correct comparison of the signals needs a transformation. In estimation error calculation the directly determined RMSE cannot be taken into consideration due to some perturbing phenomena such as baseline displacement. To realize a proper comparison the measured signal must be filtered. The role of the used filter is to eliminate various artifacts such as abrupt baseline movement and various noises.

There are other perturbing phenomena that are patient dependent, for example the baseline elevation or depression caused by the inspiration-expiration process. These displacements are not caused by artifacts, but the perturbing phenomena are not included in the simulation model, so the impact of these events cannot be simulated. The best way in our consideration is to determine the most important patient and ECG wave dependent parameters, such as QRS duration, R and T wave's positions and amplitudes and to calculate a weighted error among these parameters. This approximation is not only easier to apply, but has significantly much robustness.

4.2.5. Compression of the image sequences

Figure 4.3. present the image-estimation-based compression of the recorded data sequence. The constructed AAM-based 4-D model yields the necessary information to realize a proper image estimation.

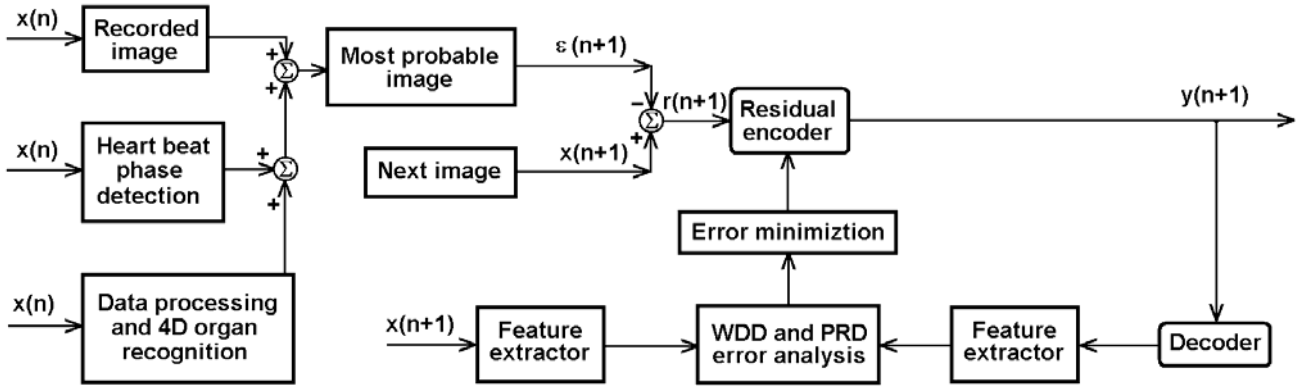

Fig. 4.4. Schematic representation of residual data construction and distortion analysis. The residual signal calculation process uses the recorded image, heart beat phase information and AAM-based 4D organ shape to determine the most probable image in the next measuring moment. As the $y(n+1)$ output signal is obtained, a WDD and PRD-based distortion analysis is realized, where the image features are determined from AAM

Due to its adaptive behavior, the compression method is able to handle patient-dependent data, and has a capability to efficiently separate the measured artifacts from the useful signal. The proposed signal compression algorithm can be divided into the following steps:

- Intelligent image sequence analysis and filtering (that involves the automatic recognition of echocardiography image, ECG signal and various changing and constant labels and letters that appear on the recorded image sequence);
- Background selection (the constantly dark region);
- ECG signal processing;
- Segmentation of echocardiographic image (see Fig. 4.3.);
- Calculation of the heart's 4D shape (3D+time) using AAM;
- Estimation of probable image;
- Residual signal estimation, entropy coding (encode and decode) and back-estimation.

The compression evaluation was implemented in two ways, using percentage root mean square difference (PRD) and weighted diagnostic distortion (WDD) (Zigel *et al.*, 2000b). WDD measures the relative preservation of the diagnostic information (such as location, duration, intensity, shapes, edges) in the reconstructed image. These diagnostic features were determined by physicians. The distortion estimation and signal (ultrasound image and all auxiliary data) coding process is presented in Fig. 4.4.

4.3. Results

The depolarization of various ventricular and two atria slices for normal case is presented in Fig. 3.6. of the previous heart modeling chapter.

In Fig. 3.9. of the heart-modeling chapter the visualization of some selected control points (used by the AAM) from various echocardiographic images is observable.

Figure 3.10.(a) from the heart modeling chapter presents two series of ultrasound slices indicating the contour of the left ventricle of the 2nd patient, detected during a ventricular contraction. The two rows of slices show two different angle views, having 60° angle difference. The four slices in each column represent subsequent images of the sequence, showing the approximately 100ms duration of the ventricular contraction. Figure 3.10.(b) exhibits the same ultrasound slices after being normalized, that is, transformed to Euclidean space. Figure 3.10.(c) contains the obtained contours of the simulated left ventricle. Figure 3.10.(d) shows two different reconstructed 3-D shapes of the left ventricle, which were obtained using 1527 distribution points.

The evolution in time of the heart volume during a normal and an ectopic (ventricular extra-systole) RR period is presented by Fig. 3.8.(a) and (b) of the previous heart modeling chapter. Four different patient data was averaged in normal case, but the fourth patient did not produce ventricular extra-systolic beats. As the depolarization wave in case of an ectopic beat starts from the ventricular area, the minimal volume is obtained earlier (the delay caused by the AV-node is skipped), and at a higher value compared to normal beats (the contraction of the heart is not optimally synchronized). The first moment of LV volumetric calculation (t = 0ms) was considered at the moment of maximal positive deflection of the ECG signal.

Figure 4.5. presents a sensibility analysis of the QRS recognition algorithm. Figure 4.5.(a) shows how the variation of the RR distances (shorter or longer than average) influences the recognition rate: the algorithm is more sensible for shorter RR periods. The effect of the variation of QT distances around the average value is shown in Fig. 4.5.(b): the same absolute difference makes significantly more damage if it occurs in positive direction. Figure 4.5.(c) reflects the relation between the shape of QRS complexes and recognition performance. The correlation coefficient of the QRS beat with the cluster averaged shape is directly proportional with the performance of the algorithm.

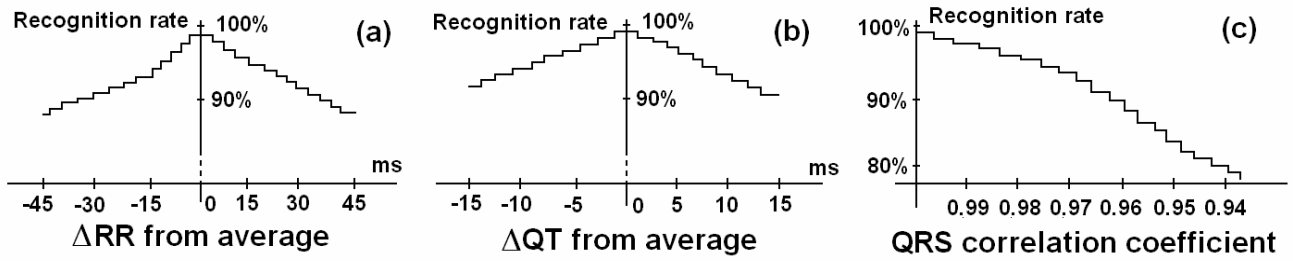

Fig. 4.5. Sensibility of QRS complex recognition algorithm to: (a) variations of RR distances, (b) variations of QT distances (both with respect to their average), (c) QRS shape correlation with average template.

Table IV.1. presents the patient-dependent recognition rates for normal beats (average duration 707 ms) and ventricular beats (average duration 671 ms). The measurements were effectuated on four patients, and three of them produced ventricular extra-systolic beats.

Table IV.1. Patient-dependent recognition rate of various QRS beats in case of optimal circumstances (average QRS shape, average RR and QT distances)

Patient\ QRS type	Normal QRS beat	Ventricular extra-systole
1st- patient	99,2%	97,6%
2nd- patient	99,4%	92,4%
3rd- patient	98,4%	95,2%
4th- patient	98,6%	Not available data

Table IV.2. Patient-dependent averaged percentual heart rate modification during aspiration and expiration. The obtained variance is presented for normal and ventricular beats. The 4th-patient had no ventricular beats.

Patient\ HR variance	Normal QRS beat	Ventricular extra-systole
1st- patient aspiration	6.2%	6.6%
2nd- patient aspiration	5.5%	3.4%
3rd- patient aspiration	9.2%	7.8%
4th- patient aspiration	5.6%	Not available data
1st- patient expiration	-4.5%	-5.7%
2nd- patient expiration	-5.2%	-3.4%
3rd- patient expiration	-6.7%	-5.9%
4th- patient expiration	-4.3%	Not available data

The recognition of the relation between echocardiographic image and simultaneously recorded ECG signal is a key element in wall movement detection. This relation can be partially hidden by various events, such as aspiration and expiration. These phenomena may influence the measured heart rate, as presented in Table IV.2.

The measurement circumstances were selected optimal (average QRS wave shape, average RR and QT distances) for performance values presented in Table IV.1. As this table reflects, the fourth patient did not produce any ventricular beats. We can observe a pronounced performance advantage of the algorithm for normal beats due its higher incidence.

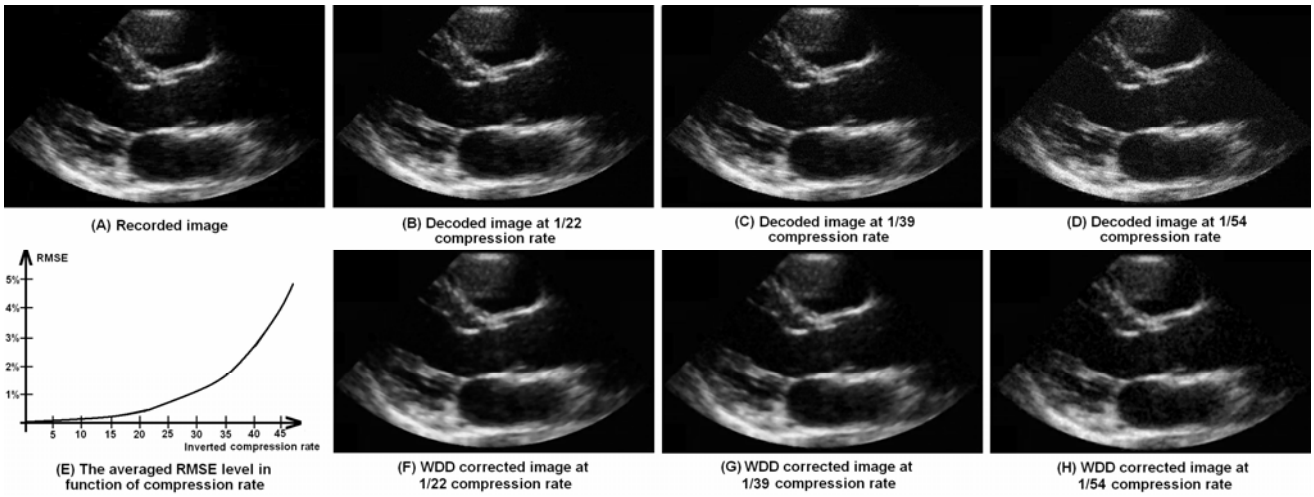

Fig. 4.6. Results of image reconstruction: (a) original image, (b) decoded image at 1/22 compression rate, (c) decoded image at 1/39 compression rate, (d) decoded image at 1/54 compression rate, (e) representation of root mean square error (RMSE) in function of inverted compression rate, (f) feature-base corrected image 'b', (g) feature-base corrected image 'c', (h) feature-base corrected image 'd'.

Figure 4.6. presents the decoded and feature-base corrected echocardiographic images at various compression rates. The variation of RMSE level against inverted compression rate is shown in Fig. 4.6.(e). The RMSE graph was created for a normal QRS beat shape and average RR and QT distances. We can observe a pronounced performance advantage of the method for normal beats due to its higher incidence. Table IV.3. summarizes the obtained compression rates.

Table IV.3. The obtained inverted compression rates obtained for normal beats using: (a) Wavelet – based compression, (b) Image comparison-based estimation, (c) QRS, long-term prediction (LTP) ECG and echocardiographic image compression, (d) JPEG 2000, (e) Matching Pursuits, (f) AAM-based compression.

RMSE\ Method type	Wavelet -based	Image comparison	QRS and LTP Image comparison	JPEG 2000	Matching Pursuits	AAM-based
1%	10.2	14.2	17.4	13.7	15.7	22.7
2%	15.4	21.2	26.6	20.5	22.9	36.3
3%	17.3	24.0	29.6	23.2	27.1	40.2
4%	18.8	26.1	31.8	25.1	29.5	44.1
5%	19.9	27.8	33.7	26.6	31.4	47.7

4.4. Discussion

The propagation of the depolarization wave in the ventricular and atrial tissue is presented in Fig. 4.6. The propagation of the depolarization wave can be seen in the consecutive slices. Using this view, we can supervise the propagation of the depolarizing waves in various circumstances, such as normal beat, ectopic beat, Wolff-Parkinson-White (WPW) syndrome and ventricular fibrillation.

The proper selection of the landmark points to train AAM is an important step of spatial shape generation. The selected points from Fig. 3.9. of the heart modeling chapter must suffer a transformation in order to create the normalized shapes for AAM. The normalization is an un-avoidable step of ultrasound image process due the recording mechanism of the echocardiographic images (the magnification value at a given image pixel depend from the position of the measuring electrode).

From Fig. 3.10. of the heart modeling chapter we can observe that the generated slices from the created deformable model have quite similar shapes (only after Procoust alignment process). From the generated and recognized shapes and ECG waveforms the deformable model can be validated. These shapes were generated during a normal beat. The realized shapes for an ectopic beat may differ significantly from the segmented contour. To validate the method in all circumstances we need more clinical measurements.

From Fig. 3.8. of the previous heart modeling chapter: a) we could observe that the variation of the RR distances (shortenings and lengthening) influences the recognition rate in different ways. The relation (connection recognition of the image and electric signal) construction algorithm is more sensible for shorter than average normal RR periods. As Fig. 3.8.(b) presents, the lengthened QT distances deteriorate the recognition performance much more than shortened ones where all QT distances are related to average QT distances for normal beats. Fig. 3.8.(c) reflects the relation between the shape of QRS beats and recognition performance. The correlation coefficient of the QRS beat with cluster averaged shape is directly proportional with the algorithm's performance. The identification of a wall segment from an image, measured in time of depolarization (before or in first part of systole) is easier than during repolarization. During a normal RR period, about 21-22 images were recorded, so from such an image sequence the first 7-9 images that are related to depolarization stage could be investigated with higher performance.

The recognition of the relation between echocardiography images and simultaneously recorded ECG signal is a key element in wall movement detection. Various events, such as aspiration and expiration influence the measured heart rate. During a whole cardiac cycle, the shape and volume of the left ventricle changes considerably.

It is difficult to determine the performance of the reconstruction method for the sporadically occurred ventricular extra-systolic beats. Even for patients that produce at least five extra beats with similar shapes in each minute that are included in the same cluster, the reconstruction performance remains well below the normal QRS cluster's accuracy, due to the sparse distribution of the processable slices.

This relatively smaller population in the cluster of ventricular beats, compared to the normal ones, implies a lower reconstruction performance. The measurement circumstances were selected optimal (average QRS wave shape, average RR and QT distances) for performance values presented in Table IV.1. As this table reflects, the fourth patient did not produce any ventricular beats. We can observe a pronounced performance advantage of the algorithm for normal beats due its higher incidence.

The volumetric variance of the heart during normal and ectopic (ventricular extra) RR period is presented by Fig. 3.8. of the previous heart modeling chapter: a) and b). As the depolarization wave in case of ectopic beats starts from ventricular area, the minimal volume is obtained earlier (the AV-node caused delay is skipped) but at a higher value (the contraction of the heart is not optimally synchronized), compared to normal beats.

The visual aspect of the heart and its environment varies in time, due to their mutual motion. AAM models include information concerning inner texture only. It would be beneficial to build another AAM for the modeling of the environment, but the invisibility of the pericardium and lung tissues represents an enormous obstacle.

As we know, the left ventricular (LV) hypertrophy has been identified as a strong and independent predictor of various adverse cardiac events even in patients without associated cardiovascular disease (Benjamin *et al.*, 1999). This important clinical parameter has been subject to extensive scientific investigation (Haider *et al.*, 1998). The conventional 2-D echocardiography is the most commonly used imaging modality that supports LV wall mass determination. However, this method is based on geometric assumptions that do not include some possible abnormal ventricular shapes and variability in the distribution of LV mass that hardens the development of an accurate, easily reproducible method for the quantification of ventricular mass.

Evaluation of intra-cardiac anatomy from two dimensional echocardiography image sequences requires a mental conceptualization process that is hardened by cardiac dynamics (MacLeod *et al.*, 1998). The dynamic modeling and visualization systems can help with the spatial interpretation of 3-D data of the heart, and make it possible to build the 3-D model of the heart (Issenberg *et al.*, 2001).

This study is an attempt to evaluate, whether a virtual modeling and visualizing method is feasible for echocardiography, and if ultrasound images in a virtual reality can advance to a clinically useful tool in the technological process of the future. Unfortunately the low number of patients and the long processing time reflect that the applicability and benefits of the presented volumetric analyzer and heart modeling method in clinical practice is still limited.

The spatial texture around voxels belonging to a dynamic organ suffers a deformation during contraction. Under such circumstances a compensation mechanism would be necessary, which is situated beyond the scope of the present paper.

The proper connection between the electric and mechanic properties of the heart is a challenging task and demands a good understanding of the constituting models describing cells, tissue or various components. An efficient parameter reduction generated by a more abstract formulation of the information may enable the development of real-time deformable models for various pathological cases.

From Fig. 4.6. we can observe that even a well-working WDD correction method cannot handle a compression rate better than 1/60 without a serious image distortion that can lead to wrong medical

diagnosis. Table IV.1. demonstrates the higher performance of the image compression method, that exist due to the advanced QRS beat analysis and spatial AAM-based organ reconstruction. Such an analysis can lead to a much better 'estimated image' quality that reduces the amplitude of the residual signal.

4.5. Conclusions

The investigation of simultaneously recorded ECG and echocardiography images enables us to study the relations between the electrical and mechanical phenomena concerning the heart. The method presented in this paper performs correctly in case of normal and ventricular beats, that is, we can monitor the volumetric variance of the heart and its main components. This kind of approach of the problem may result in deeper understanding of several pathological cases like:

- effects of ectopic beats on the heart's pumping activity;
- risk of development of arrhythmias and fibrillation in case of pathological LV wall thickening;
- mechanical effects of Wolff - Parkinson - White syndrome.

The signal and image estimation is made by using various priori medical information, and the algorithm yields lower amplitude residual signal and better compression ratio at given distortion level. The compression method presented in this paper performs well in case of normal and quite well for ventricular beats. The presence of pathological image and signal samples may lower the performance difference among the proposed method and the tested algorithms. This kind of approach of the problem may result in deeper understanding of electrical and mechanical properties of the heart that enable a much efficient compression than the results obtained algorithms using less a priori information.

5. Efficient Localization of an Accessory Pathway Using a 12-Lead ECG

Abstract: This paper presents an analysis of the Arruda accessory pathway localization method for patients suffering from Wolff-Parkinson-White syndrome, with modifications to increase the overall performance. The Arruda method was tested on a total of 79 patients, and 91.1% localization performance was reached. With modifications this performance reaches 94.9%. After a deeper analysis of each decision point of Arruda localization method we considered that the lead aVF is not as relevant as other used leads (I, II, III, V1). Despite lower decision performance of aVF sign tests in the right and septal region, they cannot be wisely replaced within the scope of the 12 lead ECG. The modified algorithm significantly improves the localization performance in the left ventricle. A high localization performance of non-invasive methods is relevant because they can enlighten the necessary invasive interventions, and also reduces the discomfort caused to the patient.

Key words: delta wave, heart regions, non-invasive method, accessory pathway localization, WPW syndrome

5.1. Introduction

5.1.1. The Wolff-Parkinson-White syndrome

The Wolff-Parkinson-White syndrome is characterized by an accessory pathway (by-pass tract) between the atria and ventricles that conducts parallel with the atrioventricular (AV) node - His bundle, but faster (Wolff *et al.*, 1930, Yee *et al.,* 1995). An accessory AV connection can conduct in both directions. The presence of these by-pass tracts may predispose to atria-ventricular reentrant tachycardia. Moreover, in the setting of atrial fibrillation, the WPW syndrome may cause a catastrophically rapid ventricular response with degeneration to ventricular fibrillation (VF).

Electrocardiographically, the WPW syndrome can be characterized by a specific sinus rhythm pattern. Its other specific features are paroxysms of re-entry tachycardia (the incidence in the young adult population is about 10% and growing up with age to 30%), more rarely paroxysm of atrial fibrillation (20–30% of patients with the syndrome), or atrial flutter (Guize *et al.,* 1985, Wellens *et al.,* 1987).

In the case of WPW syndrome, the electrocardiogram (ECG) tracing is a mixture of the electrical activities (Szilágyi *et al.*, 2003a) caused by the accessory AV connection and normal AV conduction system. The fast impulse conduction produces an initial deflection in the QRS complex (delta wave) (Szilágyi *et al.*, 2003d). The length of this delta wave is determined by the difference between the accessory AV connection and normal AV conduction times. The modified ventricular activation may cause secondary abnormalities in the ventricular repolarization such as: ST segment displacement (elevation or depression), T wave shape distortion and abnormal U wave appearance. The conduction capacity variances (changes may occur hour by hour or day by day) of the accessory AV connection may result in alternating WPW pattern (complete, partial or missing pre-excitation, concertina effect).

An adequate analysis of this phenomenon is important, since 0.1-0.2% of the population suffer from WPW syndrome (Wellens *et al.,*1990, Josephson 1993). When the refractory period of the accessory connection becomes too short, the patient's life is endangered by a possible VF. Unfortunately, the exact risk for developing VF during high ventricular rates is unknown (Goudevenos *et al.*,2000).

5.1.2. WPW syndrome analysis

Usually the WPW analysis is focused to develop and validate an accessory pathway (AcP) localization method (Rosenbaum *et al.*,1945). A number of investigations have correlated ECG patterns and processing algorithms for detecting the place of the AcP (Fitzpatrick *et al.,*1994, Reddy and Schamroth 1987, Arruda *et al.,*1992, 1993, 1994, 1998), while other studies have been focused on the localization, realized through three-dimensional (3D)-heart reconstruction by the inverse solution of the ECG (Cuppen *et al.*, 1984; Huiskamp *et al.*, 1997; Shahidi *et al.,*1994; Johnston *et al.* 1997, Oster *et al.,*1997, Guanglin *et al.*, 2001). Unfortunately, the inverse problem, in contrast to the forward approximation methods, does not possess a mathematically unique solution. Another not easily by-passable difficulty is rooted in its ill-posed nature, whereby the obtained inverse solution could be unstable and may oscillate widely with the slightest perturbation.

Several approaches have been explored to handle the problem of multiple solutions by using equivalent cardiac generators (such as equivalent dipole (De Guise *et al.,*1985) and multipole), heart surface isochrones (Cuppen *et al.*, 1984; Huiskamp *et al*., 1997), or epicardial potential (Shahidi *et al.,*1994; Johnston *et al.*, 1997; Oster *et al.,*1997; Guanglin *et al*., 2001). The high sensitivity of solutions to the different disturbances forced the investigators to explore various regularization techniques (Shahidi *et al.,*1994; Johnston *et al.*, 1997; Oster *et al.,*1997).

These methods allow a significant progress, but the diverse uncertainty elements of the processing limit the potentially beneficial ECG inverse solutions from becoming a routine clinical tool at present. The Arruda method differs from prior algorithms in its combined use of the resting ECG, utilization of only five ECG leads (I, II, III, V1, aVF), and by prospective validation of the algorithm.

In this paper we present a sensibility analysis of the Arruda's stepwise method (Arruda *et al.,*1998), and a decomposition algorithm to improve the performance of AcP localization. Our main purpose is to detect more accurately the location of the ventricular insertion.

5.2. Methods

5.2.1. Base studies

This research starts from the results and considerations published in S. M. Szilágyi's "Sensibility Analysis of the Arruda Localization Method" paper (Szilágyi *et al.,* 2004). There has been concluded, that the efficiency of the localization method – described in Arruda's "Development and Validation of an ECG Algorithm for Identifying Accessory Pathway Ablation Site in Wolff-Parkinson-White Syndrome" work (Arruda *et al.,* 1998) – depends significantly on the location of the AcP. The used measurements were realized at the Cardiology Institute of Timişoara.

5.2.2. Outline of the research

According to the above-mentioned studies, we developed a modified Arruda localization method, which was tested and evaluated through our measurements. The schematic representation of the research process can be seen on Fig. 5.1.

The *initial population* (1) of the research consisted of *85 patients* having at least one AcP (delta wave was detected in the preliminary phase of the study). For each patient a 5-10 minutes long 12-lead *ECG* recording was registered. The so-obtained data were then pre-processed and *analyzed* (2) in order to provide input for stages 3-4. Thereafter, we separately predicted the AcP locations by means of the *Arruda* (3) and *modified Arruda* (4) *algorithms*. After *radio-frequency (RF) catheter*

ablation (5), 6 patients were excluded, due to multiple AcP's, while the remaining *79* ones were selected as *test population* (6) for further study phases. In the course of *evaluation of Arruda* (7) *and modified Arruda* (8) *algorithms*, the estimated positions of both localization methods (3-4) were evaluated one by one and validated with the outcome of *RF ablation* (5). Finally, within the frame of the *sensibility analysis* (9), the results of stages 7-8 were statistically compared, followed by a vector-space dissection with regard to the spatial location of the ECG leads used by each algorithm.

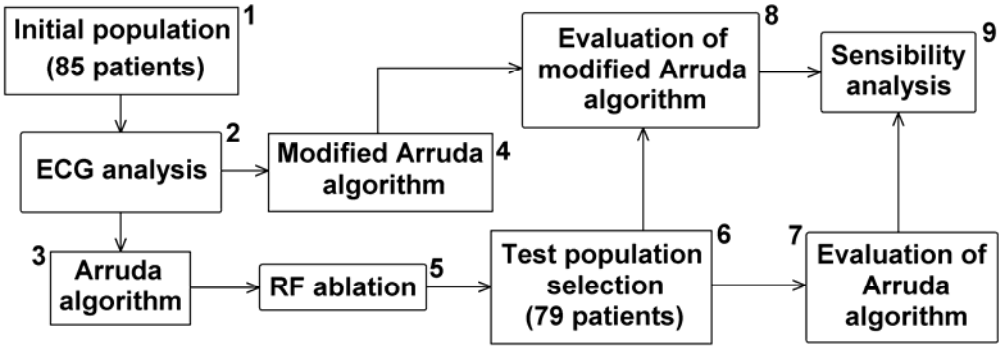

Fig. 5.1. Flow sheet of the research

5.2.3. Initial arrangements

In the preliminary phase of the study we performed a 12-lead ECG measurement for patients manifesting cardiac symptoms that served as a basis to select the subjects suffering from WPW syndrome (initial population – 85 persons). The ECG recordings were sampled at 500Hz frequency with 12-bit resolution. Our ECG signal processing concerned only accurate detection of the QRS complexes and delta (Δ) waves presented in Fig. 5.2., constituting input parameters for the Arruda and modified Arruda algorithms. As Fig. 5.2. presents, one cause for a wide QRS-complex that exceeds 0.12 seconds may be the Wolff-Parkinson-White syndrome (WPW syndrome). In this case the QRS-complex initially exhibits an early upstroke called *delta wave*. The two presented ECG signals differ significantly in shape. In both cases the interval from the P-wave to the R spike is normal, but the early ventricular excitation forming the delta wave shortens the PQ-time.

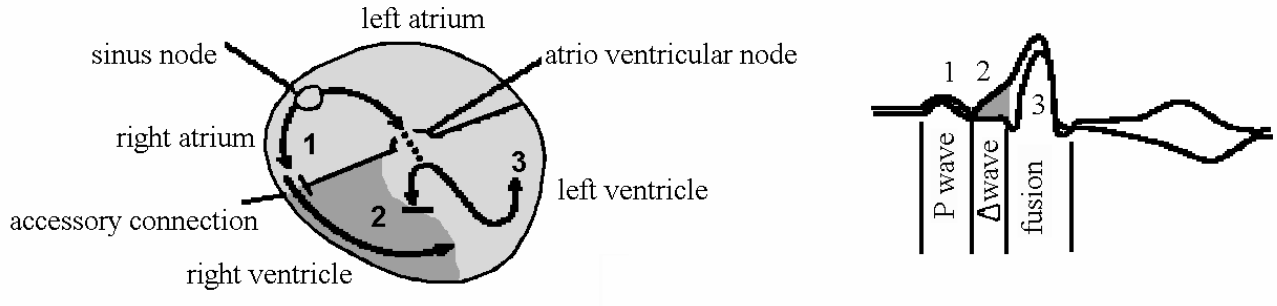

Fig. 5.2. The emergence of WPW syndrome

The cause of the WPW syndrome is the transfer of activation from the atrium (region 1 in Fig. 5.2.) directly to the ventricular muscle via an abnormal route, called AcP, which bypasses the AV junctions. This partially activates the ventricular muscle (region 2 in Fig. 5.2.) before normal activation (region 3 in Fig. 5.2.) reaches it via the normal conduction system (after a delay in the AV junction). This process is called pre-excitation, and the resulting ECG depends on the specific location of the accessory pathway (see right side of Fig. 5.2.). With the help of localization methods the place of AcP can be determined.

5.2.4. The Arruda algorithm

The Arruda algorithm is a well known, clinically tested localization method, developed in order to identify the place of a singular accessory connection, reaching up to 90% recognition rate. It uses only five leads (I, II, III, aVF, V1) from the 12-lead ECG recordings.

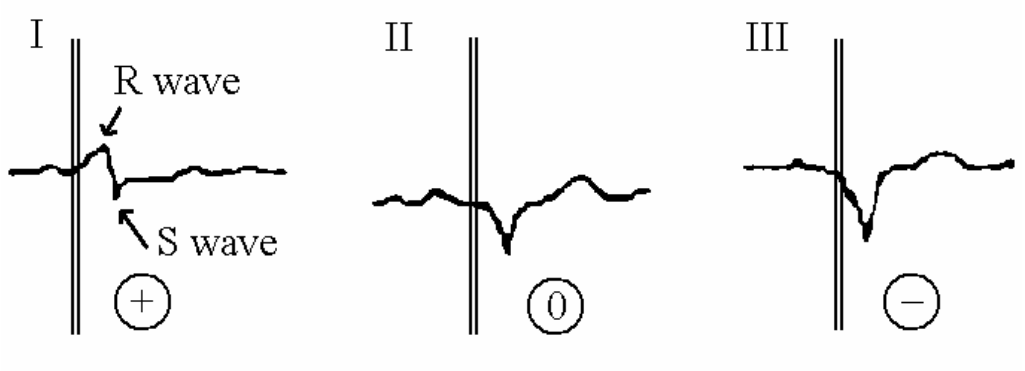

Fig. 5.3. The delta wave polarity

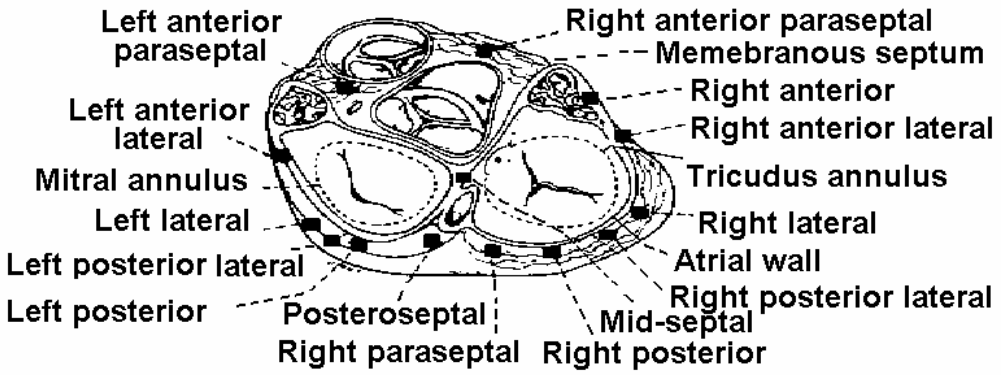

Fig. 5.4. Possible accessory pathway locations

The first step of the algorithm is to analyze the amplitude relations of the R, S and delta (Δ) waves in order to determine the AcP location (see Fig. 5.3.). The onset of the delta wave in each lead is measured from the onset of the earliest delta wave in any of the 12 leads. After 20 ms the displacement of the delta wave in each lead is classified as positive (+), negative (–) or isoelectric (0) (see Fig. 5.3.).

The Arruda algorithm specifies a heart-region as the location of the AcP. According to Arruda, the possible AcP places have been divided into three major regions, which are further divided thereafter, as follows (see Fig. 5.4.):

- Septal accessory pathways: anteroseptal tricuspid annulus and right anterior paraseptal (AS/RAPS), mid-septal tricuspid annulus (MSTA), posteroseptal tricuspid annulus (PSTA), posteroseptal mitral annulus (PSMA), subepicardial posteroseptal (SEC);
- Right free-wall accessory pathways: right anterior (RA), right anterolateral (RAL), right lateral (RL), right posterolateral (RPL), right posterior (RP);
- Left free-wall accessory pathways: left anterolateral (LAL), left lateral (LL), left posterolateral (LPL), left posterior (LP).

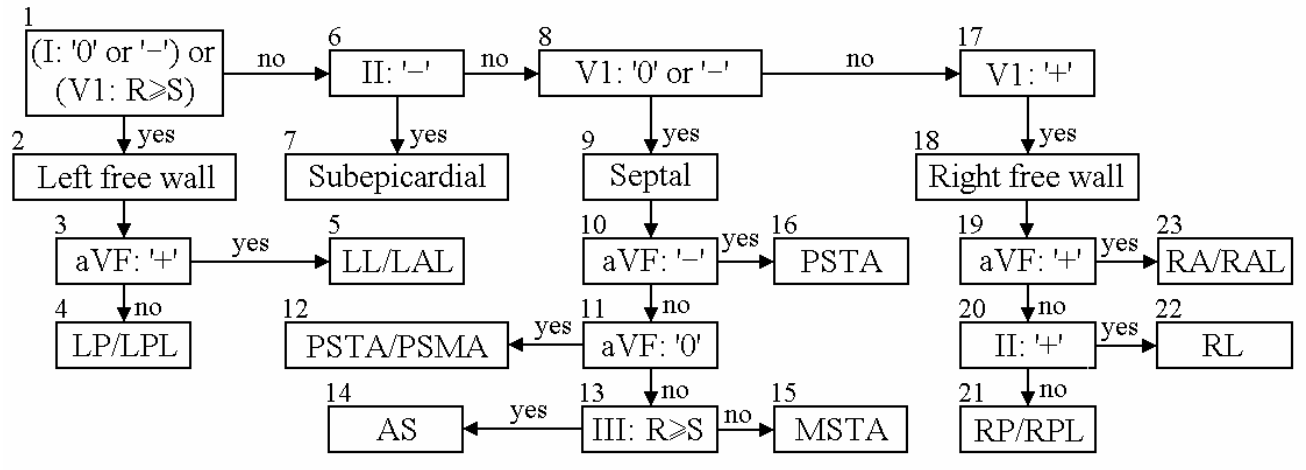

Fig. 5.5. Stepwise Arruda method for determination of AcP location

The proper Arruda algorithm might be interpreted as a decision tree consisting of simple two-way (YES/NO) ramifications, so called decision points (see Figure 5.5.). It has five leads (I, II, III, aVF, V1), R and S waves, respectively the displacement of the delta wave in each lead (+, –, 0) as input, while the above mentioned heart regions (locations) as output.

5.2.5. The modified Arruda algorithm

Although it has been statistically concluded that the performance of the Arruda algorithm is about 90%, some modifications in this localization method could be beneficial.

In (Szilágyi *et al.,* 2004) we pointed out that in most of the cases the estimation errors of the Arruda algorithm are correlated with aVF sign test. In the same place we suggested modifying the lead aVF where it is possible.

The modified Arruda algorithm (see Fig. 5.6.) developed in order to identify the place of a singular accessory connection uses the same leads, same heart regions for localization of the AcP and same displacement of the delta wave in each lead (+, –, 0) as Arruda. The algorithm might be interpreted as a decision tree consisting of simple two-way (yes/no) ramifications with one exception at place 4 (see Figure 5.6.). Although (Szilágyi *et al.*, 2004) revealed that the most sensible aVF sign tests at locations 3, 10 and 19 in Fig. 5.5. we modified only the first one at left free wall (see Fig. 5.6.). The other two sensible places are marked as places 13 and 22 in Fig. 5.6. The left free wall region is completely altered for better performance but all other tests are the same as in Arruda's work.

5.2.6. Radio-frequency catheter ablation

As presented in (Cao *et al.,*2000) the RF catheter ablation of cardiac tissue is highly effective in the invasive treatment of WPW syndrome. During RF cardiac ablation, a catheter is introduced into a heart chamber via percutaneous peripheral venous or arterial conduits and placed in contact with the target ablation region (such as an AcP) at the endocardial surface. A high frequency current is applied between the catheter electrode and a dispersive electrode attached to the patient's skin. The myocardium is heated by Joule heat and heat conduction inside the myocardium. A temperature of 50C° or higher causes irreversible loss of cellular excitability of tissue and forms a lesion (Nath *et al.,*1993).

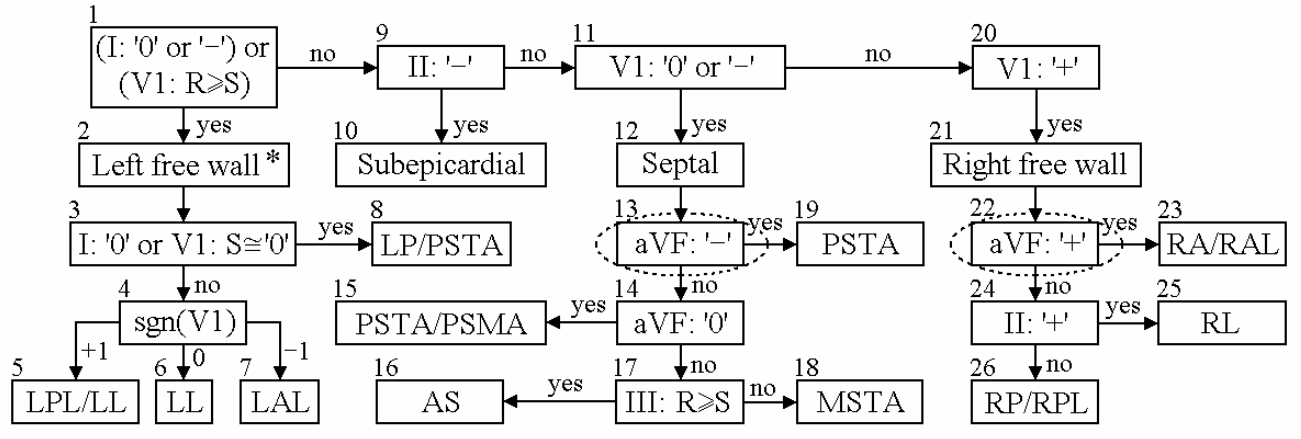

Fig. 5.6. Modified Arruda method for determination of AcP location

In the course of RF ablation, a priori knowledge about the target ablation site(s) could be beneficial due to shorter intervention time and therefore lower risk. The Arruda (as well as the modified Arruda) algorithm predicts the location of a singular AcP, serving as a starting point to the surgeon. However, the exact number and place of the AcP-s will be determined only during the surgical operation. Therefore, RF ablation plays a validation role for both localization methods. By means of RF ablation, we excluded from the research 6 patients with multiple AcP-s, thus obtaining a test population consisting of 79 subjects.

5.3. Results

To evaluate the performance of a localization method we had to analyze the relationship between the predicted location (based upon the ECG algorithm) and the real location (based upon ablation site) of the AcP.

Table V.1. Detection accuracy of the accessory pathway with Arruda localization method

Ablation Site	Number	RA/RAL	RL	RP/ RPL	AS/RASP	MSTA	PSTA	PSTA/PSM	LP/LPL	LL/ LAL	SEC	Sensitivity (%)	Specificity (%)
RA/RAL	11	11										100.0	97.1
RL	8	1	7									87.5	100.0
RP/RPL	6	1		5								83.3	100.0
AS/RASP	2				2							100.0	100.0
MSTA	3					3						100.0	98.7
PSTA	14					1	12		1			85.7	100.0
PSTA/PSMA	1							1				100.0	98.7
LP/LPL	2							1	1			50.0	96.2
LL/LAL	22								2	20		90.9	100.0
SEC	10										10	100.0	100.0
All	79											91.1	99.0

Table V.1. and Table V.2. present this relation for both algorithms, indicating the sensitivity and specificity for all AcP locations. Ablation sites are represented in vertical and the predicted locations in horizontal direction.

Table V.2. Detection accuracy of the accessory pathway with modified Arruda localization method

Ablation Site	Number	RA/RAL	RL	RP/ RPL	AS/RASP	MSTA	PSTA	PSTA/PSMA	LPL/LL	LL	LAL	LP/PSTA	SEC	Sensitivity (%)	Specificity (%)
RA/RAL	11	11												100.0	97.1
RL	8	1	7											87.5	100.0
RP/RPL	6	1		5										83.3	100.0
AS/RASP	2				2									100.0	100.0
MSTA	3					3								100.0	98.7
PSTA	14					1	13							92.9	100.0
PSTA/PSMA	1							1						100.0	100.0
LPL/LL	1								1					100.0	98.7
LL	10								1	9				90.0	100.0
LAL	12										12			100.0	100.0
LP/PSTA	1											1		100.0	100.0
SEC	10												10	100.0	100.0
All	79													94.9	99.5

Table V.3. Detailed accuracy analysis of each decision point for Arruda localization method

Place nr.	Ablation site	Total decisions	Failed decisions	Performance (decision points:total/correct/failed)
4	LP/LPL	2	1	1: 2/1/1 3: 2/2/0
5	LL/LAL	22	2	1: 22/22/0 3: 22/20/2
7	SEC	10	0	1,6: 10/10/0
12	PSTA/PSMA	1	0	1,6,8,10,11: 1/1/0
14	AS/RAPS	2	0	1,6,8,10,11,13: 2/2/0
15	MSTA	3	0	1,6,8,10,11,13: 3/3/0
16	PSTA	14	2	1,10: 14/13/1 6,8: 13/13/0 11,13: no result
21	RP/RPL	6	1	1,6,8: 6/6/0 19: 6/5/1 20: 5/5/0
22	RL	8	1	1,6,8: 8/8/0 19: 8/7/1 20: no result
23	RA/RAL	11	0	1,6,8,19: 11/11/0

Table V.4. Detailed accuracy analysis of each decision point for modified Arruda localization method

Place nr.	Ablation site	Total decisions	Failed decisions	Performance (decision points:total/correct/failed)
5	LPL/LL	1	0	1,3,4: 1/1/0
6	LL	10	1	1,3: 10/10/0 4: 10/9/1
7	LAL	12	0	1,3,4: 12/12/0
8	LP/PSTA	1	0	1,3: 1/1/0
10	SEC	10	0	1,9: 10/10/0
15	PSTA/PSMA	1	0	1,9,11,13,14:1/1/0
16	AS/RAPS	2	0	1,9,11,13,14,17: 2/2/0
18	MSTA	3	0	1,9,11,13,14,17: 3/3/0
19	PSTA	14	1	1,9,11: 14/14/0 13: 14/13/1 14,17: no result
23	RA/RAL	11	0	1,9,11,22: 11/11/0
25	RL	8	1	1,9,11: 8/8/0 22: 8/7/1 24: no result
26	RP/RPL	6	1	1,9,11: 6/6/0 22: 6/5/1 24: 5/5/0

All AcP location predictions were analyzed in order to determine the strong and weak decision points of both localization methods. The result of this analysis is deductible from Tables V.1. and V.2., and is presented in Tables V.3. and V.4. During performance determination the contribution of each decision point was taken into consideration in when it was possible. In some cases a failed decision made all further evaluation meaningless. Such cases are indicated having no result. The last column shows the decision performance for all possible algorithmic branches.

Table V.5. Global accuracy of each decision point for Arruda localization method

Place nr.	Total decisions	Failed decisions	Performance
1	79	1	98.73%
3	24	2	91.67%
6	54	0	100.00%
8	44	0	100.00%
10	20	1	95.00%
11	6	0	100.00%
13	5	0	100.00%
19	25	2	92.00%
20	5	0	100.00%

Table V.6. Global accuracy of each decision point for modified Arruda localization method

Place nr.	Total decisions	Failed decisions	Performance
1	79	0	100.00%
3	24	0	100.00%
4	23	1	95.65%
9	54	0	100.00%
11	44	0	100.00%
13	20	1	95.00%
14	6	0	100.00%
17	5	0	100.00%
22	25	2	92.00%
24	5	0	100.00%

Tables V.5. and V.6. represent the global accuracy of each decision point, deducted from Tables V.3. and V.4., respectively.

5.4. Discussion

A penetrative study of the localization method demands much more, than a simple evaluation of its overall performance, which proves to depend mostly on the least efficient decision points.

A deeper investigation of Table V.5. reflects that applying Arruda localization method the estimation errors often (about 80% of the cases) appear due to wrong decision at places 3, 10, 19 (see Fig. 5.7.). All of these decision points contain an aVF sign test. Furthermore, it is observable that in the diagram none of the aVF sign tests perform reliably.

The main goal of the modified localization method was to eliminate the most sensible decision points and thus to increase the overall performance. Unfortunately, this elimination proves to be easy only theoretically, due to the followings:

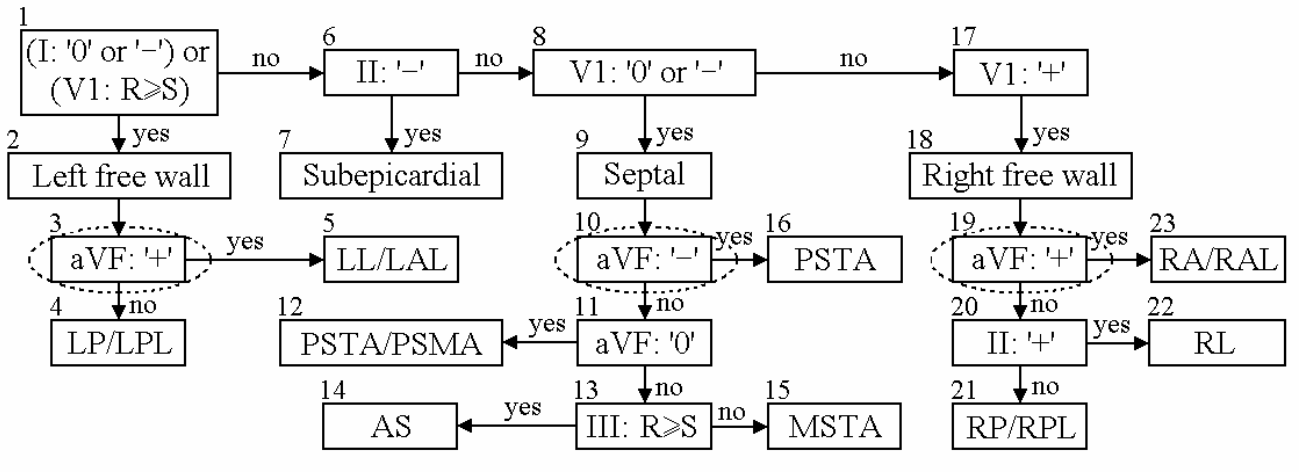

Fig. 5.7. Stepwise Arruda method with marked sensitive decision points

- The depolarization wave's sphere-symmetric propagation is highly deformed by the fact, that the right ventricle wall (4-5mm) is much thinner than the left (10-12mm) or the septal (7-8 mm) one. Taking into consideration the fact, that the depolarization wave propagates at 300-800mm/sec, and the sign of the delta wave is investigated over 20-milisecond intervals, it is obvious that vectorial calculations cannot accurately describe the behaviour of the right ventricle (see Figure 5.8.).
- As Figure 5.8. indicates, the three leads used by Arruda, namely I, V1 and aVF, are almost orthogonal. Although V2 should perform better than V1, no significant difference proved achievable. Unfortunately we have to admit, that despite Arruda's decision points 10 and 19, which detect the septal and right regions, are sensible, they cannot be wisely replaced within the scope of the 12 lead ECG. This is illustrated also in Figure 5.6., where the aVF tests are encircled to indicate the necessity of further development.

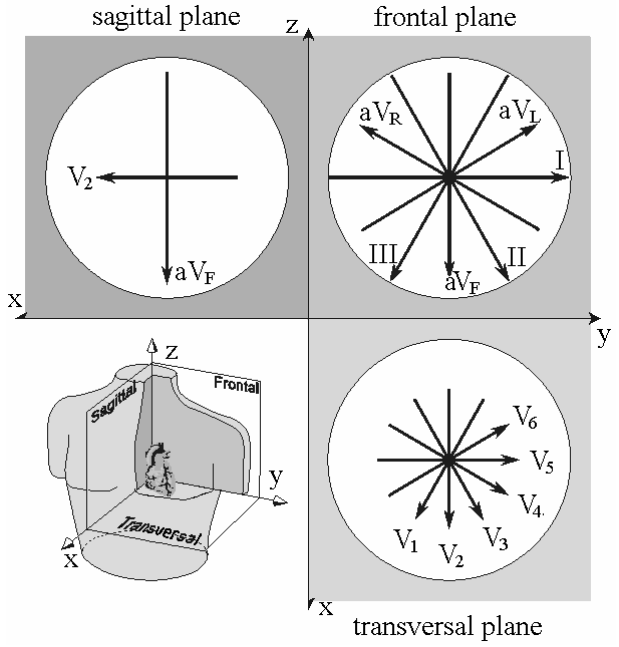

Fig. 5.8. The projections of the lead vectors of the 12-lead ECG system in three orthogonal planes

The thicker wall of the left ventricle allows us to apply vectorial analysis, therefore in this region significant improvements are possible.

Arruda's leads I and aVF (decision points 1 and 3) do not assure visibility in the direction of *x* axis (see Fig. 5.8.). The modified method (decision points 1, 3 and 4) uses the *z* direction instead, which according to Table V.6 at least partially improves the performance. Decision point 6 needs further refinement, because its 95% accuracy is relatively low.

These considerations were tested on our database, and must be used with care, due to the followings:

- Our database was too small to guarantee a solid statistical confirmation;
- The selected patients were not 100% representative (due to the small number);
- We used only few recordings from one patient, so the WPW syndrome could manifest in other way (it could change its behaviour hourly).

5.5. Conclusions

Finally we can conclude the followings:

- Arruda's leads used for the detection of septal and right regions seem to give optimal solution in the scope of 12-lead ECG.
- Significant improvements are achieved in the left ventricle.
- A more accurate analysis requires further studies and a significantly larger database.

The about 95% recognition rate we considered quite good, but a straightforward comparison with other localization methods (Boersma et al., 2002) performed on the same database would be beneficial in order to create a better non-invasive localization method (Szilágyi 2000, Benyó *et al.* 2000; Szilágyi 1999; Szilágyi *et al.*, 2003b).

A high localization performance of non-invasive methods is relevant because they can enlighten the necessary invasive interventions, and also reduce the discomfort caused to the patient.

6. Thesis Points

1st Thesis: Adaptive Processing of the ECG Signal

I have created a complex procedure for precise localization of QRS complexes and ECG signal segmentation. I have involved wavelet-transform-based event recognition to support the ECG processing adaptive neural network and genetic algorithm. I have introduced a novel neural network structure called unified neural network, which can efficiently detect and classify the cardiac events. In order to accomplish efficient information processing, I have created an iterative ECG processing method. I have created an efficient compression method for multi-channel ECG signals, which reliably preserves the medical parameter values (Szilágyi *et al.*, 2007d).

1.1. I have created a spectral transformation formula for event detection, which uses parametrized wavelets (Szilágyi *et al.*, 1997a, 1997b):

$$\Psi(t) = \frac{1}{\sqrt{2\cdot\pi}\cdot\sigma}\cdot\exp\left(-\frac{t^2}{2\cdot\sigma}\right)\cdot\sin(\alpha\cdot t\cdot\exp(-\beta\cdot|t|))$$

1.2. I have created a novel criterion function for ANN-based ECG waveform classification (Szilágyi *et al.*, 2007b, 2007d):

$$J(w) = \lambda_d\cdot\sum_{i=1}^{N}(y_{des,i} - f_s(w^T\cdot x_i))^2 + \lambda_m f_m(z) + \lambda_u\cdot\sum_{i=1}^{N} f_u(w^T\cdot x_i)$$

1.3. I have formulated a long term estimation based signal prediction method, that uses a priori patient-based information to improve its performance in case of both single and multiple channel ECG (Szilágyi *et al.*, 2007a).

1.4. Based on medical parameter values, I have accomplished an efficient compression and automatic diagnosis procedure (Szilágyi *et al.*, 2007d), which has the great advantage that it compares the measured and processed ECG signal from the point of view of the diagnosis, instead of computing RMS errors.

1.5. I have created an iterative procedure for ECG signal filtering and segmentation (Szilágyi *et al.*, 2007a). The segmentation process, because of the involved medical parameters, is reliable even in case of highly noise contaminated signals.

1.6. I have created a complex algorithm for ECG waveform identification that works in both single- and multi-channel mode. The information provided by the pre-filtering, together with the specific morphological features of the signal, are both involved in the artifact separation process. I have realized that this novel approach of the problem is what makes it more efficient, than the available methods from literature (Szilágyi *et al.*, 2007d).

1.7. Using an extended coding mechanism, I have significantly reduced the redundancy of the compacted data (Szilágyi *et al.*, 1997c).

2nd Thesis: Dynamic Heart Modeling

I have created a new computerized method for the simulation of the ECG signal formation and identification of the human inner structure. I have established an ECG processing system, which combines the empirical knowledge, the traditional analysis methods, and the extra information provided by the model. Instead of using the traditional "black box" approach, I have created a model that describes the inner functions of the human body (Szilágyi *et al.*, 2004a, 2004b, 2005c).

2.1. I have created a dynamic compartmental heart structure model based on 3D connections, which can accurately simulate both normal and pathological cases. The accomplished

model can successfully deal with various difficulties like heart movement and position, etc. (Szilágyi *et al.*, 2005a, 2006a).

2.2. By applying inverse ECG processing, I have established a stimulus conduction model of the whole heart or any part of it. In order to improve its efficiency, this model is able to dynamically vary the spatial and temporal resolution of the investigated wave front (Szilágyi *et al.*, 2007c).

2.3. Based on the ECG signal and echocardiography data, I have created an electrical-mechanical heart model that successfully simulates the interactions between electrical and mechanical events (Szilágyi *et al.*, 2007c, 2007e, 2007g).

2.4. I have established a wave front modeling algorithm, which can efficiently use the computation power of massive parallel systems, causing only reduced amount of simulation errors (Szilágyi *et al.*, 2007c).

3rd Thesis: Volumetric Analysis of the Heart based on Echocardiography Images

I have accomplished the volumetric analysis of the heart based on simultaneously registered ECG signal and echocardiography sequences. Based on the simultaneous processing, I have determined the electrical and mechanical properties of the heart, and obtained a more exact description of the heart's inner structure. The investigated heart wall contours were detected using an active appearance model. The time varying volumetric analysis made it possible to create a 4D model of normal and ectopic beats (Szilágyi *et al.*, 2007e, 2007g).

3.1. I have established a heart volumetric reconstruction procedure based on ECG signals and echocardiography images, which for synchronization uses not only the QRS complex, but the whole cardiac cycle, creating thus a more exact electro-mechanical connection, especially in the final stages of the cycle (Szilágyi *et al.*, 2007f, 2007g).

3.2. Based on ECG signal analysis, I have created an image processing method, which takes into consideration the specificities of pathological events. The initial control points of the active appearance model are completely different in case of normal and ectopic beats, and vary from patient to patient (Szilágyi *et al.*, 2007e, 2007g).

3.3. I have created a complex method for the compression of echocardiography image sequences, based on heart wall position estimation and volumetric reconstruction, which by the intensive exploitation of the medical data, reduces significantly the errors of the image estimation model. This method produces better image quality at fixed compression rate and quality criteria, than the available algorithms in the literature (Szilágyi *et al.*, 2007e, 2007f).

4th Thesis: Localization of Accessory Pathway

Starting from Arruda's accessory pathway localization method based on 12-lead ECG signal analysis, I have created a new localization algorithm, which performs better than other published methods (Szilágyi *et al.*, 2004c, 2005b). The new localization method reforms Arruda's procedure in its least reliable decision point, namely the aVF sign test, which is responsible for locations in the left ventricle. A more precise localization of the accessory pathway causing WPW syndrome, before proceeding with the RF ablation, can reduce the duration and improve the efficiency of the intervention (Szilágyi *et al.*, 2006e).

List of Publications and References

Journal Papers

1. **Szilágyi SM**, Szilágyi L, Benyó Z: *Spatial Visualization of the Heart in Case of Ectopic Beats and Fibrillation.* Lecture Notes in Computer Science, Springer Verlag, 2007, accepted paper, ISSN 0302-9743, IF: 0.402
2. **Szilágyi SM**, Szilágyi L, Benyó Z: *Unified Neural Network Based Pathologic Event Reconstruction Using Spatial Heart Model.* Lecture Notes in Computer Science, Springer Verlag, 2007, vol. 4756, pp. 851-860, ISSN 0302-9743, IF: 0.402
3. **Szilágyi SM**, Szilágyi L, Benyó Z: *Echocardiography Image Sequence Compression Based on Spatial Active Appearance Model.* Lecture Notes in Computer Science, Springer Verlag, 2007, vol. 4756, pp. 841-850, ISSN 0302-9743, IF: 0.402
4. **Szilágyi SM**, Szilágyi L, Benyó Z: *Adaptive ECG Compression Using Support Vector Machine.* Lecture Notes in Computer Science, Springer Verlag, 2007, vol. 4756, pp. 594-603, ISSN 0302-9743, IF: 0.402
5. Szilágyi L, **Szilágyi SM**, Benyó Z: *A Modified Fuzzy C-Means Algorithm for MR Brain Image Segmentation,* Lecture Notes in Computer Science, Springer Verlag, 2007, vol. 4633, pp. 866-877, ISSN 0302-9743, IF: 0.402
6. Szilágyi L, **Szilágyi SM**, Benyó Z: *Efficient Feature Extraction for Fast Segmentation of MR Brain Images.* Lecture Notes in Computer Science, Springer Verlag, 2007, vol. 4522, pp. 611-620, ISSN 0302-9743, IF: 0.402
7. **Szilágyi SM**, Szilágyi L, Benyó Z: *Volumetric Analysis of the Heart Using Echocardiography.* Lecture Notes in Computer Science, Springer Verlag, 2007, vol. 4466, pp. 81-90, ISSN 0302-9743, IF: 0.402
8. **Szilágyi SM**, Szilágyi L, Benyó Z: *Spatial Heart Simulation and Analysis Using Unified Neural Network,* Series of Advances in Soft Computing, Springer Verlag, 2007, pp. 346–354, ISSN 1615-3871
9. **Szilágyi SM**, Szilágyi L, Benyó Z: *Support Vector Machine Based ECG Compression,* Series of Advances in Soft Computing, Springer Verlag, 2007, pp. 737-745, ISSN 1615-3871
10. Szilágyi L, **Szilágyi SM**, Benyó Z: *A Modified Fuzzy C-Means Classifier for Fast Segmentation of MR Brain Images*, Series of Advances in Soft Computing, Springer Verlag, 2007, pp. 119-127, ISSN 1615-387
11. **Szilágyi SM**: *3D Heart Simulation and Analysis,* Periodica Polytechnica, Ser. Electrical Engineering, BME, vol. 50, no. 1-2, pp. 79-90, 2006, ISSN 0324-6000
12. **Szilágyi SM**, Szilágyi L, Iclănzan D, Benyó Z: *Unified Neural Network Based Adaptive ECG Signal Analysis and Compression,* Scientific Bulletin of Polytechnica University of Timişoara (Romania), Transactions on Automatic Control and Computer Science, vol. 51(65), no. 4., pp. 27-36, 2006**,** ISSN 1224-600X
13. Máthé Zs, Stan J, **Szilágyi SM**: A nyilvános kulcsú kriptográfia egy lehetséges alkalmazása I., Firka, 2005-06(5), 182-186.
14. Máthé Zs, Stan J, **Szilágyi SM**: A nyilvános kulcsú kriptográfia egy lehetséges alkalmazása II., Firka, 2005-06(6), 223-227.

15. **Szilágyi SM**, Frigy A, Görög LK, Szilágyi L, Benyó Z: *A pitvar-kamrai járulékos nyalábok Arruda-féle lokalizációs módszerének érzékenységi analízise.* ORKI Orvos- és Kórháztechnika, XLII. évf., 6. sz., pp. 164-167, 2004**,** ISSN 1585-7360
16. **Szilágyi SM**, Benyó Z: *Event Recognition from ECG Signal Analysis and 3D Heart Model.* Scientific Bulletin of Polytechnica University of Timişoara (Romania), Transactions on Automatic Control and Computer Science, vol. 49(63), no. 2., pp. 123-128, 2004**,** ISSN 1224-600X
17. **Szilágyi SM**, Frigy A, Benyó Z: *Sensibility Analysis of the Arruda Localization Method.*Scientific Bulletin of Polytechnica University of Timişoara (Romania), Transactions on Automatic Control and Computer Science, vol. 49(63), no. 2., pp. 129-132, 2004**,** ISSN 1224-600X
18. **Szilágyi SM**, Benyó Z: *Szívmodell alapú diagnosztika,* ORKI Orvos- és Kórháztechnika, XLII. évf., 3. sz., pp. 84-86, 2004**,** ISSN 1585-7360
19. Benyó Z, Benyó B, **Szilágyi SM**, Várady P, Szilágyi L: *Research Activity of the Biomedical Engineering Laboratory at TU Budapest*, Research News, TU Budapest, pp. 8-13, 1999, ISSN 1587-2149

Book Chapters

20. **Szilágyi SM**, Szilágyi L, Frigy A, Görög LK, Benyó Z: *Spatial Heart Simulation and Adaptive Wave Propagation*, Encyclopaedia of Healthcare Information Systems, IDEA Group (USA), in press.
21. **Szilágyi SM**, Szilágyi L, Benyó Z: *Volumetric Analysis and Modeling of the Heart Using Active Appearance Model*, Encyclopaedia of Healthcare Information Systems, IDEA Group (USA), in press.
22. **Szilágyi SM**, Szilágyi L, Benyó Z: *Echocardiographic Image Sequence Compression Based on Spatial Active Appearance Model*, Encyclopaedia of Healthcare Information Systems, IDEA Group (USA), in press.
23. **Szilágyi SM**, Szilágyi L, Benyó Z: *Spatial Heart Simulation and Analysis Using Unified Neural Network,* Encyclopaedia of Healthcare Information Systems, IDEA Group (USA), in press.
24. **Szilágyi SM**, Szilágyi L, C. T. Luca, D. Cozma, G. Ivanica, Benyó Z: *Modification of Arruda's Accessory Pathway Localization Method to Improve the Performance of WPW Syndrome Interventions.* Encyclopaedia of Healthcare Information Systems, IDEA Group (USA), in press.
25. Szilágyi L, **Szilágyi SM**, Benyó Z: *Fast and Robust Fuzzy C-Means Algorithms for Automated Brain MR Image Segmentation,* Encyclopaedia of Healthcare Information Systems, IDEA Group (USA), in press

Conference Proceedings – International

26. Szilágyi L, Benyó B, **Szilágyi SM**, Benyó Z: *Medical Image Segmentation Techniques for Virtual Endoscopy,* MCBMS'06, 6th IFAC Symposium on Modeling and Control in Biomedical Systems, Reims (France), pp. 243-248, 2006, ISBN 0080445306.
27. **Szilágyi SM**, Szilágyi L, Benyó Z: *Sensibility Analysis of the Arruda Localization Method and Modifications in Left Ventricle Analysis.* EMBC'06, 28th Annual Int'l Conf. of IEEE

Engineering in Medicine and Biology Society, New York (NY USA), pp. 3998-4001, 2006, ISBN 1424400333.

28. Szilágyi L, **Szilágyi SM**, G. Fördős, Benyó Z: *Quick ECG Analysis for On-Line Holter Monitoring Systems.* EMBC'06, 28th Annual Int'l Conf. of IEEE Engineering in Medicine and Biology Society, New York (NY USA), pp. 1678-1681, 2006, ISBN 1424400333
29. **Szilágyi SM**, Szilágyi L, Benyó Z: *Inverse 3D Heart Model for ECG Signal Simulation and Analysis*. WC2006, World Congress on Medical Physics and Biomedical Engineering, Seoul (South Korea), IFMBE Proc. vol. 14., pp. 27-31, 2006, ISSN 1727-1983
30. **Szilágyi SM**, Szilágyi L, Görög LK, Máthé Zs, Benyó Z: *Modifications in Arruda's Localization Method in Left Ventricle Analysis*, WC2006 World Congress on Medical Physics and Biomedical Engineering, Seoul (South Korea), IFMBE Proceedings vol. 14, pp. 117-120, ISSN 1727-1983, 2006
31. Szilágyi L, **Szilágyi SM**, Benyó Z: *Automated Medical Image Processing Methods for Virtual Endoscopy*, WC 2006 World Congress on Medical Physics and Biomedical Engineering, Seoul (South Korea), IFMBE Proceedings vol. 14, pp. 2267-2270, ISSN 1727-1983, 2006
32. Szilágyi L, **Szilágyi SM**, Benyó Z: *Quick ECG Segmentation, Artifact Detection, and Risk Estimation Methods for On-Line Holter Monitoring Systems*, WC 2006 World Congress on Medical Physics and Biomedical Engineering, Seoul (South Korea), IFMBE Proceedings vol. 14, pp. 914-917, ISSN 1727-1983, 2006
33. **Szilágyi SM**, Szilágyi L, Iclănzan D, Benyó Z: *Adaptive ECG Signal Analysis for Enhanced State Recognition and Diagnosis.* CONTI 2006, Int'l Conference on Technical Informatics, Timişoara (Romania), pp. 209-214, 2006, ISBN 9736253201
34. Szilágyi L, **Szilágyi SM**, Iclănzan D, Benyó Z: *Quick ECG Signal Processing Methods for On-Line Holter Monitoring Systems.* CONTI 2006, Int'l Conference on Technical Informatics, Timişoara (Romania), pp. 221-226, 2006, ISBN 9736253201.
35. Iclănzan D, **Szilágyi SM**, Szilágyi L, Benyó Z: *Advanced Heuristic Methods for ECG Parameter Estimation*. CONTI 2006, Int'l Conference on Technical Informatics, Timişoara (Romania), pp. 215-220, 2006, ISBN 9736253201.
36. Máthé Zs, Görög LK, Creţ O, László SE, **Szilágyi SM:** *Iterative ECG Signal Filtering for Better QRS Recognition,* EMBEC'05, 3rd European Medical & Biological Engineering Conference, Prague, IFMBE Proc. vol 11., paper#2260, pp. 1-6, 2005, ISSN 1727-1983
37. Görög LK, Máthé Zs, Creţ O, **Szilágyi SM:** *Sensibility Analysis of the Arruda Localization Method,* EMBEC'05, 3rd European Medical & Biological Engineering Conference, Prague, IFMBE Proc. vol 11., paper#2309, pp. 1-5, 2005, ISSN 1727-1983
38. **Szilágyi SM**, Szilágyi L, Frigy A, Görög LK, László SE, Benyó Z: *3D Heart Simulation and Recognition of Various Events*, EMBC 2005 - 27th Annual Int'l Conference of IEEE Engineering in Medicine and Biology Society, Shanghai (China), pp. 4038-4041, ISBN 0708387414, 2005
39. Szilágyi L, **Szilágyi SM**, Frigy A, László SE, Görög LK, Benyó Z: *Quick QRS Complex Detection for On-Line ECG and Holter Systems*, EMBC 2005 - 27th Annual Int'l Conference of IEEE Engineering in Medicine and Biology Society, Shanghai (China), pp. 3906-3908, ISBN 0708387414, 2005
40. **Szilágyi SM**, Szilágyi L, Benyó Z: *Risk Estimation Techniques in Case of WPW Syndrome.* 16th IFAC World Congress, Prague, paper #4785, pp. 1-6, 2005, ISBN 008045108X

41. **Szilágyi SM**, Szilágyi L, Benyó Z: *Recognition of Various Events from 3-D Heart Model.* 16th IFAC World Congress, Prague, paper #4695, pp. 1-6, 2005, ISBN 008045108X

42. [1,2] Szilágyi L, Benyó Z, **Szilágyi SM**: *Brain Image Segmentation for Virtual Endoscopy*, EMBC 2004 - 26th Annual Int'l Conference of IEEE Engineering in Medicine and Biology Society, San Fransisco (CA USA), pp. 1730-1732, ISBN 0780384393, 2004

43. [3,4,5] **Szilágyi SM**, Szilágyi L, Dávid L, Benyó Z: *Adaptive Wavelet-Transform-Based ECG Waveforms Detection.* EMBC'03, 25th Annual Int'l Conf. of IEEE Engineering in Medicine and Biology Society, Cancún (Mexico), pp. 2412-2415, 2003, ISBN 0780377893.

44. [6,7,8,9] Szilágyi L, **Szilágyi SM**, Benyó Z, Adam HS: *MR Brain Image Segmentation Using an Enhanced Fuzzy C-Means Algorithm.* EMBC'03, 25th Annual Int'l Conf. of IEEE Engineering in Medicine and Biology Society, Cancún (Mexico), pp. 724-726, 2003, ISBN 0780377893.

45. **Szilágyi SM**, Benyó Z, Dávid L: *Heart Model Based ECG Signal Processing*. MCBMS'03, 5th IFAC Symposium on Modeling and Control in Biomedical Systems, Melbourne (Australia), pp. 213-217, 2003, ISBN 0080441599.

46. **Szilágyi SM**, Benyó Z, Dávid L: *Iterative ECG Filtering for Better Malfunction Recognition and Diagnosis*. MCBMS'03, 5th IFAC Symposium on Modeling and Control in Biomedical Systems, Melbourne (Australia), pp. 295-300, 2003, ISBN 0080441599.

47. **Szilágyi SM**, Benyó Z, Dávid L - *ECG Signal Compression and Noise Distortion Effect Analysis*, World Congress on Medical Physics and Biomedical Engineering, Sydney, Australia (2003), 4391.pdf, ISBN: 1-877040-14-2.

48. **Szilágyi SM**, Benyó Z, Dávid L - *WPW Syndrome Identification and Classification Using ECG Analysis*, World Congress on Medical Physics and Biomedical Engineering, Sydney, Australia (2003), 4423.pdf, ISBN: 1-877040-14-2.

49. **Szilágyi SM**, Szilágyi L, Benyó Z: *Comparison of Malfunction Diagnosis Sensibility for Direct and Inverse ECG Signal Processing Methods.* EMBC'02, 24th Annual Int'l Conf. of IEEE Engineering in Medicine and Biology Society – 2nd Joint Conference of IEEE EMBS and BMES, Houston (TX USA), pp. 244-245, 2002, ISBN 0780376129.

---

[1] Song J, Zhao Q, Wang Y, Tian J: *Gain field correction fast fuzzy c-means algorithm for segmenting magnetic resonance images,* Lect. Notes Comp. Sci **4099**:1242-1247, 2006

[2] Zhao Q, Song J, Wu J: *Improved Fuzzy C-means Segmentation Algorithm for Images with Intensity Inhomogeneity,* Ser. Adv. Soft Comput. (IFSA 2007) **41**:150-159, 2007

[3] Kim TS, Min CH: *ECG based patient recognition model for smart healthcare systems*, Lect. Notes Artif. Intell. **3398**: 159-166, 2005

[4] Wang LC, Chen YQ, Pan M: *Development of QRS Detection Technique*, Space Medicine and Medical Engineering, **19**(3):231-234, 2006, ISSN: 1002-0837

[5] Ghosh D, Midya BL, Koley C, Purkait P: *Wavelet Aided SVM Analysis of ECG Signals for Cardiac Abnormality Detection*, Annual International Conference IEEE INDICON, pp. 9-13, 2005

[6] Yuan K, Wu L, Cheng Q, Bao S, Chen C, Zhang H: *A novel fuzzy c-means algorithm and its application*, Int'l J. Patt. Recogn. Artif. Intell. **19**(8): 1059-1066, 2005, ISSN 0218-0014

[7] Moussaoui A, Benmahammed K, Ferahta N, Chen V: *A New MR Brain Image Segmentation Using an Optimal Semi-supervised Fuzzy C-means and pdf Estimation*, El. Lett. Comp. Vis. Imag. Anal. **5**(4):1-11, 2005, ISSN: 1577-5097

[8] Cai W, Chen S, Zhang D: *Fast and Robust Fuzzy C-Means Clustering Algorithms Incorporating Local Information for Image Segmentation*, Patt. Recogn. **40**(3):825-838, 2007

[9] Pan W, Fu J, Wang XF, Hao CY: *An Automatic Classification Weighted Fuzzy C-Means Image Segmentation Algorithm*, Per. Ocean Univ. China, 37(3):485-488, 2007, ISSN 1672-5174

50. [10,11,12,13,14,15,16] Szilágyi L, **Szilágyi SM**, Benyó Z: *A New Method for Epileptic Waveform Recognition Using Wavelet Decomposition and Artificial Neural Networks*. EMBC'02, 24th Annual Int'l Conf. of IEEE Engineering in Medicine and Biology Society – 2nd Joint Conference of IEEE EMBS and BMES, Houston (TX USA), pp. 2025-2026, 2002, ISBN 0780376129.

51. **Szilágyi SM**, Szilágyi L: *Efficient ECG Signal Compression Using Adaptive Heart Model.* EMBC'01, 23th Annual Int'l Conf. of IEEE Engineering in Medicine and Biology Society, Istanbul (Turkey), pp. 2125-2128, 2001, ISBN 0780372115.

52. [17,18,19] Szilágyi L, Benyó Z, **Szilágyi SM**, Á. Szlávecz, L. Nagy: *On-Line QRS Complex Detection Using Wavelet Filtering*. EMBC'01, 23th Annual Int'l Conf. of IEEE Engineering in Medicine and Biology Society, Istanbul (Turkey), pp. 1872-1874, 2001, ISBN 0780372115.

53. **Szilágyi SM**: *The limits of heart-model-based computerized ECG diagnosis*. EMBC'2000, 22nd Annual Int'l Conf. of IEEE Engineering in Medicine and Biology Society, WC2000 – World Congress on Medical Physics and Biomedical Engineering, Chicago (IL USA), pp. 1913-1916, 2000, ISBN 0780364651.

54. **Szilágyi SM**, Szilágyi L: *Wavelet Transform and Neural-Network-Based Adaptive Filtering for QRS Detection*. EMBC'2000, 22nd Annual Int'l Conf. of IEEE Engineering in Medicine and Biology Society, WC2000 – World Congress on Medical Physics and Biomedical Engineering, Chicago (IL USA), pp. 1267-1270, 2000, ISBN 0780364651.

55. **Szilágyi SM**: *Non-linear adaptive prediction based ECG signal filtering.* EMBC'1999, 21st Annual Int'l Conf. of IEEE Engineering in Medicine and Biology Society – 1st Joint Conference of IEEE EMBS and BMES, Atlanta (GE USA), pp. 296, 1999, ISBN 0780356748.

[10] Firpi H, Goodman E, Echauz J: *Epileptic Seizure Detection by Means of Genetically Programmed Artificial Features*, GECCO'05 Gen. Evol. Comput. Conf., Washington DC, 2005, pp. 461-466, ISBN: 1-59593-010-8.

[11] Firpi H, Goodman E, Echauz J: *On Prediction of Epileptic Seizures by Computing Multiple Genetic Programming Artificial Features*, Lect. Notes Comp. Sci., pp. 321-330, ISSN: 0302-9743

[12] Firpi H, Goodman E, Echauz J: *Genetic Programming Artificial Features with Applications to Epileptic Seizure Prediction*, Proc. 27th Ann. Int'l Conf. of IEEE EMBS, Shanghai, pp. 4510-4513, 2005

[13] Firpi H, Goodman E, Echauz J: *Epileptic Seizure Detection Using Genetically Programmed Artificial Feature*, IEEE Trans. Biomed. Eng. **54**(2):212-224

[14] Ataee P, Avanaki AN, Shariatpanahi HF, Khoee SM: *Ranking features of wavelet-decomposed EEG based on significance in epileptic seizure detection*, Proc 14th Europ. Sign. Proc. Conf., Florence, 1568982271.pdf, pp. 1-4

[15] Xia MF, Liu JB: *Waveform Identification Technology in Intelligent Fault Diagnosis*, Electro-Mechanical Engineering, 2006, **22**(6):49-51,63, ISSN 1008-5300

[16] Urrestarazu E, Iriarte J: *Mathematical analyses in the study of electroencephalographic signals (Analísis matemáticos en el estudio de señales electroencefalograficas)*, Revista de Neurologia, **41**(7):423-434, 2005, ISSN 0210-0010

[17] Darrington J: *Towards real time QRS detection: a fast method using minimam pre-processing*, Biomedical Signal Processing and Control **1**:169-176, 2006.

[18] Alexandridi A, Panagopoulos I, Manis G, Papakonstantinou G: *R-Peak Detection with Alternative Haar Wavelet Filter*, Proc. ISSPIT 2003, paper MP4-4.pdf, pp. 1-4

[19] Duraj A: *Algorytmy rozpoznawania zespołu QRS w sygnałach elektrokardiograficznych pochodzących od pacjentów zwszczepionym układem stymulującym*, PhD Thesis, Universytet Zielonogórski, Wydział Elektrotechniki, Informatyki i Telekomunikacji, Zielona Góra, 2007

56. [20,21,22,23,24] **Szilágyi SM**: *Event recognition, separation and classification from ECG recordings*. EMBC'1998, 20th Annual Int'l Conf. of IEEE Engineering in Medicine and Biology Society, Hong Kong, pp. 236-239, 1998, ISBN 0780351673.

57. Benyó Z, **Szilágyi SM**, Várady P, Benyó B: *Biomedical engineering education in Hungary*. EMBC'1998, 20th Annual Int'l Conf. of IEEE Engineering in Medicine and Biology Society, Hong Kong, pp. 3359-3360, 1998, ISBN 0780351673.

58. [25,26,27,28,29,30,31,32,33,34,35,36,37] **Szilágyi SM**, Szilágyi L, Dávid L: *Comparison Between Neural-Network-Based Adaptive Filtering and Wavelet Transform for ECG Characteristic Points Detection*. EMBC'1997, 19th Annual Int'l Conf. of IEEE Engineering in Medicine and Biology Society, Chicago (IL USA), pp. 272-274, 1997, ISBN 0780342623.

59. **Szilágyi SM**, Szilágyi L, Dávid L: *ECG Signal Compression Using Adaptive Prediction*. EMBC'1997, 19th Annual Int'l Conf. of IEEE Engineering in Medicine and Biology Society, Chicago (IL USA), pp. 101-104, 1997, ISBN 0780342623.

60. **Szilágyi SM**: *Comparison of the neural-network-based adaptive filtering and wavelet transform for R, T and P waves detection*. ITAB'1997, Information Technology in Applications Biomedicine, IEEE Engineering in Medicine and Biology Society Region 8 Conference, Prague, pp. 73-75, 1997, ISBN 0780343182

---

[20] Dokur Z, Ölmez T: *ECG beat classification by a novel hybrid neural network*, Computer Methods and Programs in Biomedicine, **66**(2-3):167-181, 2001, ISSN: 0169-2607

[21] Ölmez T, Dokur Z: *Application of InP Neural Network to ECG Beat Classification*, Neural Comp. Appl. **11**:144-155, 2003

[22] Huang XM, Zhang YH: *A new application of rough set to ECG recognition*, Int'l Conf. Mach. Learn. Cybern. **3**:1729-1734, 2003

[23] Huang XM, Zhang YH: *A new application of Fuzzy Neural Network to ECG Recognition based on Rough Set Theory*, MED'03 - The 11th Mediter. Conf. Contr. Autom. paper #T3-021, pp. 1-6, 2003

[24] Olvera FE: *Electrocardiogram Waveform Feature Extraction Using the Matched Filter*, ECE510: Statistical Signal Processing II, pp. 1-6, 2006

[25] Wen LF, Meng ZH, Zhang YH: *New developments of QRS complex detection methods,* Tsinghua Report, pp.1-9, http://york.eea.tsinghua.edu.cn/6.pdf, 2000

[26] Wen LF, Meng ZH, Zhang YH, Bai J: *New developments of QRS complex detection methods*, Foreign Medicine: Biomedical Engineering, **24**(5):193-197, 2001, ISSN 1001-1110

[27] Stadler RW, Shannon N: *Axis shift analysis of electrocardiogram signal parameters especially applicable for multivector analysis by implantable medical devices, and use of same*, US Patent 6324421, 2001

[28] Stadler RW, Shannon N: *Axis shift analysis of electrocardiogram signal parameters especially applicable for multivector analysis by implantable medical devices, and use of same*, US Patent 6397100, 2002

[29] Li XJ, Chen YQ: *New progress in QRS detection algorithm based on frequency transform*, Biomed. Eng. Foreign Med. Sci. **28**(5):281-286, 2005

[30] Benyó Z: *Education and research in biomedical engineering of the Budapest University of Technology and Economics*, Acta Physiol. Hung. **93**(1):13-21, 2006

[31] Tian XL, Yan CH, Yu YQ, Wang TX: *R-wave Detection of ECG Signal by Using Wavelet Transform*, J. Biomed. Eng. (Shengwu Yixue Gongchengxue Zazhi) **23**(2):257-261, 2006, ISSN 1001-5515

[32] Benyó B.: *Analysis of Temporal Patterns of Physiological Parameters*, in R. Begg, J. Kamruzzaman, R. Sarker (Eds.) *Neural Networks in Healthcare. Potential and Challenges*, Idea Group Publishing, Hershey – London – Melbourne – Singapore, pp. 284-316, 2006, ISBN 159140849-0

[33] Tsipouras MG, Exarchos TP, Fotiadis DI, Kotsia A, Naka A, Michails LK: *A decision support system for the diagnosis of coronary artery disease*, IEEE Symp. Comp. Based Med. Syst., Article #1647582, pp. 279-284, 2006

[34] Botter EA, Nascimento CL Jr, Yoneyama T: *Redes neurais auto-organizáveis para classificação de sinais eletro-cardiográficos atriais*, Integração, **XI**(40):51-56, 2005

[35] Matsuyama A, Jonkman M: *The Application of Wavelet and Feature Vectors to ECG Signals*, TENCON'05, Melbourne, Article number 4085178, pp. 1-4, 2005

[36] Matsuyama A, Jonkman M: *The application of wavelet and feature vectors to ECG signals*, Australasian Phys. Eng. Sci. Med. **29**(1), pp. 13-17, 2006

[37] Matsuyama A, Jonkman M, de Boer F: *Improved ECG Signal Analysis Using Wavelet and Feature Extraction*, Methods of Information in Medicine **46**(2):227-230, 2007

Conference Proceedings – Others

61. László SE, **Szilágyi SM**: *Mobil EKG mérés és ritmusanalízis*, X. Fiatal Műszakiak Tudományos Ülésszaka, Kolozsvár, 2005, p. 193-196, ISBN 973-8231-44-2
62. Görög LK, **Szilágyi SM**: *Using reading Techniques in Complex Software-developing Systems*, 15th International Conference in Computer Science and Education, Kolozsvár, 2005, pp. 153-159, ISBN 973-7840-08-1
63. **Szilágyi SM**, László SE, Görög LK: *Complex Heart Diagnosis Methods*, 15th International Conference in Computer Science and Education, Kolozsvár, 2005, pp. 192-201, ISBN 973-7840-08-1
64. László SE, **Szilágyi SM**, Görög LK: *ECG Signal Measurement and Rhythm Analysis*, 15th International Conference in Computer Science and Education, Kolozsvár, 2005, pp. 202-209, ISBN 973-7840-08-1
65. Szász ZE, **Szilágyi SM**: *MRI Image Analysis with Genetic Algorithms*, 15th International Conference in Computer Science and Education, Kolozsvár, 2005, pp. 210-219, ISBN 973-7840-08-1
66. László SE, **Szilágyi SM**: *3D Modellezés Lehetőségei*, IX. Fiatal Műszakiak Tudományos Ülésszaka, Kolozsvár, 2004., p. 147-150, ISBN 973-8231-33-7
67. Görög LK, Máthé Zs, Komáromi L, **Szilágyi SM**: *A mesterséges intelligencia labirintusa*, IX. Fiatal Műszakiak Tudományos Ülésszaka, Kolozsvár, 2004., p. 171-174, ISBN 973-8231-33-7
68. Görög LK, Komáromi L, Máthé Zs, **Szilágyi SM**: *Az őrült labirintus*, IX. Fiatal Műszakiak Tudományos Ülésszaka, Kolozsvár, 2004, p. 174-178, ISBN 973-8231-33-7
69. Máthé Zs, Görög LK, Komáromi L, **Szilágyi SM**: Mesterséges intelligencia társasjátékokban, 14 th International Conference in Computer Science and Education, Kolozsvár, 2004, ISBN 973-86097-8-X
70. **Szilágyi SM**: *Szívmodell alapú számítógépes EKG diagnosztika*, BUDAMED'99, 4pp, Budapest, 1999.
71. **Szilágyi SM**, Szilágyi L: *Artifact Separation and Classification from ECG Recordings*, Proceedings of the Conference on the Latest Results in Information Technology, Budapest, 1998, pp. 85-90, ISBN: 963-421-548-3.
72. Szilágyi L, **Szilágyi SM**: *Paraméterbecslő módszerek alkalmazása szívaritmiák felismerésére,* III. Fiatal Műszakiak Tudományos Ülésszaka, Kolozsvár, 1998, pp. 61-64.
73. **Szilágyi SM**, Szilágyi L: *Adaptive Estimator for ECG Signal Compression,* Proceedings of the Conference on the Latest Results in Information Technology, Budapest, 1997, pp. 50-53, ISBN: 963-421-545-9.
74. Szilágyi L, **Szilágyi SM**: *Az EKG jel tömörítése genetikai algoritmus alkalmazásával,* II. Fiatal Műszakiak Tudományos Ülésszaka, Kolozsvár, 1997, pp. 149-152.
75. **Szilágyi SM**, Szilágyi L, Moldován IZ: *Új lehetőségek az orvostudományban az EKG jelek feldolgozása terén,* I. Fiatal Műszakiak Tudományos Ülésszaka, Kolozsvár, 1996, pp. 1-4.

Other Presentations - Abstracts

76. **Szilágyi SM**, Szilágyi L, Benyó Z: *Paralellism in Inverse 3-D Heart Modeling*, MACS06 – 6th Joint Conference on Mathematics and Computer Science, Pécs, pp. 88, 2006

77. Szilágyi L, **Szilágyi SM**, Benyó Z: *Level Set Methods in 3-D Medical Imaging*, MACS06 – 6th Joint Conference on Mathematics and Computer Science, Pécs, pp. 87, 2006
78. **Szilágyi SM**: *Térbeli szívmodellezés és elemzés,* 10 éves az Orvosbiológiai Mérnökképzés Magyarországon Konferencia, Budapest, 2005
79. **Szilágyi SM**: *Szívmodell alapú számítógépes EKG diagnosztika*, A Magyar Élettani Társaság LXIV. Vándorgyűlése, Budapest, 1999, pp. 137.
80. **Szilágyi SM**, Szilágyi L, Frigy A, Incze A: *Holter Telemetry in the Study of Heart Rate Variability,* Romanian Heart Journal, Vol. 2., Nr. 6, 1996, pp. 143.
81. **Szilágyi SM**, Moldován IZ, Szilágyi L: *EKG jelek feldolgozásának hardver és szoftver kérdései,* Orvosbiológiai Mérnökképzés Kutatások és Oktatás nemzetközi tudományos konferencia, Budapest, 1996, pp. 24.
82. **Szilágyi SM**, Moldován IZ, Szilágyi L: *Új lehetőségek az orvostudományban az EKG jelek feldolgozása terén,* Orvosbiológiai Mérnökképzés Kutatások és Oktatás nemzetközi tudományos konferencia, Budapest, 1996, pp. 23.

References

Afonso VX, Tompkins WJ (1995) Detecting ventricular fibrillation. *IEEE EMBS Mag.* **14**(2):152–159.

Ahmed SM, Al-Shrouf A, Abo-Zahhad M (2000) ECG data compression using optimal non-orthogonal wavelet transform. *Medical Engineering & Physics* **22**:39–46.

Amano A, Nishi T, Sarai N, Matsuoka S, Matsuda T, Noma A (2003) Evaluation of two cardiac cell in the context of whole cell simulation. *Proc. Ann. Int. Conf. IEEE EMBS*, Cancún **25**:2780–2783.

Angelini ED, Laine AF, Takuma S, Holmes JW, Homma S (2001) LV volume quantification via spatiotemporal analysis of real-time 3-D echocardiography. *IEEE Trans. Med. Imag.* **20**:457–469.

Antzelevitch C, Shimizu W, Yan GX, Sicouri S, Weissenburger J, Nesterenko VV, Burashnikov A, di Diego J, Saffitz J, Thomas GP (1999) The M cell: its contribution to the ECG and to normal and abnormal electrical function of the heart. *J. Cardiovasc. Electrophys.*, **10**:1124–1152.

Arruda MS, Wang X, McClelland JH (1992) ECG algorithm for predicting radiofrequency ablation site in posteroseptal accessory pathways. *PACE* 15(Pt II):535.

Arruda MS, Wang X, McClelland JH (1993) ECG algorithm for predicting sites of successful radiofrequency ablation of accessory pathways. *PACE* 16(Pt II) 865.

Arruda MS, Wang X, McClelland JH (1994) Negative delta wave in lead II identifies posteroseptal accessory pathways requiring ablation in venous branches of the coronary sinus. *J Am Coll Cardiol* (Suppl) 224A.

Arruda MS, McClelland JH, Wang X, Beckman KJ, Widman LE, Gonzalez MD, Nakagawa H, Lazzara R, Jackman WH (1998): Development and validation of an ECG algorithm for identifying accessory pathway ablation site in Wolff-Parkinson-White syndrome, *J Cardiovascular Electrophysiology* **9**(1):2–12.

Belohlavek M, Manduca A, Behrenbeck T, Seward J, Greenleaf JF (1996) Image analysis using modified self-organizing maps: automated delineation of the left ventricular cavity in serial echocardiograms. *Proc. Visual. Biomed. Comp. Conf.* 247–252.

Benjamin EJ, Levy D (1999) Why is left ventricular hypertrophy so predictive of morbidity and mortality? *Am. J. Med. Sci.* **317**:168–175.

Benyó B, Asztalos B (2000) Detection of pathologic alterations of the heartwall based on ultrasound and echocardiographic pictures. *ORKI Medical and Hospital Engineering,* **38**(2):36–40.

Besl PJ, McKay ND (1992) A method for registration of 3-D shapes. *IEEE Trans. Patt. Anal. Mach. Intell.* **14**:239–256.

Boersma L, Moran EG, Mont L, Brugada J (2002) Accessory pathway localization by QRS polarity in children with Wolff-Parkinson-White syndrome. *J Cardiovasc Electrophysiol* **13**(12):1222–1226.

Bosch JG, Mitchell SC, Lelieveldt BPF, Nijland F, Kamp O, Sonka M, Reiber JHC (2002) Automatic segmentation of echocardiographic sequences by active appearance motion models. *IEEE Trans. Med. Imag.* **21**:1374–1383.

Brotherton T, Pollard T, Simpson P, DeMaria A (1994) Echocardiogram structure and tissue classification using hierarchical fuzzy neural networks. *Proc. IEEE Conf. Acoustics Speech Sign. Proc.* **2**:573–576.

Burges C (2000) A tutorial on support vector machines for pattern recognition. In: Fayyad U: *Knowledge discovery and data mining*, Kluwer, 1–43.

Caillerie D, Mourad A, Raoult A (2002) Toward a fiber-based constitutive law for the myocardium. *Proc. Mod. Sim. Comp. Aid. Med. Surg. (MS4CMS'02), ESAIM Proceedings,* **12**:25–30.

Campbell KB, Razumova MV, Kirkpatrick RD, Slinker BK (2001) Nonlinear myofilament regulatory process affect frequency development muscle fiber stiffness, Biophys. J. **81**(4):2278–2296.

Cao H, Vorperian VR, Tsai JZ, Tungjitkusolmun S, Woo EJ, Webster JG (2000) Temperature measurement within myocardium during in vitro RF catheter ablation. *IEEE Trans. Biomed. Eng.* **47**:1518–1524.

Chalana V, Linker DT, Haynor DR, Kim Y (1996) A multiple active contour model for cardiac boundary detection on echocardiographic sequences. *IEEE Trans. Med. Imag.* **15**:290–298.

Cherry EM, Greenside HS, Henriquez CS (2000) A space-time adaptive method for simulating complex cardiac dynamics. *Phys. Rev. Lett.* **84**:1343–1346.

Cherry EM, Greenside HS, Henriquez CS (2003). Efficient simulation of threedimensional anisotropic cardiac tissue using an adaptive mesh refinement method. *Chaos* **13**:853–865.

Chiu E, Vaisey J, Atkins MS (2001) Wavelet-based space-frequency compression of ultrasound images. *IEEE Trans. Inf. Tech. Biomed. Eng.* **5**:300–310.

Cohen A, Zigel Y (1998) Compression of multichannel ECG through multichannel long-term prediction. *IEEE Engineering in Medicine and Biology Magazine* 16(4):109–115.

Colella D, Heil C (1994) Characterizations of scaling functions: continuous solutions. *SIAM Journal of Matrix Analysis Applications* **13**(2):496–518.

Cootes TF, Edwards GJ, Taylor CJ (2001) Active appearance models. *IEEE Trans. Patt. Anal. Mach. Intell.* **23**:681–685.

Couderc JP, Zareba W, Moss AJ (1998) New-method for the quantification of beat-to-beat T wave temporal variability based on interscale changes in wavelet transform of the ECG: application to simulated ECG signals. *Proc. of IASTED International Conference, IEEE* 213–216.

Courtemanche M (1996) Complex spiral wave dynamics in a spatially distributed ionic model of cardiac electrical activity. *Chaos* **6**:579–600.

Crammer K., Singer Y (2000) On the learnability and design of output codes for multi-class problems. *Proc. 13th Conf. Comput. Learn. Theory* 35–46.

Cuppen JJM, van Oosterom A (1984) Model studies with inversely calculated isochrones of ventricular depolarization. *IEEE Trans. Biomed. Eng.* **31**:652–659.

Dias JMB, Leitão JMN (1996) Wall position and thickness estimation from sequences of echocardiographic images. *IEEE Trans. Med. Imag.* **15**:25–38.

Dumoulin SO, Hoge RD, Baker CL Jr., Hess RF, Achtman RL, Evans AC (2003) Automatic volumetric segmentation of human visual retinotopic cortex. *Neuroimage* **18**:576–587.

Duncan JS, Ayache N (2000) Medical image analysis: progress over two decades and the challenges ahead. *IEEE Trans. Patt. Anal. Mach. Intell.* **22**:85–105.

Edwards GJ, Taylor CJ, Cootes TF (1998) Interpreting face images using Active Appearance Models. *Proc. 3rd Int. Conf. Face and Gesture Recogn. Japan*, 300–305.

Erickson BJ, Manduca A, Palisson P, Persons KR, Earnest D, Savcenko V (1998) Wavelet compression of medical images. *Radiology* **206**:599–607.

Erickson BJ (2002) Irreversible compression of medical images. *J. Digital Imaging* **15**:5–14.

Evans AN, Nixon MS (1996) Biased motion-adaptive temporal filtering for speckle reduction in echocardiography. *IEEE Trans. Med. Imag.* **15**:39–50

Evans FG, Rogers JM, Smith WM (1999) Automatic detection of conduction block based on time-frequency analysis of unipolar electrograms, *IEEE Trans. on Biomed. Eng.* **46**:1090–1097.

Fast VG, Rohr S, Gillis AM, Kléber AG (1998) Activation of cardiac tissue by extracellular electrical shocks: formation of 'secondary sources' at intercellular clefts in monolayers of cultured myocytes. *Circ. Res.* **82**:375–385.

Fenster A, Downey DB, Cardinal HN (2001) Three-dimensional ultrasound imaging. *Physics in Medicine and Biology* **46**:67–99.

Fidler A, Skaleric U (2006) The impact of image information on compressibility and degradation in medical image compression. *Med. Phys.* **33:**2832–2838.

Fitzpatrick AP, Gonzales RG, Lesh MD, Modin GW, Lee RJ, Scheinmen MM (1994) New algorithm for the localization of accessory atrioventricular connections using a baseline electrocardiogram. *J. Am. Coll. Cardiol.* **23**:107–116.

Friesen GM, Jannett TC, Jadallah MA, Yates SL, Quint SR, Nagle HT (1990) A comparison of the noise sensitivity of nine QRS detection algorithms. *IEEE Trans. Biomed. Eng.* **37**(1):85–97.

García J, Sörnmo L, Olmos S, Laguna P (2000) Authentic detection of ST-T complex changes on the ECG using filtered RMS difference series: application to ambulatory ischemia monitoring. *IEEE Trans. Biomed. Eng.* **47**:1195–1201.

Geiser EA, Wilson DC, Wang DX, Conetta DA, Murphy JD, Hutson AD (1998) Autonomous epicardial and endocardial boundary detection in echocardiographic shor-axis images. *J. Amer. Soc. Echocardiogr.* **11**:338–348.

Ghuran A, Reid F, La Rovere MT, Schmidt G, Bigger JT, Camm AJ, Schwartz PJ, Malik M (2002) Heart rate turbulence-based predictors of fatal and nonfatal cardiac arrest (The autonomic tone and reflexes after myocardial infarction substudy). *Am. J. Cardiol.* **89**:184–190.

Godefroid P, Khurshid S (2002) Exploring very large state spaces using genetic algorithms. *Lect. Notes Comp. Sci.* **2280**:266–280.

Gomis P, Jones DL, Caminal P, Berbari EJ, Lander P (1997) Analysis of abnormal signals within the QRS complex of the high-resolution electrocardiogram, IEEE Trans. Biomed. Eng. **44**:681–693.

Goudevenos JA, Katsouras CS, Graekas G, Argiri O, Giogiakas V, Sideris DA (2000) Ventricular pre-excitation in the general population: a study on the mode of presentation and clinical course. *Heart* **83**:29–34.

Guanglin L, Bin H (2001) Localization of the site of origin of cardiac activation by means of a heart-model-based electrocardiographic imaging approach. *IEEE Trans. Biomed. Eng.* **48**:660–669.

de Guise J, Gulrajani RM, Savard P, Guardo R, Roberge FA (1985) Inverse recovery of two moving dipoles from simulated surface potential distributions on a realistic human torso model. *IEEE Trans. Biomed. Eng.* **32**:126–135.

Guize L, Soria R, Chaouat JC, Chrétien JM, Houe D, Le Heuzey JY (1985) Prevalence and course of Wolff-Parkinson-White syndrome in population of 138,048 subjects. *Ann Med Interne* (Paris) **136**:474–489.

Häfner J, Sachse F, Sansour C, Seemann G, Dössel O (2002) Hyperelastic description of elastomechanic properties of the heart: a new material law and its application. *Biomed. Tech.* **47**:770–773.

Haider AW, Larson MG, Benjamin EJ, Levy D (1998) Increased left ventricular mass and hypertrophy are associated with increased risk for sudden death. *J. Am. Coll. Cardiol.* **32**:1454–1459.

Hamarneh G, Gustavsson T (2004) Deformable spatio-temporal shape models: extending ASM to 2D+time. *J. Imag. Vis. Comput.* **22**:461–470

Hang X, Greenberg NL, Zheng YF, Thomas JD (2006) Compression of 3-D echocardiographic images using a modified 3-D set-partitioning-in-hierarchical-trees algorithm based on a 3-D wavelet packet transform. *J. Electronic Imaging* **15**:2, 023016 (13 pages).

Harrild DM, Henriquez CS (2000) A computer model of normal conduction in the human atria. *Circ. Res.* **87**:25–36.

Hsu E., Henriquez CS (2001) Myocardial fiber orientation mapping using reduced encoding diffusion tensor imaging. *J. Cardiovasc. Magn. Reson.* **3**:325–333

Huiskamp G, Greensite F (1997) A new method for myocardial activation imaging. *IEEE Trans. Biomed. Eng.* **44**:433–446.

Ishijima M (1993) Fundamentals of the decision of optimum factors in the ECG data compression, *IEICE Trans. Inform. Syst.*, **E76-D**(12) 1398–1403

Issenberg SB, Gordon MS, Gordon DL, Safford RE, Hart IR (2001) Simulation and new learning technologies. *Med. Teach.* **23**:16–23.

Istepanian RSH, Petrosian AA (2000) Optimal zonal wavelet-based ECG compression for mobile telecardiology system, IEEE Trans. Inform. Tech. Biomed. **4**(3):200–211.

Johnson CR, MacLeod RS (1998) Adaptive local regularization methds for the inverse ECG problem. *Progr. Biophys. Mol. Biol.* **69**:405–423.

Johnston PR, Gulrajani RM (1997) A new method for regularization parameter determination in the inverse problem of electrocardiography. *IEEE Trans. Biomed. Eng.* **44**:19–39

Joho S, Asanoi H, Remah H, Igawa A, Kameyama T, Nozawa T, Umeno K, Inoue H (1999) Time-varying spectral analysis of heart rate and left ventricular pressure variability during balloon coronary occlusion in humans. *J. Amer. Coll. Cardiol.* **34**(7):1924–1931.

Josephson M (1993) Preexcitation syndromes. In: Josephson M (Ed.): *Clinical Cardiac Electrophysiology*, Lea & Febiger: Philadelphia, 311–416.

Joshi D, Li J, Wang JZ (2006) A computationally efficient approach to the estimation of two- and three-dimensional hidden Markov models. *IEEE Trans. Image Proc.* **15**:1871–1886.

Khamene A, Negahdaripour S (2000) A new method for the extraction of fetal ECG from the composite abdominal signal. *IEEE Trans. Biomed. Eng.* **47**(4):507–516.

Lagerholm M, Peterson C, Braccini G, Edenbrandt L, Sörnmo L (2000) Clustering ECG complexes using Hermite functions and self-organizing maps. *IEEE Trans. Biomed. Eng.* **47**:838–848.

Lelieveldt BPF, Mitchell SC, Bosch JG, van der Geest RJ, Sonka M, Reiber JHC (2001) Time continuous segmentation of cardiac image sequences using active appearance motion models. *Lect. Notes Comp. Sci.* **2082**:446–452.

Lelieveldt BPF, van der Geest RJ, Mitchell SC, Bosch JG, Sonka M, Reiber JHC (2002) 3-D active appearance models: fully automatic detection of endoand epicardial contours in short-axis cardiac MR data. *Proc. Int. Soc. Magn. Res. Med.* (ISMRM) **2**:1668.

Lemire D, Pharand C, Rajaonah JC, Dubé B, LeBlanc AR (2000) Wavelet time entropy, T wave morphology and myocardial ischemia. *IEEE Trans. on Biomed. Eng.* **47**(7):967–970.

Li C, Zheng C, Tai C (1995) Detection of ECG characteristic points using wavelet transforms. *IEEE Trans. on Biomed. Eng.* **42**(1):21–27.

Lux RL, Smith CR, Wyatt RF, Abildskov JA (1978) Limited lead selection for estimation of body surface potential maps in electrocardiography, *IEEE Trans. Biomed. Eng.* **25**:270–276.

MacLeod RS, Brooks DH (1998) Recent progress in inverse problems in echocardiology. *IEEE EMBS Mag*. **17**(1):73–83.

Mallat S, Hwang WL (1992) Singularity detection and processing with wavelets. *IEEE Trans. Inform. Theory* **38**(3):617–643.

Masood S, Yang G, Pennell D, Firmin D (2000) Investigating intrinsic myocardial mechanics: the role of MR tagging, velocity phase mapping and diffusion imaging. *J. Magn. Reson. Imag.* **12**:873–883.

Meste O, Rix H, Caminal P, Thakor NV (1994) Ventricular late potentials characterization in time-frequency domain by means of a wavelet transform, *IEEE Trans. Biomed. Eng.* **41**(7):625–634.

Minami K, Nakajima H, Yoyoshima T (1999) Real time discrimination of the ventricular tachyarrhythmia with Fourier-transform neural network. *IEEE Trans. Biomed. Eng.* **46**:179–185.

Mirvis DM (1988) Validation of body surface electrocardiographic mapping. In: Mirvis DM (Ed.): *Body Surface Electrocardiographic Mapping*. Kluwer Acad. Publ., Boston-Dordrecht-London 63–74.

Mitchell SC, Bosch JG, Lelieveldt BPF, van der Geest RJ, Reiber JHC, Sonka M (2002a) 3-D active appearance models: segmentation of cardiac MR and ultrasound images. *IEEE Trans. Med. Imag.* **21**:1167–1178.

Mitchell SC, Lelieveldt BPF, Bosch JG, van der Geest RJ, Reiber JHC, Sonka M (2002b) Segmentation of cardiac MR volume data using 3D active appearance models. *Proc. SPIE Med. Imag.* 433–443.

Montagnat J, Delingette H, Malandain G (1999) Cylindrical echocardiographic image segmentation based on 3-D deformable models. *Lect. Notes Comp. Sci.* (MICCAI' 99) **1679**:168–176.

Moreau-Villéger V, Delingette H., Sermesant M, Ashikaga H., McVeigh E, Ayache N (2006) Building maps of local apparent conductivity of the epicardium with a 2-D electrophysiological model of the heart. *IEEE Trans. Biomed. Eng.* **53**:1457–1466.

Nath S, Lynch C, Whayne JG, Haines DE (1993) Cellular electrophysiological effects of hyperthermia on isolated guinea pig papillary muscle implications for catheter ablation. *Circulation* **88**:1826–1831.

Nave G, Cohen A (1993) ECG compression using long-term prediction, *IEEE Trans. Biomed. Eng.* **40**:877–885.

Negroni J, Lascano E (1996) A cardiac muscle model relation sarcomere dynamics to calcium kinetics, *J. Mol. Cell. Cardiol.* **28**:915–929.

Noble D (2004) Modeling the heart. *Physiol.* **19**(4):191–197.

Nygren A, Fiset C, Firek L, Clark JW, Lindblad DS, Clark RB, Giles WR (1998) Mathematical model of an adult human atria cell: the role of K+ currents in repolarization. *Circ. Res.* **82**:63–81.

Osowski S, Hoai LT (2001) ECG beat recognition using fuzzy hybrid neural network. *IEEE Trans. Biomed. Eng.* **48**:1265–1271.

Osowski S, Hoai LT, Markiewicz T (2004) Support vector machine-based expert system for reliable heartbeat recognition. *IEEE Trans. Biomed. Eng.* **51**:582–589.

Oster HS, Taccardi B, Lux RL, Ershler PR, Rudy Y (1997) Noninvasive electrocardiographic imaging: Reconstruction of epicardial potentials, electrograms, and isochrones and localization of single and multiple electrocardiac events. *Circulation* **96**:1012–1024.

Panfilov AV (1999) Three-dimensional organization of electrical turbulence in the heart. *Phys. Rev. E,* **59**:R6251–R6254.

Park K, Metaxas D, Axel L (2003) A finite element model for functional analysis of 4D cardiac-tagged MR images. *Lect. Notes Comp. Sci.* **2878**:491–498.

Pommert A, Höhne KH, Pflesser B, Richter E, Riemer M, Schiemann T, Schubert R, Schumacher U, Tiede U (2001) Creating a high-resolution spatial/symbolic model of the inner organs based on the visible human. *Med. Image Anal.* **5**:221–228.

Prado R, García I (2001) Analysis of electrocardiogram signals via wavelet based Bayesian models. *Ann. Inst. Statist. Math.* **52**(1):1–18.

Provazník I, Kozumplík J (1997) Wavelet transform in electrocardiography – data compression. *Int. J. Med. Inform.* **45**:111–128.

Provazník, I (2001) Wavelet analysis for signal detection – applications to experimental cardiology research. Habil. Thesis, Brno Univ. Tech.

Quan W, Evans SJ (1998) Efficient integration of a realistic two-dimensional cardiac tissue model by domain decomposition. *IEEE Trans. Biomed. Eng.* **45**:372–384.

Reddy GV, Schamroth L (1987) The localization of bypass tracts in the Wolff-Parkinson-White syndrome from the surface electrocardiogram. *Amer. Heart. J.* **113**(4): 984-993.

Rix H, Meste O (1997) Fine structure of ECG signal using wavelet transform. In: D'Attelis CE, Fernández-Bergauder EM (Eds.) Wavelet Theory and Harmonic Analysis in Applied Sciences. Birkhäuser: Boston.

Rosenbaum FF, Hecht HH, Wilson FN, Johnston FD (1945) The potential variation of the thorax and the esophagus in anomalous antrioventricular excitation (Wolff–Parkinson–White syndrome). *Amer. Heart J.* **29**:281–326.

Said A, Pearlman WA (1996) A new, fast, and efficient image codec based on set partitioning in hierarchical trees. *IEEE Trans. Circ. Syst. Video Techn.* **6**:243–250.

Sanches JM, Marques JS (2000) A Rayleigh reconstruction/interpolation algorithm for 3D ultrasound. *Patt. Recogn. Lett.* **21**:917–926.

Schmidt G, Malik M, Barthel P, Schneider R, Ulm K, Rolnitzky L, Camm AJ, Bigger JT Jr, Schömig A (1999) Heart-rate turbulence after ventricular premature beats as a predictor of mortality after acute myocardial infarction. *Lancet* **353**:1390–1396.

Senhadji L, Carrault G, Bellanger JJ, Passerielo G (1995) Comparing wavelet transforms for recognizing cardiac patterns. *IEEE EMBS Mag.* **14**(2):167–173.

Sermesant M, Moireau P, Camara O, Sainte-Marie J, Andriantsimiavona R, Cimrman R, Hill DLG, Chapelle D, Razavi R (2006a) Cardiac function estimation from MRI using a heart model and data assimilation: advances and difficulties. *Med. Imag. Anal.* **10**:642–656.

Sermesant M, Delingette H, Ayache N (2006b) An electromechanical model of the heart for image analysis and simulation. *IEEE Trans. Med. Imag.* **25**:612–625.

Shahidi AV, Savard P, Nadeau R (1994) Forward and inverse problems of electrocardiography: modeling and recovery of epicardial potentials in humans. *IEEE Trans. Biomed. Eng.* **41**:249–256.

Shapiro J (1993) Embedded image coding using zerotrees of wavelet coefficients. *IEEE Trans. Sign. Proc.* **41**:3445–3462.

Sheehan F, Wilson DC, Shavelle D, Geiser EA (2000) Echocardiography. In: Sonka M, Fitzpatrick JM (Eds.): Handbook of medical imaging. Volume 2. Medical image processing and analysis. SPIE:Bellingham, WA, 609–674.

Sher DB, Revankar S, Rosenthal S (1992) Computer methods in quantitation of cardiac wall parameters from two dimensional echocardiograms: a survey. *Int. J. Card. Imag.* 8(1):11–26.

Shiao YH, Chen TJ, Chuang KS, Lin CH, Chuang CC (2007) Quality of compressed medical images. *J. Digit. Imag.* **20**:149–159.

Smola A, Scholkopf B (1998) A tutorial on support vector regression. Royal Holloway College, Univ. London, London, U.K., NeuroColt Tech. Rep. NV2-TR-1998-030.

Stegmann M, Pedersen D (2005) Bi-temporal 3D active appearance models with applications to unsupervised ejection fraction estimation. *Progr. Biomed. Opt. Imag. Proc. SPIE* **5746**:336–350.

Struzik ZR (2000) Revealing local variability properties of human heartbeat intervals with the local effective Hoelder exponent. Tech. Rep. INS-R0015, CWI, Amsterdam, The Netherlands.

Szilágyi SM, Szilágyi L, Dávid L (1997a) ECG signal compression using adaptive prediction. *Ann. Int. Conf. of IEEE EMBS* (Chicago) **19**:101–104.

Szilágyi SM, Szilágyi L, Dávid L (1997b) Comparison between neural-network-based adaptive filtering and wavelet transform for ECG characteristic points detection. *Ann. Int. Conf. of IEEE EMBS* (Chicago) **19**:272–274.

Szilágyi SM (1998) Event recognition, separation and classification from ECG recordings. *Ann. Int. Conf. of IEEE EMBS* (Hong Kong) **20**:236–239.

Szilágyi L (1999) Wavelet-transform-based QRS complex detection in on-line Holter systems. *Ann. Int. Conf. of IEEE EMBS* (Atlanta) **21**:271.

Szilágyi SM (2000) The limits of heart model based computerized ECG diagnosis. *Ann. Int. Conf. of IEEE EMBS* (Chicago) **22**:1913–1916.

Szilágyi SM, Benyó Z, Dávid L (2003a) Heart model based ECG signal processing. In: Feng DD, Carson ER (Eds.): Modelling and Control in Biomedical Systems (MCBMS'03), Elsevier: Oxford, 213–217.

Szilágyi SM, Benyó Z, Dávid L (2003b) Iterative ECG filtering for better malfunction recognition and diagnosis. In: Feng DD, Carson ER (Eds.): Modelling and Control in Biomedical Systems (MCBMS'03), Elsevier: Oxford, 295–300.

Szilágyi SM, Benyó Z, Dávid L (2003c) ECG signal compression and coise distortion effect analysis. *World Congr. Med. Phys. Biomed. Eng.* (Sydney), IFMBE Proc. **4**, paper #4391.

Szilágyi SM, Benyó Z, Dávid L (2003d) WPW syndrome identification and classification using ECG analysis. *World Congr. Med. Phys. Biomed. Eng.* (Sydney), IFMBE Proc. **4**, paper #4423.

Szilágyi SM, Benyó Z, Frigy A (2004) Sensibility analysis of the ARRUDA localization method. *Sci. Bull. Univ. Timisoara, Trans. Autom. Contr. Comp. Sci.* **49(63)**(2):129–32.

Szilágyi SM, Benyó Z, Szilágyi L (2005) Recognition of various events from 3–D heart model, *16th IFAC World Congress Preprint* (Prague), paper #4695, 1–6.

Szilágyi SM (2006) 3D heart simulation and analysis. *Periodica Polytech. Ser. El. Eng.* **50**(1-2):79–90.

Szilágyi SM, Szilágyi L, Benyó Z (2007a) Spatial heart simulation and analysis using unified neural network. *Ser. Adv. Soft Comput.* **41**:346–354.

Szilágyi SM, Szilágyi L, Benyó Z (2007b) Volumetric analysis of the heart using echocardiography. *Lect. Notes Comp. Sci.* **4466**:81–90.

Thaker NV, Ferrero JM (1998) Electrophysiologic models of heart cells and cell networks. *IEEE EMBS Mag.* **17**(5):73–83.

Tkacz EJ, Kostka P (2000) An application of wavelet neural network for classification patients with coronary artery disease based on HRV analysis, *Ann. Int. Conf. of IEEE EMBS* (Chicago) **22**:1391–1393.

Trahanias PE (1993) An aproach to QRS complex detection using mathematical morphology. *IEEE Trans. Biomed. Eng.* **40**(2):201–205.

ten Tusscher KHWJ, Noble D, Noble PJ, Panfilov AV (2004) A model for human ventricular tissue. *Amer. J. Physiol. Heart. Circ. Physiol.* **286**:H1573–H1589.

ten Tusscher KHWJ, Bernus O, Hren R, Panfilov AV (2006) Comparison of electrophysiological models for human ventricular cells and tissues. *Prog. Biophys. Mol. Biol.* **90**:326–345.

Vapnik V (1998) Statistical learning theory. Wiley: New York.

Vuille C, Weyman AE (1994) Left ventricle I: general considerations, assessment of chamber size and function. In: Weyman AE (Ed.) Principles and practice of echocardiography. Lippincott Williams & Wilkins 575–624.

Watanabe MA (2003) Heart rate turbulence: a review. *Indian Pacing Electrophysiol. J.* **3**(1):10–22.

Webster JG (Ed.) (1978) Medical instrumentation - application and design. Houghton Mifflin: Boston.

Wellens HJJ, Fare J, Bar FW (1987) The Wolff-Parkinson-White syndrome. In: Mandel WJ (Ed.): Cardiac arrhythmias. Their mechanisms, diagnosis and management.JP Lippincott: Philadelphia 274–296.

Wellens HJJ, Brugada P, Penn OC *et al* (1990) Pre-excitation syndromes: clinical presentation, course and therapy. In: Zipes DP, Jalife J (Eds.) Cardiac electrophysiology. From cell to bedside. WB Saunders Co: Philadelphia 691–702.

Winfree AT (1994) Electrical turbulence in three-dimensional heart muscle. *Science* **266**:1003-1006.

Winslow RL, Scollan DF, Holmes A, Yung CK., Zhang J, Jafri MS (2000) Electrophysiological modeling of cardiac ventricular function: from cell to organ. *Ann. Rev. Biomed. Eng.* **2**:119–155.

Winslow RL, Hinch R, Greenstein JL (2005) Mechanisms and models of cardiac excitation-contraction coupling, Lect. Notes Math. **1867**:97–131.

Wolff L, Parkinson J, White P (1930) Bundle branch block with short PR interval in healthy young people prone to paroxysmal tachycardia. *Amer. Heart J.* **5**:685–704.

Wood JC, Barry DT (1995) Time frequency analysis of the first heart sound, *IEEE EMBS Mag.* **14**(2):144-151.

Wu X, Memon N (1997) Context-based adaptive lossless image coding. *IEEE Trans. Comm.* **45**:437–444.

Wu X, Bao P (2000) L-infinity constrained high-fidelity image compression via adaptive context modeling. *IEEE Trans. Image Proc.* **9**:536–542.

Xue Q, Hu YH, Tompkins WJ (1992) Neural-network-based adaptive matched filtering for QRS detection. IEEE Trans. Biomed. Eng. **39**:317–329.

Yee R, Klein GJ, Guiraudon GM (1995) The Wolff-Parkinson-White syndrome. In: Zipes DP, Jalife J (Eds.) Cardiac electrophysiology. From cell to bedside. WB Saunders Co: Philadelphia 1199–1214.

Yuan Y, Evans AN, Monro DM (2004) Low complexity separable matching pursuits. IEEE Int. Conf. Acoustics, Speech, Sign. Proc. III. 725–728.

Zhenga Z, Yang J (2006) Supervised locality pursuit embedding for pattern classification. Imag. Vis. Comput. **24**:819–826.

Zigel Y (1998) ECG signal compression. Electr. Comput. Eng. Dept., Ben-Gurion Univ. Israel. Available: http://www.ee.bgu.ac.il/~spl

Zigel Y, Cohen A, Katz A (2000a) ECG signal compression using analysis by synthesis coding. IEEE Trans. Biomed. Eng. **47**(10):1308–1316.

Zigel Y, Cohen A, Katz A (2000b) The weighted diagnostic distortion (WDD) measure for ECG signal compression. IEEE Trans. Biomed. Eng. **47**(11):1422–1430.